Precise Mass Measurements of ^{252}Cf Fission Fragments With The Canadian Penning Trap Mass Spectrometer (CPTMS)

BY

Yuyan Wang

A Thesis
Submitted to the Faculty of Graduate Studies
in Partial Fulfillment of the Requirements
for the Degree of

MASTER OF SCIENCE

Department of Physics and Astronomy
University of Manitoba
Winnipeg, Manitoba

To my parents,
for their unconditional love and support

Abstract

The Canadian Penning Trap Mass Spectrometer (CPTMS) located at the ATLAS (Argonne Tandem Linear Accelerator System) facility of Argonne National Laboratory makes precise mass measurements on both stable and unstable isotopes. A ^{252}Cf fission source has been used as the ion source for the unstable isotope mass measurements. This thesis concentrates on the mass measurements of the fission fragments from the ^{252}Cf fission source using the CPTMS system. It is the first time that the masses of such fission fragments have been measured with a mass spectrometer.

The masses of ^{108}Tc, ^{108}Ru, ^{109}Ru and ^{110}Ru have been measured to a precision of 10^{-7}. The results have been compared to exiting mass measurements and the Atomic Mass Evaluation (AME2003). In general good agreement between this work and existing data is realized. A few discrepancies are identified.

Acknowledgements

First of all, I would like to express the greatest gratitude to my supervisor Kumar Sharma for his guidance, help and patience throughout my program of study. Thank him for giving me the opportunity to work on such an inspiring and challenging project. Thank him for guiding me to become a logic and careful person. Thank him for spending long hours to read and edit my thesis.

Special thanks should be given to Dr. Guy Savard at Argonne National Lab for his guidance on my work and for his commitment and inspiration to the whole project.

I would like to sincerely thank the post doctor Zhen Zhou. Without his help, much of this work wouldn't have been possible. Thank Dr. Jason Clark, for helping me to truly understand the mass measurement operation procures. He is an example of intelligent, careful, and diligent young physicists. I feel really lucky to know him. Thank the post doctor Jicheng Wang, for patiently teaching me how to operate such a complicate apparatus as the CPTMS. Thank post doctor H.P Sharma, for helping me conduct the experiments and for kindly inviting me to have delicious Indian meals.

Many thanks should also be given to the staff members and the students in the CPT research group. They were always more than willing to lend me a hand. For the teachers, I would like to thank Dr. S. A. Page, for patiently answering all of my questions in the nuclear physics class.

Thanks NSERC and the Department of Physics & Astronomy in the University of Manitoba for providing the financial assistance for this program.

Last but certainly not least I would like to thank my parents for their unconditional love and ongoing support. In Chinese tradition, as an adult, I have the responsibility to take care of my parents. However, for years, I have been thousands of miles away from them. They never complain and always try to find a way to help, support and encourage me. To express my gratitude, I dedicate this thesis.

Table of Contents

List of Tables

List of Figures

Chapter 1

Introduction

1.1 Physics of Nuclear Masses

The atom is considered the basic unit of all kinds of matter in the world. It consists of electrons orbiting around the core of the atom, which is called the nucleus. A nucleus consists of protons and neutrons. In nuclear physics, we use "Z" to represent the number of protons (also called atomic number) and use "N" to represent the number of neutrons. Therefore, the sum of Z and N gives the total number of the nucleons, which is called the mass number (A). Nuclei with the same proton number Z but different neutron number N are called isotopes. Nowadays, about 2300 different nuclides are known, 230 of which exist in nature.

Nuclear mass is one of the fundamental characteristics of a nucleus. The mass of the nucleus is smaller than the mass of its individual components, the sum of protons and neutrons. The binding energy ($B(Z,A)$) is reflected by the "mass difference" between the mass of the bound nucleus $m_{nuclear}({}^{A}_{Z}X)$ and the masses of the free protons m_p and neutrons m_n [Krane1987], shown in the equation 1.1:

$$B(Z,A) = Zm_p + (A-Z)m_n - m_{nuclear}({}^{A}_{Z}X) \tag{1.1}$$

Based on the equation 1.1, the commonly used form "binding energy per nucleon" can be written as $B(Z,A)/A$. The average binding energy of most nuclei is about 8 MeV per nucleon. Figure 1.1 shows the variation of $B(Z,A)/A$ with nucleon number:

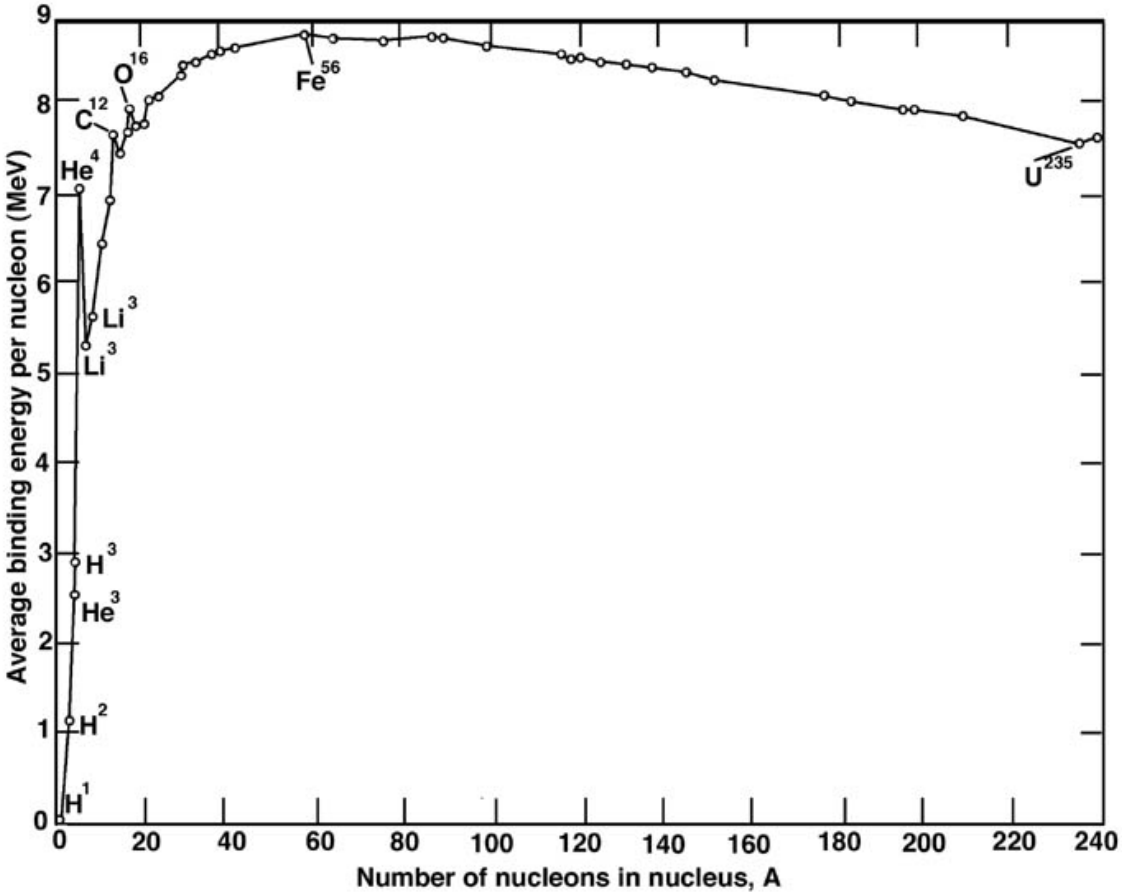

FIG. 1.1. The average binding energy per nucleon as a function of number of nucleons in the atomic nucleus [NASA].

Energy is released when nuclei with smaller binding energies combine or split to form nuclei with larger binding energies. Fission occurs when a heavy nucleus splits into several tightly bound lighter nuclei. The heavy element ^{252}Cf fissions into two main fragments: the light fission fragment and the heavy fission fragment as seen on the figure 3.7 in chapter 3.

The mass of the nucleus can be extracted from the atomic mass, corrected for the mass and binding energy of the atomic electrons [Duckworth 1990].

$$m_{nuclear}\left({}^{A}_{Z}X\right) = m_{Atomic}\left({}^{A}_{Z}X\right) - Zm_e + \sum_{i=1}^{Z} B_i \tag{1.2}$$

B_i represents the electron binding energy of the ith electron. Therefore the atomic mass measurements provide a way to determine the nuclear masses directly. The last neutron or proton separation energy in a nuclide can be calculated from mass difference of two nuclear masses. For example, the last neutron separation energy ($E_{separation}$) can be derived from the following equation:

$$E_{separation} = (m_n - (m({}^{A}_{Z}X) - m({}^{A-1}_{Z}X))) \times C^2 \tag{1.3}$$

Studying the separation energy will help us to further understand the nuclear structure.

The atomic masses have been widely used to calculate the reaction energy "Q" value, which is defined as the energy released in the nuclear reaction. Many kinds of nuclear reactions occur by absorbing the particles such as neutrons or protons. Other types of reactions may involve the absorption of gamma rays. A typical nuclear reaction is written:

$$a + X \rightarrow Y + b \tag{1.4}$$

or

$$X(a,b)Y \tag{1.5}$$

Where a is the projectile particle, X is the target, and Y *and* b are the reaction products. Based on the conservation law of the total energy:

$$m_X c^2 + T_X + m_a c^2 + T_a = m_Y c^2 + T_Y + m_b c^2 + T_b \tag{1.6}$$

where the T's are kinetic energies and m's are rest masses [Krane1987]. Therefore the Q value can be expressed as:

$$Q = \left(m_{initial} - m_{final}\right)c^2 = \left(m_X + m_a - m_Y - m_b\right)c^2 \quad (1.7)$$

The Q is positive if the total mass of the products is less than the total mass of the projectile and target, indicating that the total nuclear binding energy has increased.

Also the atomic masses of the nuclides far away from β-stability line will provide stringent tests for nuclear models [Lunney2003]. A detailed description is given in the chapter 5 of this thesis. Due to the importance of the nuclear and atomic masses, more and more mass spectrometers have been built and the mass measurement techniques have developed very quickly in the past several decades.

1.2 Brief History of Mass Measurement Techniques

The first practical mass spectrometer, introduced by Aston, was constructed right after the First World War [Aston1920]. Later on, an improved idea was employed in the Dempster-type "double focusing" mass spectrometer consisting of a 90^o radial electrostatic analyzer followed by a semicircular magnetic analyzer. Manitoba I is one of such type of machine located at University of Manitoba in the early sixties [Barber1964]. The resolving power of Manitoba I could reach up to 100,000. Improvement was made on Manitoba II ("Betsy") by employing sector fields in a relatively compact configuration during the mid-sixties [Barber1971].

Nowadays, ion traps have become a standard technology used as mass spectrometers in many accelerator laboratories [Savard1997]. They are used to capture, accumulate and confine the charged particles in the vacuum. The choice of the type of ion

trap depends on the specific use. The most commonly used ion traps are the Penning trap [Penning1936] and the Paul trap [Paul1989]. The Paul trap is mostly used for accumulating and storing the ions. In the Penning trap, the mass m of the stored ions can be determined by measuring the cyclotron frequency ω_c ($\omega_c = (q/m)B$). The cyclotron frequency can be measured using Time of Flight (TOF) technique [Bollen1990]. The details are described in the following chapter 2. In order to measure the masses of nuclides far from the stability (known as "exotic" nuclei), experimenters coupled such "ion trap" mass spectrometers with an accelerator system, for instance, the ISOLTRAP at CERN, Geneva [Bollen1996]; the NSCL, at MSU, Michigan, USA [Bollen2003]; the ESR at GSI, Darmstadt [Radon2000]; IGISOL at JYFL, Jyvaskyla, Finland [Szerypo2002]; the ISAC at TRIUMF, Vancouver [Dilling2003] and of course the CPTMS at ANL, Argonne, USA [Sharma1998].

The purpose of this thesis is to describe the Canadian Penning Trap Mass Spectrometer (CPTMS) system and some of the mass measurements being done with it.

1.3 The Canadian Penning Trap Mass Spectrometer

Back to 1994, a group of people from University of Manitoba, the TASCC (Tandem Accelerator Superconducting Cyclotron) facility of Chalk River Laboratory, and McGill University proposed to build a device named the Canadian Penning Trap Mass Spectrometer (CPTMS), which would conduct high precision mass measurements on both stable and unstable isotopes. The apparatus was designed and assembled at Chalk River Laboratory between 1994 and 1997. In 1997, the CPTMS was moved to Argonne National Lab (ANL) in Argonne, IL, USA due to the shutdown of TASCC facility. First,

the system was tested with the laser-desorption ion source. Mass measurements on gold (Au) and platinum (Pt) isotopes were made and the data were used to test the precision and consistency of the CPTMS [Vaz2002]. By the end of 2003 great improvements have been made on the injection system of the CPTMS system [Clark2003]. Since then, the mass measurements of radioactive nuclides have been successful with this system, such as the mass measurements of ^{68}Se [Clark2004], ^{22}Mg [Savard2004] and ^{46}V [Savard2005]. Also the masses of neutron-rich nuclei from the ^{252}Cf fission source have been measured to a very high precision. In 2005, the APT (Advanced Penning Trap) system, composed with a gas-filled Penning trap in a 7 Tesla super-conducting magnet, was assembled and connected with the CPTMS to further improve the efficiency and precision of the whole system. Now, the CPTMS system has become a powerful machine to conduct mass measurements with high precision on part of 10^{-8}. This thesis will concentrate on the mass measurements of the light fission fragments from the ^{252}Cf fission source using the CPTMS system.

Chapter 2

Theory of the Ion Traps

"Traps" have become one of the most important devices in mass measurements over the last 30 years [Savard1997]. There are two types of ion trap used by the CPTMS system. ***The RFQ*** (Radio Frequency Quadrupole) ***trap*** is an ion trap using a two-dimensional quadrupole field to confine ions and select a certain range of m/q. Two RFQ traps are used in the CPTMS system. One is located in the last section of the gas cooler and the other is assembled below the Penning trap. Helium gas with the room temperature fills in both of the RFQ traps to cool down the ions. ***The Penning trap*** uses a three-dimensional quadrupole field and a homogenous magnetic field. Two Penning traps have been employed in the CPTMS system. One filled with the buffer gas, the "isobar separator", is used to remove the contaminant ions from the sample. The other, the "precision trap", is located in a 5.9 Tesla superconducting magnet. The ion mass is determined by measuring the cyclotron (ω_c) frequency of an ion in this Penning trap. This chapter explores the theories associated with these two types of ion trap and describes the ion motions inside traps. Then, a brief description is given of the Time of Flight (TOF) technique used to measure the cyclotron frequency of the trapped fission fragments.

2.1 The RFQ Trap

In experiment, a two-dimensional (x-y plane) quadrupole field is achieved by using a set of four-rod electrodes and applying DC voltages on each of them, as shown in figure 2.1. In the CPTMS system, the defined RFQ trap is the device that uses such a two-dimensional quadrupole field.

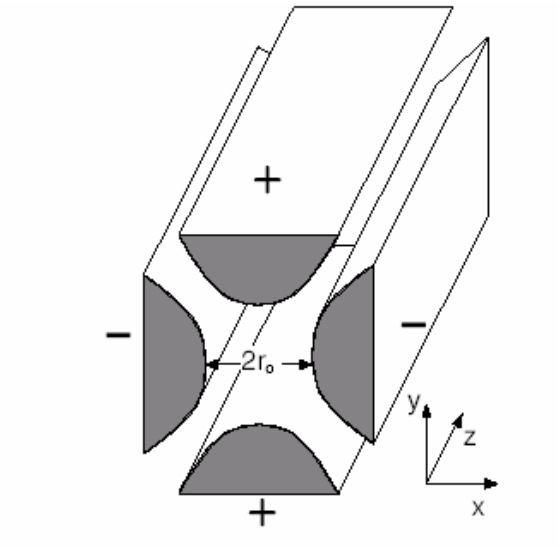

FIG. 2.1. A set of four-rod electrodes provides a two dimensional quadrupole electric field on x-y plane. The distance between two opposite rods is $2r_o$ and each rod has a hyperbolic surface [Boudreau2001].

The potential of a two-dimensional quadrupole field in the Cartesian coordinates can be expressed as:

$$\Phi = \frac{\Phi_0}{2r_0^2}\left(\lambda x^2 + \sigma y^2\right) \tag{2.1}$$

Where Φ_0 is an applied electric potential difference between the two pairs of opposite rod electrodes; λ and σ are the constants and r_0 depends on the physical structure of the electrodes. Applying the Laplace's equation to equation 2.1, we get:

$$\nabla^2\Phi = \frac{\Phi_0}{2r_0^2}(2\lambda + 2\sigma) = 0 \tag{2.2}$$

Therefore:

$$\lambda + \sigma = 0 \tag{2.3}$$

Setting $\lambda = -\sigma = 1$. The equation 2.1 becomes:

$$\Phi = \frac{\Phi_0}{2r_0^2}(x^2 - y^2) \tag{2.4}$$

The "saddle" shape potential Φ can be plotted based on equation 2.4 in the Cartesian coordinates, as shown in figure 2.2:

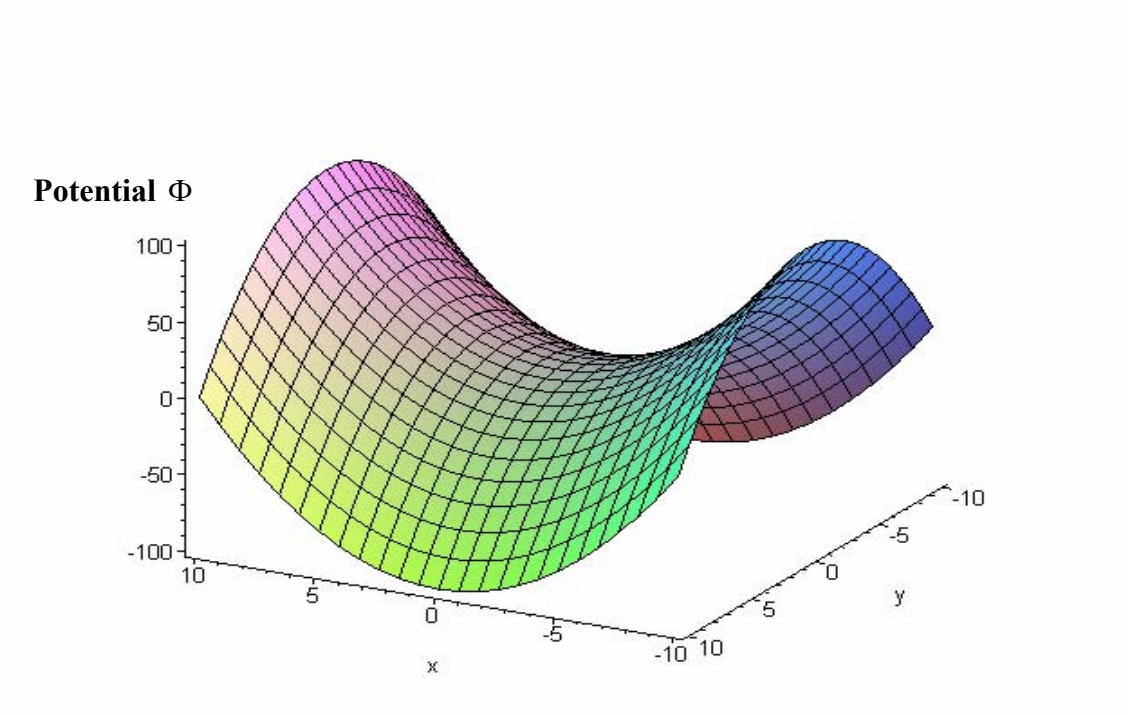

FIG. 2.2. The plot of the quadrupole potential in the RFQ trap, ions are confined along the x-axis direction and repulsed along the y-axis direction.

As shown in figure 2.2, with the quadrupole potential, ions will be confined in one direction and repulsed in the other. Therefore the potential Φ_0 must be variable in time in order to trap the ions within both x and y directions. In the experiments, this condition can be achieved by applying a DC voltage U plus an oscillating radio-frequency voltage $V\cos\Omega t$. Applying this to equation 2.4, we get:

$$\Phi(x,y,t) = (U - V\cos\Omega t)\frac{x^2 - y^2}{2r_0^2} \tag{2.5}$$

In any direction (x, or y), the ion motion is a harmonic oscillation; then the equation of motion can be written as $m\ddot{x} = -e\cdot\partial\Phi/\partial x$:

$$\begin{aligned} &\ddot{x} + \frac{e}{mr_0^2}(U - V\cos\Omega t)x = 0 \\ &\ddot{y} - \frac{e}{mr_0^2}(U - V\cos\Omega t)y = 0 \\ &\ddot{z} = 0 \end{aligned} \tag{2.6}$$

In order to solve this equation, we introduce three parameters a, q and ζ [Daw76]:

$$\begin{aligned} a &= a_x = a_y = \frac{4eU}{mr_o^2\Omega^2} \\ q &= q_x = q_y = \frac{2eV}{mr_o^2\Omega^2} \\ \zeta &= \frac{\Omega t}{2} \end{aligned} \tag{2.7}$$

Equation 2.6 then can be changed to Mathieu differential equation:

$$\frac{d^2u}{d\zeta^2} + (a - 2q\cos 2\zeta)u = 0 \tag{2.8}$$

The Mathieu equation has both stable and unstable solutions depending on the values of the parameters a and q. Solutions are in a form of:

$$u(\varsigma) = Ae^{\mu\varsigma}\sum_{n=-\infty}^{+\infty} C_{2n}e^{2in\varsigma} + Be^{-\mu\varsigma}\sum_{n=-\infty}^{+\infty} C_{2n}e^{-2in\varsigma} \tag{2.9}$$

Constants A and B depend on the initial conditions. C_{2n} and the complex μ ($\mu = \alpha \pm i \cdot \beta$) depend only on the parameters a and q. The stable solutions, which means $u(\varsigma)$ remains finite as $\varsigma \to \infty$, are what we need for the device. In order to achieve that, μ must be a pure imaginary, i.e. $\alpha = 0$. Equation 2.9 becomes:

$$u(\varsigma) = A\sum_{n=-\infty}^{+\infty} C_{2n}e^{(2n\pm\beta)i\varsigma} + Be^{-\mu\varsigma}\sum_{n=-\infty}^{+\infty} C_{2n}e^{-(2n\pm\beta)i\varsigma} \tag{2.10}$$

The stable solutions of equation 2.8 form the stability regions in both x and y directions. It is convenient to operate the trap at the lowest stability region (closest to the origin) as shown in figure 2.3. Only ions following the stable trajectories can be collected and others will be lost on the electrodes.

Equation 2.7 shows that $a/q \sim 2U/V$. A fixed a/q ratio implies a straight line, which is also called the operation line. Based on equation 2.7, at the lowest stability region as shown in figure 2.3, the lowest and the highest q value can be expressed respectively:

$$\begin{aligned} q_{low} &= (e/m)_{low}\frac{2V}{r_0^2\Omega^2} \\ q_{high} &= (e/m)_{high}\frac{2V}{r_0^2\Omega^2} \end{aligned} \tag{2.11}$$

If r_0, V and Ω are fixed, the range of q (between q_{low} and q_{high}) will decide the range of the masses lying in the stable region. If U is fixed, the ratio of a/q will only depend on the value of V. By reducing V, we can narrow the range of q and consequently increase the resolution of the masses ($m/\Delta m = \infty$ at the peak of the stability zone in figure 2.3).

The resolution is limited, in other words, $m/\Delta m = \infty$ cannot be achieved due to the imperfect operation condition and systematic uncertainties.

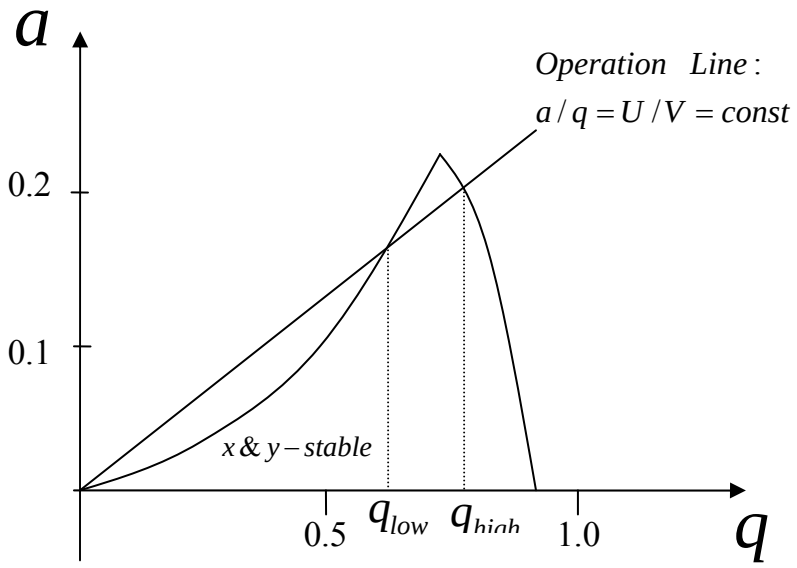

FIG. 2.3. An approximate schematic sketch shows the lowest positive common stability region in both x and y directions and the operation line with a slope of a/q.

In practice, the hyperbolic cylinders of the RFQ trap are often replaced by circular rods. The rod radius r ($r = 1.146 r_o$) is often chosen as the best approximation to provide the quadrupole potential given by the hyperbolic cylinders [Denison1971]. In the CPTMS, the circular rods of the RFQ trap are cut into three isolated segments. Independent DC potentials can be applied to each of the segments. If a lower potential is applied to the middle segment and higher potential employed to the two neighbouring segments, a potential well is formed. Thus, a linear trap is made along the axial direction. Detailed description is given in chapter 3.3.6. Also the buffer gas, usually helium, was introduced into the RFQ trap during the experiments. Ions lose energy by colliding with

the buffer gas in the trap reducing the energy. Finally the cooled ions are trapped in the bottom of the potential well.

2.2 The Penning Trap

Unlike the RFQ trap, the Penning trap consists of both an electrostatic quadrupole field and a homogenous magnetic field. The electrostatic field and the magnetic field inside the Penning trap are illustrated in figure 2.4.

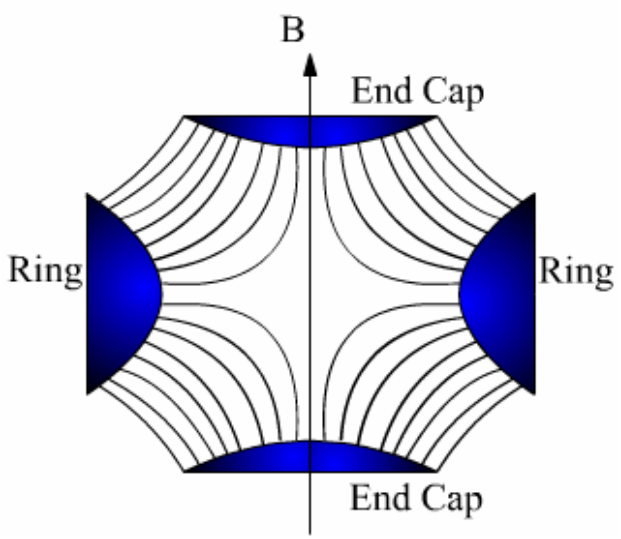

FIG. 2.4. The graph shows the magnetic field and electric field provided by the Penning trap; the magnetic field is along the axial direction and the electric field is a three dimensional quadrupole field given by the two end-caps and the ring electrode in the Penning trap.

Due to the quadrupole field, an ion experiences a harmonic oscillation along the axial (z) direction with the frequency ω_z. In the x-y plane, the electric force is repulsive and pushes the ions out of the trap in the radial direction. A strong uniform magnetic field of the magnitude B, applied along the axial direction (z-axis), is used to confine the ions into a orbit.

$$\omega_c = \frac{qB}{m} \tag{2.12}$$

Where q is the charge of the ion. Finally, the ion masses can be determined by measuring the cyclotron frequency ω_c.

The quadrupole potential can be written in Cartesian coordinates as [Daw76]:

$$\Phi(x, y, z) = \frac{\Phi_o}{4d^2}\left(2z^2 - (x^2 + y^2)\right) \tag{2.13}$$

Where

$$d^2 = \frac{1}{2}\left(z_o^2 + \frac{r_o^2}{2}\right) \tag{2.14}$$

The quadrupole electric potential Φ can be produced by placing three ideal electrodes along the equipotential surface. Figure 2.5 on the next page shows the structure of an ideal Penning trap. The two end-cap electrode surfaces can be described by equation 2.15, where z_o is the minimum axial distance between the centre of the Penning trap and the end-cap electrodes.

$$z^2 - \frac{(x^2 + y^2)}{2} = z_o^2 \tag{2.15}$$

The ring electrode surface can be described by equation 2.16, where r_o is the minimum radial distance between the centre of the Penning trap and ring electrode.

$$z^2 - \frac{(x^2 + y^2)}{2} = -\frac{r_o^2}{2} \tag{2.16}$$

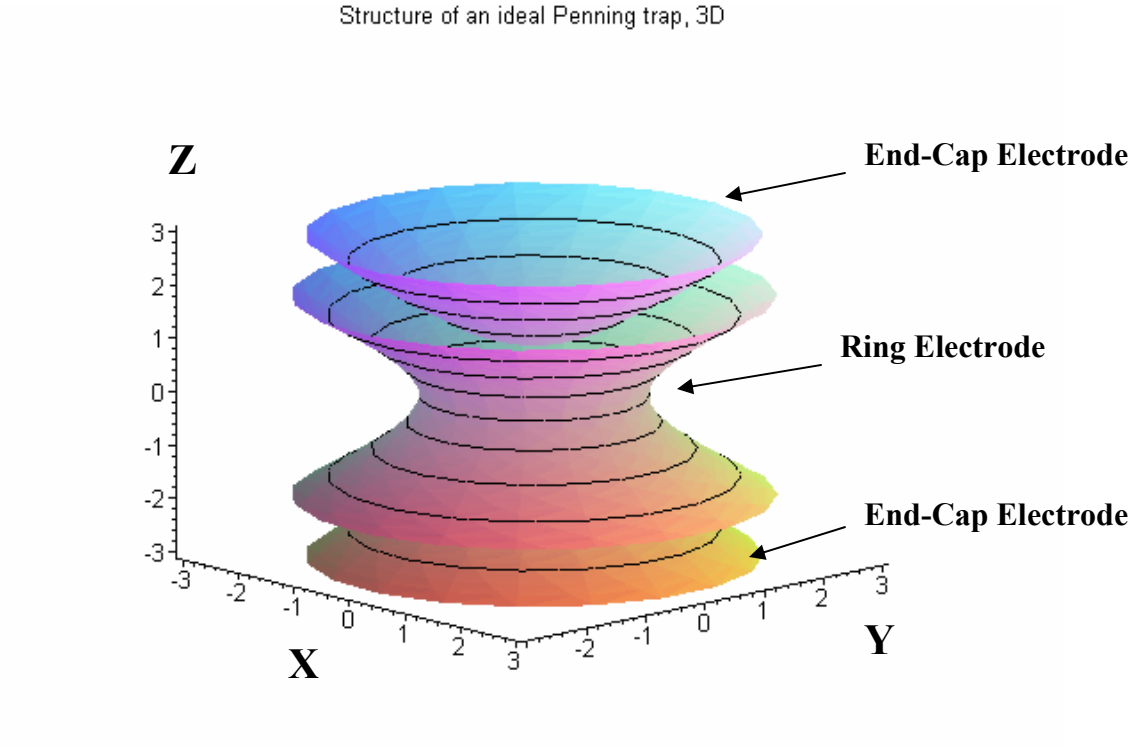

FIG. 2.5. A 3-dimensional graph showing the surfaces of three electrodes along the equipotential surfaces in an ideal Penning trap: two end-cap electrodes and one ring electrode with the hyperbolic surface

In an ideal Penning trap, all electrodes are hyperboloids of revolution with $r_o = \sqrt{2} z_o$. Based on equation 2.13, the electric fields along the x, y and z directions can be derived as following equation 2.17:

$$E = -\nabla\Phi = \frac{\Phi_0}{2d^2} \cdot \begin{bmatrix} x \\ y \\ -2z \end{bmatrix} \tag{2.17}$$

Forces due to the electric field are shown below respectively in Cartesian coordinates:

$$F = qE = \frac{q\Phi_o}{2d^2} \cdot \begin{bmatrix} x \\ y \\ -2z \end{bmatrix} \tag{2.18}$$

The axial motion (along z-axis) is purely electric field dependent. The equation is given by:

$$m\ddot{z} + \frac{qV_o}{d^2} z = 0 \tag{2.19}$$

This equation describes a simple harmonic oscillation. Based on the definition, the frequency can be written as:

$$\omega_z = \sqrt{\frac{qV_o}{md^2}} \tag{2.20}$$

The force on the radial direction can be described as:

$$\vec{F} = m\vec{a} = q\vec{E} + q\vec{r} \times \vec{B} \tag{2.21}$$

Therefore the equation of motion can be written as:

$$\begin{bmatrix} \ddot{x} \\ \ddot{y} \\ \ddot{z} \end{bmatrix} = \frac{q\Phi_o}{2md^2} \begin{bmatrix} x \\ y \\ -2z \end{bmatrix} + \frac{qB}{m} \begin{bmatrix} \dot{y} \\ -\dot{x} \\ 0 \end{bmatrix} \tag{2.22}$$

Using equations 2.12 and 2.20 to simplify the equation 2.22:

$$\begin{bmatrix} \ddot{x} \\ \ddot{y} \\ \ddot{z} \end{bmatrix} = \frac{\omega_z^2}{2} \begin{bmatrix} x \\ y \\ -2z \end{bmatrix} + \omega_c \begin{bmatrix} \dot{y} \\ -\dot{x} \\ 0 \end{bmatrix} \tag{2.23}$$

On the radial direction (x and y plane), the first two equations on equation 2.23 can be combined to:

$$\ddot{u} + i\omega_c \dot{u} - \frac{\omega_z^2}{2} u = 0 \tag{2.24}$$

The solution of this equation is calculated with a Maple program:

$$u(t) = C_1 e^{-i\omega_+ t} + C_2 e^{-i\omega_- t} \tag{2.25}$$

Where C_1 and C_2 are constants. The two eigenfrequencies ω_+ and ω_- are:

$$\omega_{\pm} = \frac{\omega_c}{2} \pm \sqrt{\frac{\omega_c^2}{4} - \frac{\omega_z^2}{2}} \tag{2.26}$$

Transfer the solution 2.25 back into Cartesian coordinates:

$$\begin{bmatrix} x \\ y \end{bmatrix} = R_+ \begin{bmatrix} \cos(\omega_+ t - \phi_+) \\ -\sin(\omega_+ t - \phi_+) \end{bmatrix} + R_- \begin{bmatrix} \cos(\omega_- t - \phi_-) \\ -\sin(\omega_- t - \phi_-) \end{bmatrix} \tag{2.27}$$

Therefore the ions undergo two decoupled ion motions in the x and y plane: 1) the magnetron motion with the frequency ω_- and the constant radius R_- and 2) the modified cyclotron motion with the frequency ω_+ and the constant radius R_+. Figure 2.6 shows the three independent ion motions in the Penning trap. Three frequencies-axial oscillation (ω_z), modified cyclotron motion (ω_+), and magnetron motion (ω_-)- define the final ion motion and are interrelated as shown in equation 2.28 below:

$$\begin{aligned} \omega_+ + \omega_- &= \omega_c \\ \omega_+ \omega_- &= \frac{\omega_z^2}{2} \\ \omega_+^2 + \omega_-^2 + \omega_z^2 &= \omega_c^2 \end{aligned} \tag{2.28}$$

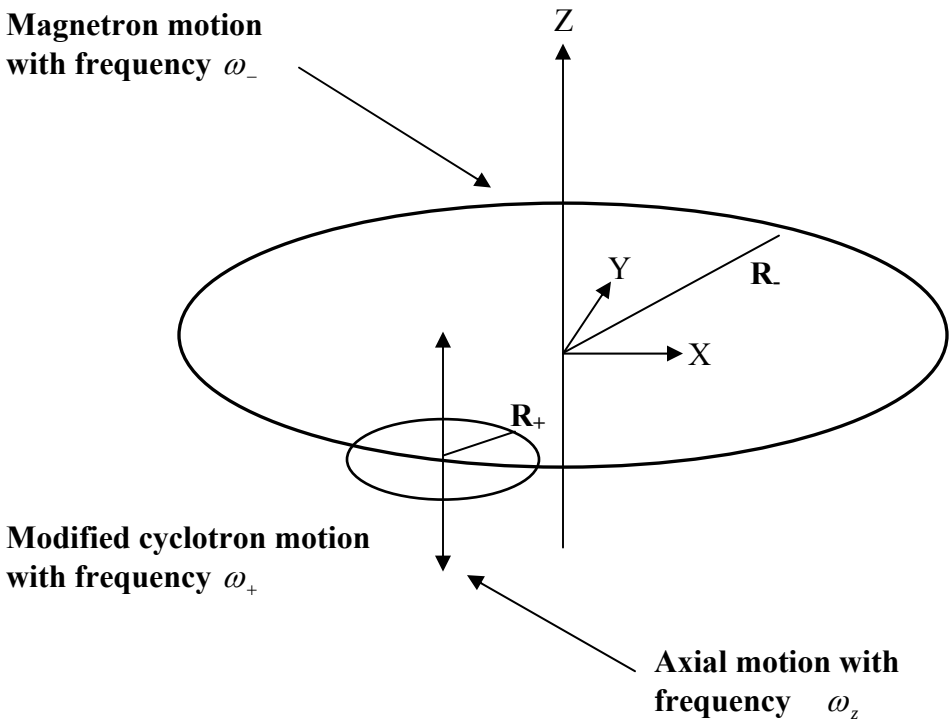

FIG. 2.6. The schematic sketch of the ion motions in a Penning trap. The overall ion motion is superposed of the circular magnetron motion with low frequency ω_-, the modified cyclotron motion with high frequency ω_+ and the axial oscillation with frequency ω_z.

The axial motion along the z-axis only depends on the electric field, while the modified cyclotron and magnetron motions are dependent on both the electric and magnetic fields. The true cyclotron frequency is solely dependent on the magnetic field, which is stable and precisely known. For this reason, in the mass measurements, the mass *m* is determined by the true cyclotron frequency ω_c ($\omega_c = (q/m)B$) of ions stored in a Penning trap. This frequency is measured from the stored ions excited by a radio frequency (RF) field and the resonance is detected by a time of flight (TOF) technique. The details are described in the following sections.

2.3 Excitation of stored ion motion in the Penning Trap

In order to excite the motion of the stored ions, RF voltages are applied to the ring electrode of the Penning trap, which is split into quarters. Thus, two modes of excitation, dipole excitation and quadrupole excitation, can be applied in the radial plane of the trap.

2.3.1 Dipole Excitation of the Stored Ions

The RF excitation is an auxiliary electric field applied to the system. In an ideal Penning trap, an oscillating dipole potential has the form:

$$\Phi_d = A_0 \cdot \cos(\omega_d t - \phi_d) \cdot x \tag{2.29}$$

where ϕ_d is the initial phase, ω_d is the excitation frequency, and A_0 is a constant depending on the amplitude of the applied excitation and the geometric factor of the trap as well. Also refer to the following figure 2.7 about dipole excitation.

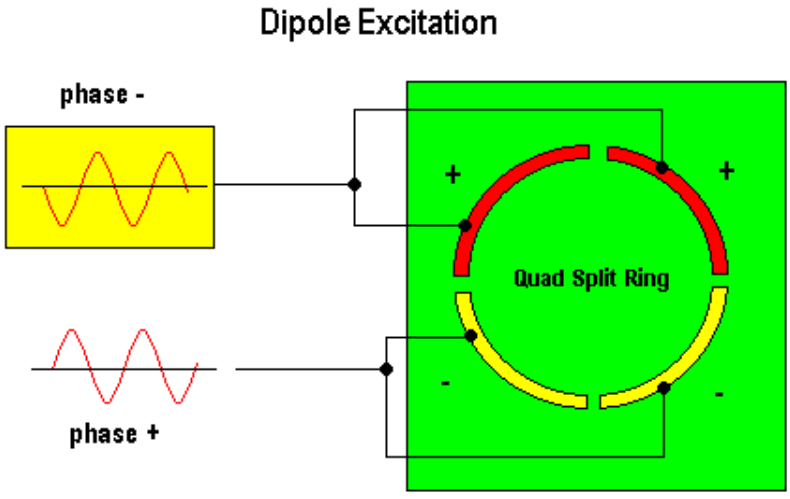

FIG. 2.7. The sketch of the dipole excitation. A RF voltage is applied to two opposite segments of the ring electrode of the Penning trap, producing a dipole potential.

Based on equation 2.29, the additional electric field E_d can be written in the Cartesian coordinates:

$$E_d = -\nabla\Phi_d = -A_0 \cdot \cos(\omega_d t - \phi_d) \cdot \begin{bmatrix} 1 \\ 0 \\ 0 \end{bmatrix} \tag{2.30}$$

Add this additional force to the equation of motion 2.23 in the Cartesian coordinates:

$$\begin{bmatrix} \ddot{x} \\ \ddot{y} \\ \ddot{z} \end{bmatrix} - \frac{\omega_z^2}{2} \begin{bmatrix} x \\ y \\ -2z \end{bmatrix} - \omega_c \begin{bmatrix} \dot{y} \\ -\dot{x} \\ 0 \end{bmatrix} = \begin{bmatrix} -k_0 \cos(\omega_d t - \phi_d) \\ 0 \\ 0 \end{bmatrix} \tag{2.31}$$

With

$$k_0 = A_0 \cdot \frac{q}{m} \tag{2.32}$$

The axial motion remains unaffected by and the solution of the radial motion is similar to the solution of equation 2.24:

$$\begin{bmatrix} x \\ y \end{bmatrix} = R_-(t) \begin{bmatrix} \cos(\omega_- t - \phi_-) \\ -\sin(\omega_- t - \phi_-) \end{bmatrix} + R_+(t) \begin{bmatrix} \cos(\omega_+ t - \phi_+) \\ -\sin(\omega_+ t - \phi_+) \end{bmatrix} \tag{2.33}$$

In contrast to from the solution 2.27, $R_\pm(t)$ are now the ***time-varying*** functions, representing the radius of the magnetron motion and the modified cyclotron motion. If the phase shift ($\phi_d - \phi_\pm$) equals to $3\pi/2$ for excitations at ω_+ and $\pi/2$ for excitations at ω_-, the $R_\pm(t)$ can be simplified as:

$$R_\pm(t) = R_\pm(0) + \frac{k_0 t}{2(\omega_+ - \omega_-)} \tag{2.34}$$

In the dipole excitation mode, the ion motions are excited at their eigenfrequencies ω_+ or ω_-. The ω_+ excitation is highly mass selective and ω_-

excitation is less mass selective. Therefore, in the CPTMS experiments, the ω_+ dipole excitation is used to remove the unwanted isotopes by increasing their cyclotron motion orbit until they are lost from the trap. The ω_- dipole excitation is employed to establish the initial orbit of the desired ions.

2.3.2 Quadrupole Excitation of the Stored Ions

Similarly an oscillating quadrupole potential has the form:

$$\Phi_q = B_0 \cos(\omega_q t - \phi_q) \cdot (x^2 - y^2) \tag{2.35}$$

Where ϕ_q is the initial phase, ω_q is the excitation frequency, and B_0 is the constant depending on the amplitude and the geometric factor of the trap. The following schematic sketch shows the application of the quadrupole excitation:

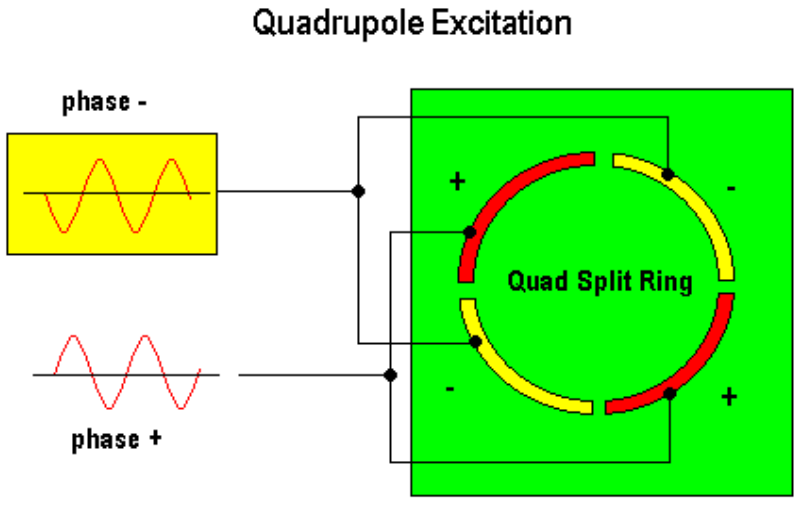

FIG. 2.8. The schematic sketch of quadrupole excitation, a RF voltage is applied between two pairs of opposite segments, producing a quadrupole potential.

Based on equation 2.35, the additional electric field E_q can be written in Cartesian coordinates:

$$E_q = -\nabla\Phi_q = -2B_0 \cdot \cos(\omega_q t - \phi_q) \cdot \begin{bmatrix} x \\ -y \\ 0 \end{bmatrix} \tag{2.36}$$

Add this term to equation 2.23:

$$\begin{bmatrix} \ddot{x} \\ \ddot{y} \\ \ddot{z} \end{bmatrix} - \begin{bmatrix} \left\{\frac{\omega_z^2}{2} - 2k_0 \cos(\omega_q t - \phi_q)\right\} x \\ \left\{\frac{\omega_z^2}{2} + 2k_0 \cos(\omega_q t - \phi_q)\right\} y \\ -\omega_z^2 z \end{bmatrix} - \omega_c \begin{bmatrix} \dot{y} \\ -\dot{x} \\ 0 \end{bmatrix} = 0 \tag{2.37}$$

with

$$k_0 = B_0 \cdot \frac{q}{m} \tag{2.38}$$

where ω_q is the applied RF frequency and ϕ_q is the initial phase of the applied frequency. Once again the axial motion remains unaffected and the equation of the radial motion can be solved:

$$\begin{bmatrix} x \\ y \end{bmatrix} = R_-(t) \begin{bmatrix} \cos(\omega_- t - \phi_-) \\ -\sin(\omega_- t - \phi_-) \end{bmatrix} + R_+(t) \begin{bmatrix} \cos(\omega_+ t - \phi_+) \\ \sin(\omega_+ t - \phi_+) \end{bmatrix} \tag{2.39}$$

However, $R_\pm(t)$ is a time-varying function. If the frequency of the RF is exactly equal to the sum of the frequencies of the radial motion ($\omega_q = \omega_+ + \omega_- = \omega_c$), the radial amplitudes are given [Kellerbauer2002] by:

$$R_\pm(t) = R_\pm(0)\cos(\frac{\omega_{conv}}{2}t) \mp R_\mp(0)\sin(\frac{\omega_{conv}}{2}t)\cos(\phi_q - \phi_+ - \phi_-) \tag{2.40}$$

where

$$\omega_{conv} = \frac{k_0}{2(\omega_+ - \omega_-)} \tag{2.41}$$

If the initial phase shift $(\phi_q - \phi_+ - \phi_-)$ equals to π, equation 2.40 becomes:

$$R_{\pm}(t) = R_{\pm}(0)\cos(\frac{\omega_{conv}}{2}t) \pm R_{\mp}(0)\sin(\frac{\omega_{conv}}{2}t) \tag{2.42}$$

Two radial motions are coupled by an excitation at the sum of their frequencies. A complete conversion can be obtained when the conversion time

$T_{conv} = \frac{\pi}{\omega_{conv}}, \frac{3\pi}{\omega_{conv}} \cdots \frac{(2n+1)\pi}{\omega_{conv}}$.

In the quadrupole excitation mode, the ion motions can be excited at the sum of the eigenfrequencies. During the CPTMS experiment, the quadrupole excitation at the frequency of $\omega_+ + \omega_-$ is used to determine the true cyclotron frequency ω_c.

2.4 Cooling technique In the Penning Trap

Cooling techniques are widely used in mass measurements. There are two functions of the cooling technique: 1) ***Cooling***: The energy of the ions is reduced by colliding with the buffer gas pumped into the trap. 2) ***Purification***: By applying a quadrupole excitation on the gas-filled Penning trap, we are able to concentrate the desired ions and remove the contaminants. The theory is described in the following.

In a gas-filled Penning trap, ions lose kinetic energy by colliding with the buffer gas. The average force on the particle can be expressed as:

$$F = -\delta \cdot \dot{r} \tag{2.43}$$

where the damping coefficient δ is given by [McDa1973] and is dependent on the ion species, gas pressure and gas temperature.

By adding this force to equation 2.23 in Cartesian coordinates, we get:

$$\begin{bmatrix} \ddot{x} \\ \ddot{y} \\ \ddot{z} \end{bmatrix} - \frac{\omega_z^2}{2} \begin{bmatrix} x \\ y \\ -2z \end{bmatrix} - \begin{bmatrix} \omega_c \dot{y} - \frac{\delta}{m}\dot{x} \\ -\omega_c \dot{x} - \frac{\delta}{m}\dot{y} \\ -\frac{\delta}{m}\dot{z} \end{bmatrix} = 0 \tag{2.44}$$

The axial motion (z-direction) is simply damped harmonic oscillation and the solution can be expressed as:

$$z = A_z e^{-(\delta/2m)t} \cos(\omega_z' t - \phi_z) \tag{2.45}$$

with

$$\omega_z' = \sqrt{\omega_z^2 - (\frac{\delta}{2m})^2} \tag{2.46}$$

The solution for the radial part of the equation of motion (x-y plane) in Cartesian coordinates is given by [Kellerbauer2002] as:

$$\begin{bmatrix} x \\ y \end{bmatrix} = R_- e^{\alpha_- t} \begin{bmatrix} \cos(\omega_- t - \phi_-) \\ -\sin(\omega_- t - \phi_-) \end{bmatrix} + R_+ e^{\alpha_+ t} \begin{bmatrix} \cos(\omega_+' t - \phi_+) \\ \sin(\omega_+' t - \phi_+) \end{bmatrix} \tag{2.47}$$

where

$$\begin{aligned} \omega_\pm' &= \omega_\pm \pm \Delta\omega \\ \Delta\omega &= \frac{1}{16} \cdot (\frac{\delta}{m})^2 \cdot \frac{8\omega_z^2 + (\frac{\delta}{m})^2}{(\omega_c^2 - 2\omega_z^2)^{3/2}} \end{aligned} \tag{2.48}$$

and the time constant $\alpha_\pm$ is:

$$\alpha_\pm = -\frac{\delta}{2m}\left\{1 \pm \left(1 + \frac{1}{8} \cdot \frac{8\omega_z^2 + (\frac{\delta}{m})^2}{\omega_c^2 - 2\omega_z^2}\right)\right\} \tag{2.49}$$

Compared with the undamped ion motion, two eigenfrequencies (ω_+ and ω_-) shift up and down respectively by a very small amount ($\Delta\omega$). However, their sum still remains the same as the true cyclotron frequency ω_c, which depends only on the mass of trapped ions and the magnetic field. The change of the radius of the ion motion depends on the time constant $\alpha_\pm$. For the modified cyclotron motion, $\alpha_+ \approx -\delta/m$, the radius decreases in the gas-filled Penning trap. For the magnetron motion, $\alpha_- \approx (\delta/2m)\cdot(\omega_z/\omega_c)^2$, the radius increases in the trap. Since $|\alpha_+| << |\alpha_-|$, the radius of modified cyclotron motion decreases much faster than the radius of magnetron motion increases.

As described above, the radius of the magnetron motion keeps increasing in a gas-filled Penning trap. Eventually, all the ions will be lost at the electrode. However, if we apply a quadrupole excitation at the true cyclotron frequency $\omega_c = \omega_+ + \omega_-$ to the Penning trap, magnetron motion will be converted into modified cyclotron motion whose radius decreases through collisions with the buffer gas. Hence the ions will be cooled and centred [Savard1991].

Note that, because the true cyclotron frequency depends on the mass of the ions, this technique can be used for mass selection. The desired ions will be centred while the contaminants can be removed. In the CPTMS system, the Isobar Separator is the example equipment using such cooling technique.

2.5 Detection of resonance Using Time of Flight (TOF) Technique

The Time of Flight (TOF) technique provides a way to determine the true cyclotron frequency ω_c, which depends only on the magnetic field and the mass of the

trapped ion. This method was first applied to the precision mass measurements by Graff in 1980 [Graf1980].

In the CPTMS experiments, ions are initially trapped near the centre of the Penning trap with a very small radius. A dipole excitation at the magnetron (ω_-) frequency is applied first to establish the radius of the initial orbit. When ions reach a small magnetron orbit, a quadrupole RF excitation is then applied with the duration time of $T_{RF} = T_{conv} = \pi / \omega_{conv}$ (refer to equation 2.42). If the applied frequency corresponds to the resonance frequency ($\omega_q = \omega_c$), the magnetron motion will be completely converted into modified cyclotron motion. The energy gain, ΔE_r , during this process can be expressed as [Bollen1996]:

$$\Delta E_r = \frac{m}{2}(\omega_+^2 - \omega_-^2) \cdot (R_{-,0}^2 - R_{+,0}^2) \tag{2.50}$$

where $R_{-,0}$ and $R_{+,0}$ are the radii of the magnetron motion and cyclotron motion respectively at the beginning of the excitation. Larger $R_{-,0}$ and smaller $R_{+,0}$ will make a bigger energy gain ΔE_r , which is used to detect the cyclotron resonance. The energy gained at the excitation frequencies that are not equal to ω_c is given by [Koni1995] as:

$$E_r(\omega_q) = \frac{q^2 V_d^2}{2mr^4} \cdot \frac{\omega_+^2}{(\omega_+ - \omega_-)^2} \cdot \frac{\sin^2(\omega_b T_{RF})}{\omega_b^2} \tag{2.51}$$

with

$$\omega_b = \frac{1}{2}\sqrt{(\omega_c - \omega_q)^2 + \left(\frac{\pi}{T_{conv}}\right)^2} \tag{2.52}$$

where V_d is the amplitude of the potential of the driving azimuthal quadrupole field at radius r, and ω_q is applied frequency. Since $E_r \propto \frac{\sin^2(\omega_b T_{RF})}{\omega_b^2}$, the energy gain relative to the resonance can be plotted as in figure 2.9:

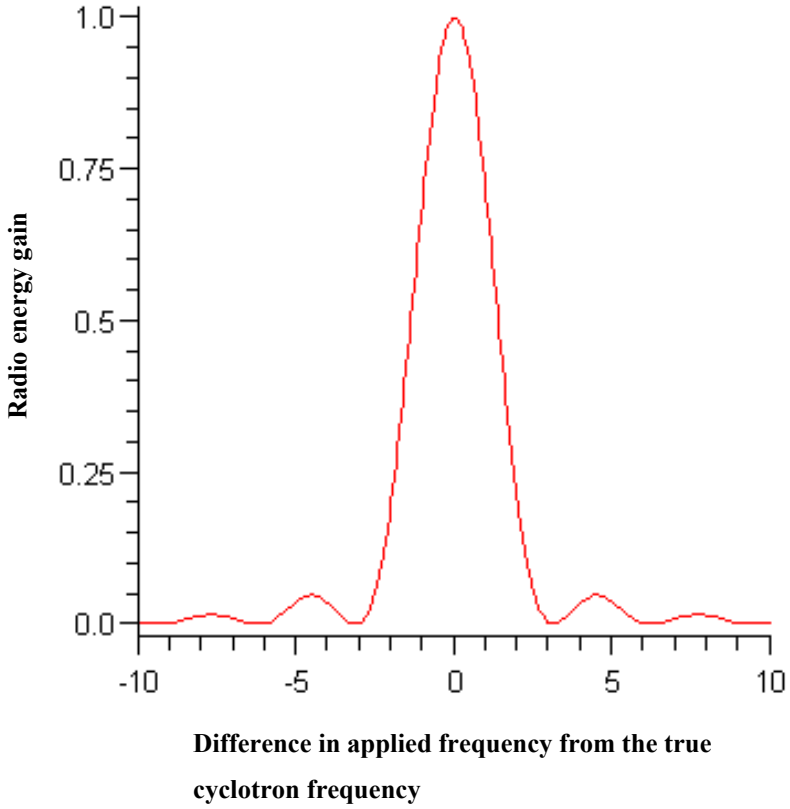

FIG. 2.9. The plot of the energy gain is shown in the condition that a complete conversion from a pure magnetron motion to a modified cyclotron motion is obtained.

One way to detect this energy gain is to eject the ions from the Penning trap and allow them to drift into a region of non-uniform magnetic field. Then, the cyclotron energy will be converted to axial kinetic energy due to the interaction with the gradient of the magnetic field. The axial force can be expressed as following:

$$F = -\mu(\nabla B) = -\frac{E_r}{B} \cdot \frac{\partial B}{\partial z}\hat{z} \tag{2.53}$$

The effect of the magnetic field gradient on the ion motion is also shown schematically in figure 2.10:

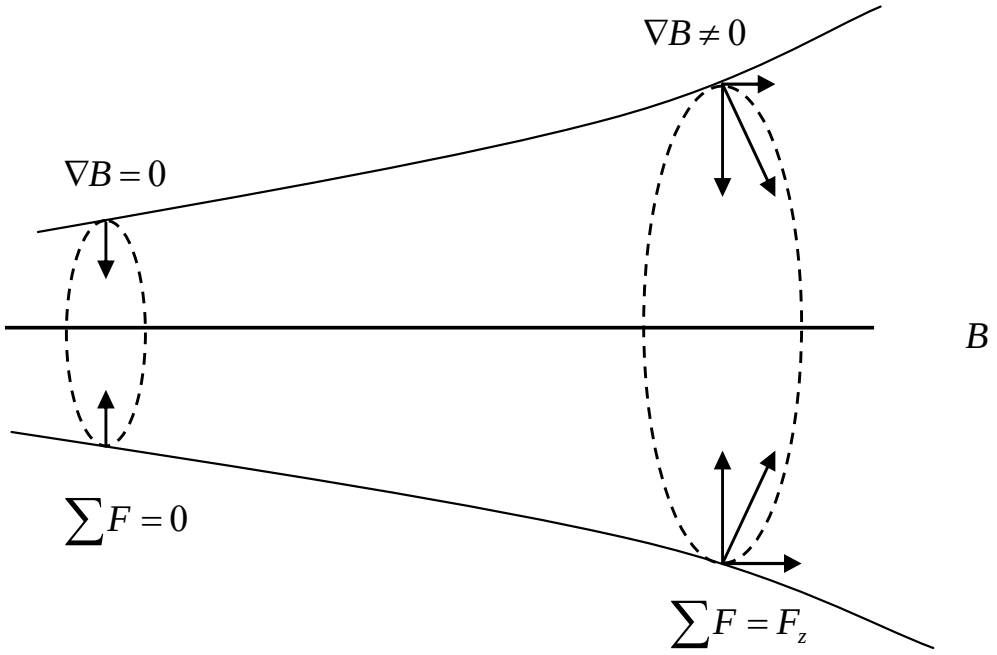

FIG. 2.10. Conversion of cyclotron energy to axial energy

Therefore, the axial energy is increased if the cyclotron radial energy is gained during resonance. At the resonant frequency, the ions gain the most energy, hence fly with the shortest time of flight. By repeating the excitation/ejection process over a range of frequencies, a time-of-flight versus frequency spectrum is obtained. Resonance at the true cyclotron frequency of the ions is observed as reduction in the time of flight of the ions. Figure 2.11 is an example of the time of flight spectrum. It comes from the ^{108}Ru mass measurement. The horizontal axis represents the 23 sweeping frequencies and the vertical axis is the average time of flight in microseconds.

^{108}Ru

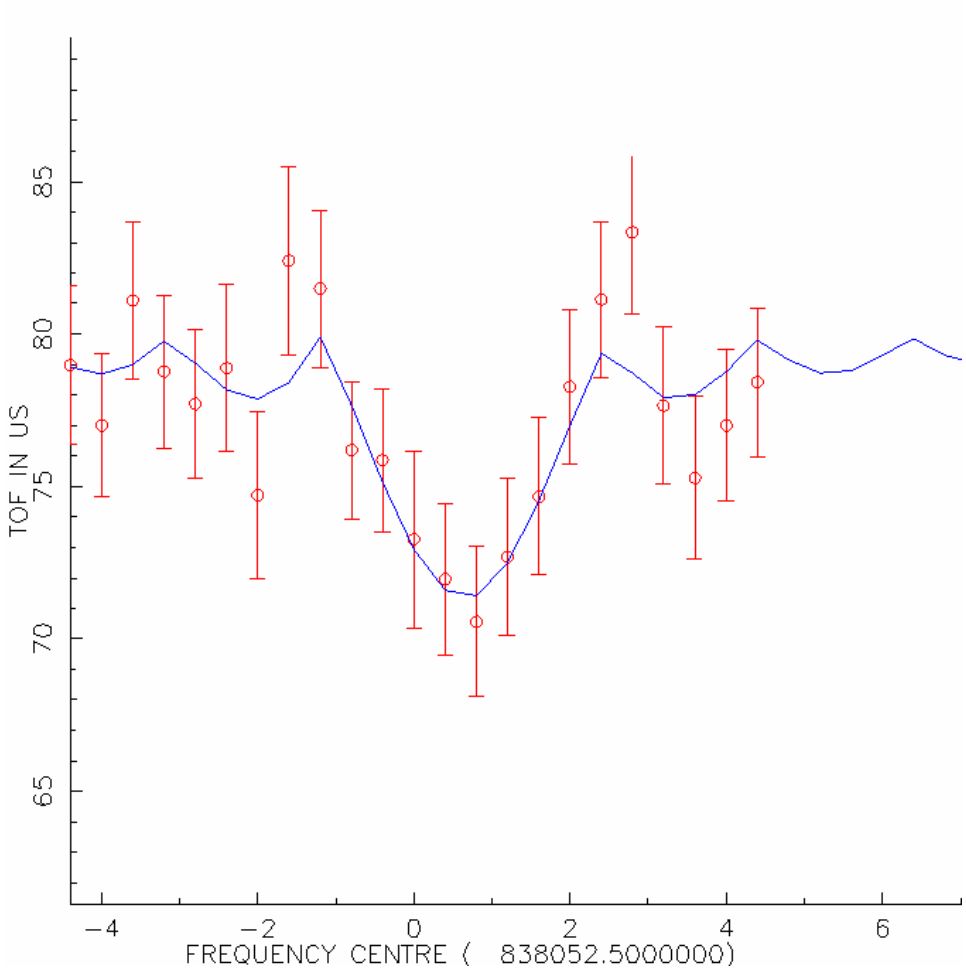

FIG. 2.11. The time of flight spectrum for ^{108}Ru mass measurement

Chapter 3

The Canadian Penning Trap Mass Spectrometer System

The Canadian Penning Trap Mass Spectrometer (CPTMS) system is located at the ATLAS (Argonne Tandem Linear Accelerator System) facility of Argonne National Laboratory. It is an ideal apparatus to carry out precise mass measurements for radioactive nuclides obtained from nuclear reactions [Clark2004]. In 2004, the APT (Advanced Penning Trap) system was successfully installed and shares the ion injection and production system with the CPTMS through a quadrupole deflector. This chapter presents an overview of the whole CPTMS system and provides details on each part of the apparatus.

3.2 General Experiment Set-Up

In general, six essential components were used in the mass measurements on neutron rich nuclei (refer to the figure 3.1). First, fission fragments produced from the ^{252}Cf fission source stop in the ***Gas Cell*** filled with the pure Helium gas and are

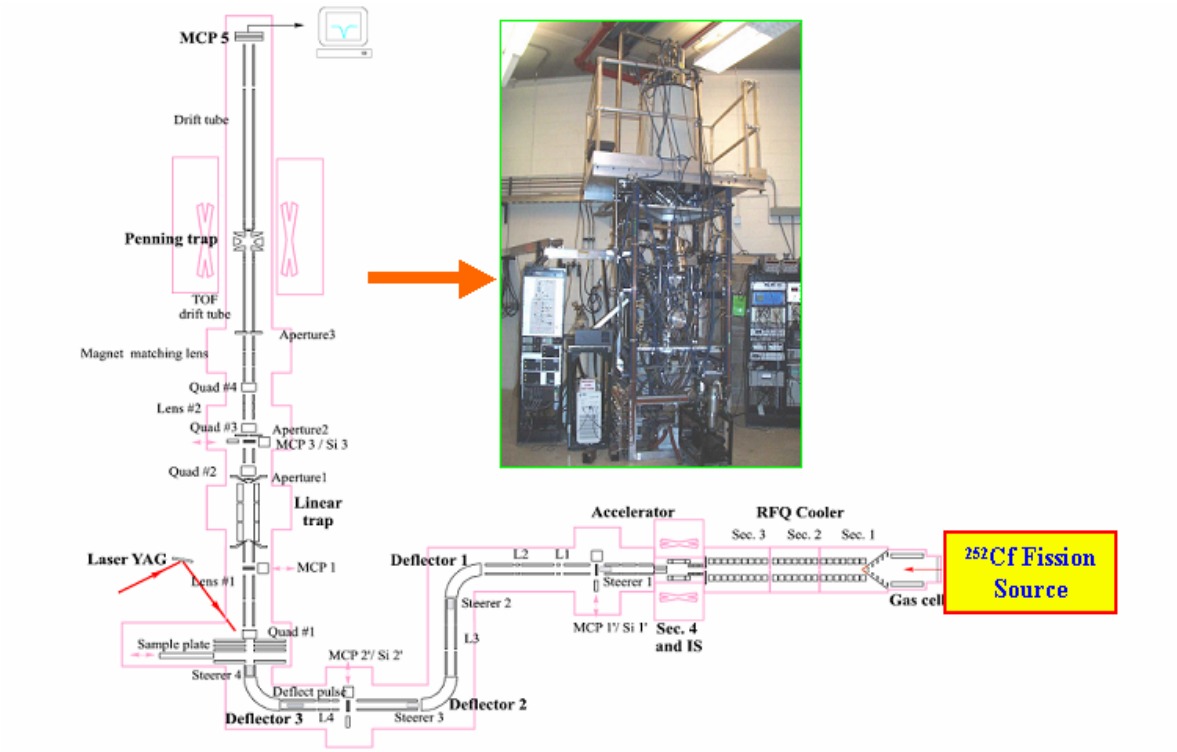

FIG. 3.1. Overview of the CPTMS system used for the fission fragment mass measurements.

guided to the exit nozzle of cell by gas flow and radio frequency (RF) and DC electric fields [Savard2003]. Due to the interaction with the buffer gas, the fission fragments predominantly emerge as singly or doubly charged particles when they are extracted out of the gas cell. Second, the ***RFQ cooler*** is used as an ion guide and a mass filter [Boudreau2001]. The ions from the gas cell are captured here and ejected as ion bunches with the rate of 2Hz -20 Hz into the isobar separator, which is the next essential part. Third, a quadrupole RF excitation of several hundred millisecond duration time is applied to the ions in the ***Isobar Separator*** to separate the contaminant molecules and the desired isotopes using the cooling Penning trap described in chapter 2.4. The ions are then

ejected from the isobar separator and travel to the RFQ trap. Fourth, a voltage pulse (so called ***Deflection Pulse***), applied to one of the electrodes along the beam transport line, is used to further select the desired ions by removing the lighter ones and heavier ones based on the time of flight information of those ions. Fifth, the ***RFQ linear trap*** is used to accumulate several bunches of ions and cool the ions prior to injection into the precision Penning trap [Clark2003]. Finally the bunched ions are delivered to the precision ***Penning trap*** to make precise mass measurements using the time of flight (TOF) method. Ion detectors are installed at various points along the whole system to monitor the number of the ions arriving at different positions.

Throughout the mass measurement, a suitable molecule is used as the calibration. For the ^{109}Ru mass measurement as an example. The molecule $^{12}C_8{}^{1}H_{13}$, which has the same nominal mass unit as ^{109}Ru, is used as a calibration. It is much easier to detect the hydrocarbon molecular ions than that of the activities because the number of such ions is hundreds of times more than the activity, ^{109}Ru, ions during the measurement. By detecting the number of the $^{12}C_8{}^{1}H_{13}$ ions, we can adjust the value of the DC voltages, capture/ejection pulses, RF frequencies, and gas pressures for the purpose of transferring more ions to the RFQ trap. Then, the adjusted value is used to calculate the proper value for the isotope ^{109}Ru. By applying the proper value on the system, we are able to bring more desired ions (isotope ^{109}Ru) to the RFQ trap. Finally, the molecule $^{12}C_8{}^{1}H_{13}$ is removed by the isobar separator and the precision Penning trap.

3.3 Overview of CPTMS System

The whole CPTMS system can be considered as a composition of four systems: ***the mechanical system***, ***the electronic system***, ***the vacuum system*** and ***the acquisition/control system***. Precise mass measurements can only be made if all of the four systems work properly. A description of these four systems is given below.

3.3.1 The Mechanical System

The mechanical system consists of the Aluminum frames, the vacuum chambers, the super-conducting magnet, the magnet for the isobar separator, the ion detectors (Silicon detectors and Micro-Channel Plate detectors) and series of the electronic devices such as the gas cell, the RFQ cooler, the isobar separator, the RFQ linear trap, the Penning trap and beam transport elements (steerers, lenses and drift tubes). Most of the electrodes are made of stainless steel to avoid oxidization and to stand the high vacuum. The parts inside the bore of the super-conducting magnet are made of oxygen-free copper in order to reduce magnetic effects. The vacuum chamber is made of molybdenum (Mo), which has material with low magnetic susceptibility. The chambers and the electronic devices are thoroughly cleaned by electro-polishing and appropriate etching and outgassed before assembling together. Another important component in the Mechanical System is the super-conducting magnet. In CPTMS, it is located on a 4-meter high platform as seen on the following picture:

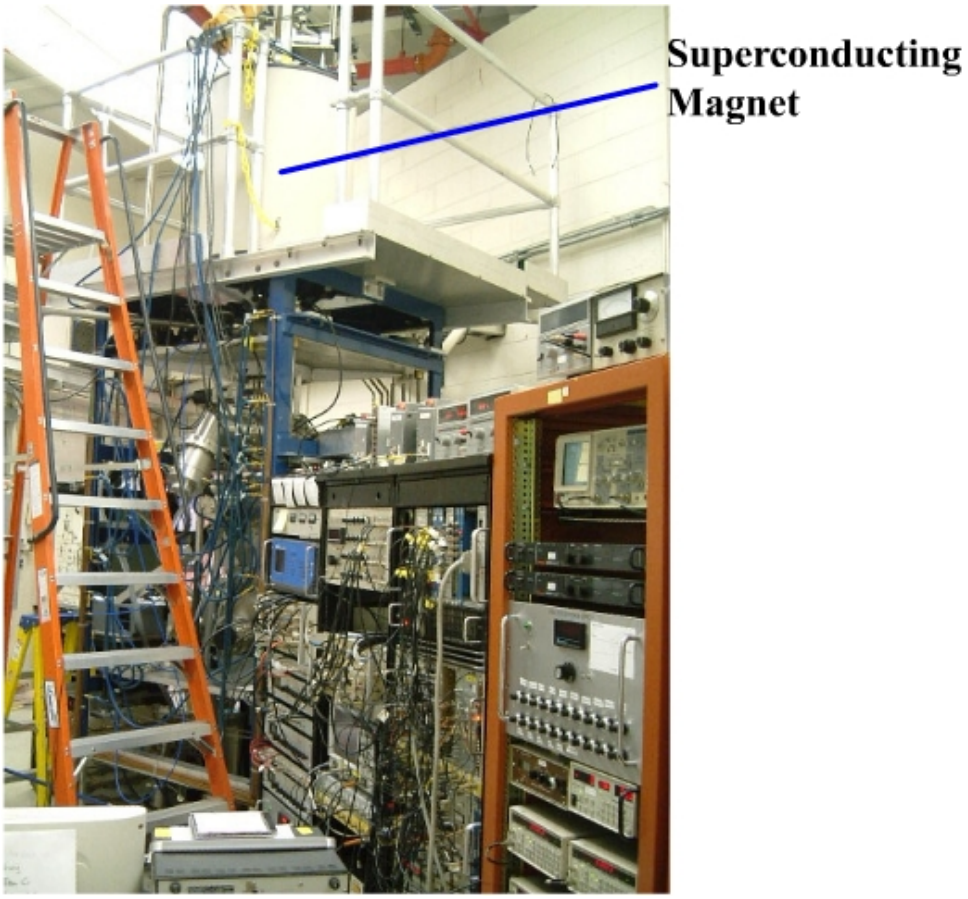

FIG. 3.2. The photo of the CPTMS in the laboratory, the 5.9T super-conducting magnet is indicated.

The super-conducting magnet is designed to produce a highly homogeneous 5.9T magnetic field over a volume of one cubic centimeter. A schematic diagram is shown in the figure 3.3 on the next page. The Penning trap is located in the center of the magnet. The magnet is made of super-conducting coils, surrounded by liquid helium and liquid nitrogen as shown on the following figure:

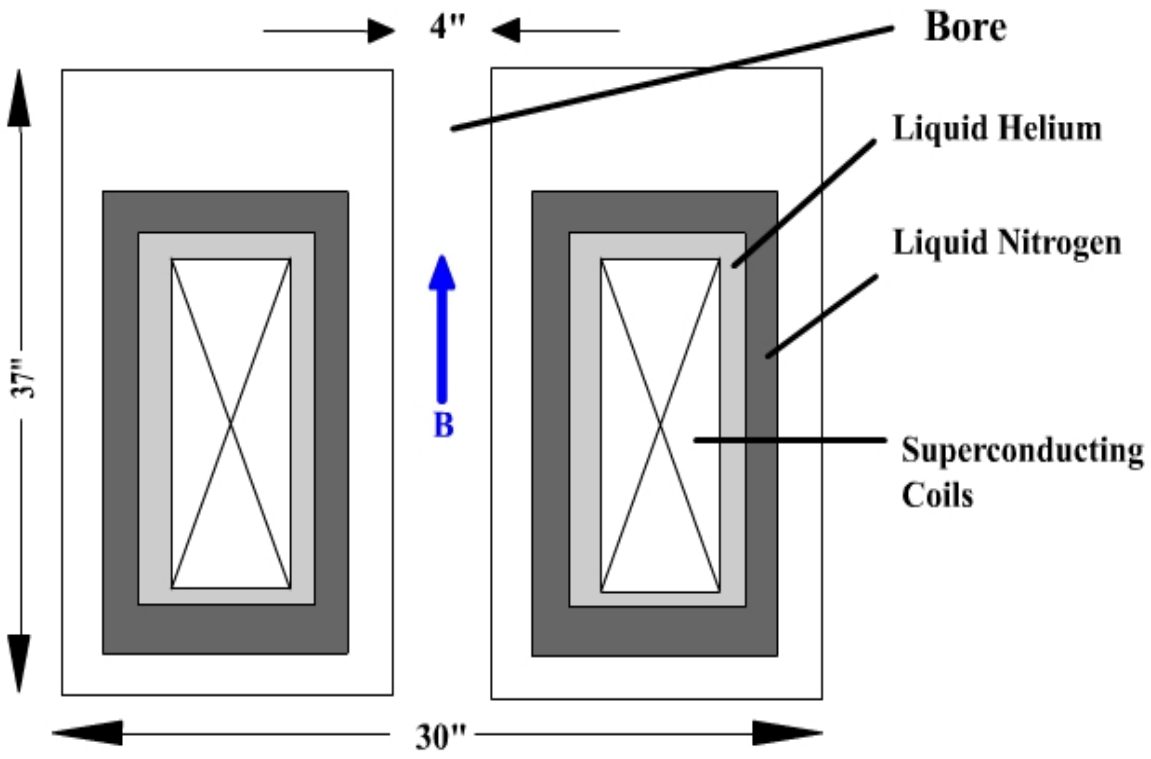

FIG. 3.3. The schematic diagram of super-conducting magnet, it is 93.98cm tall with a hollow bore of 10.16cm diameter. The super-conducting coil is sitting in a liquid Helium tank, which is surrounded by the liquid Nitrogen.

3.3.2 The Electronic System

The electronic system provides all the voltages needed to operate the CPTMS system. It includes:

1) ***The high power supplies*** LeCroy (model 1454) and C.A.E.N (model SY2527) providing DC voltages on most of the electrodes. They can be programmed to ramp voltages on all its outputs at the desired rate up to the final settings. The drift tube potential (floating voltage) of the whole system is provided by these two power supplies.

2) ***The high precision DC power supply*** (Kenwood PD56-AD) provides highly stable DC voltages to the part of a millivolt for the Penning trap.

3) ***The DC power supplies***, they provide one to two hundred volts, which is applied on the beam transport elements (steerers and lenses) to bend or focus the beam.

4) ***The pulse boxes*** are used to provide all kinds of capture/ejection pulses on the electrodes;

5) ***The synthesized function generators*** (Stanford Research System DS345 and DS340) offering RF (radio frequency) up to 30.2MHz for the ion traps with the resolution of 1 μHz. For the gas cooler and the RFQ trap, a few hundreds volts RF is applied through an amplifier. For the Penning trap, millivolts need to be used; hence the output of the function generator is sent through an attenuator.

The mechanical system and electronic system work together creating the electric fields and the magnetic fields needed for transferring, confining and exciting the ions.

3.3.3 The Vacuum System

The vacuum system consists of series of the pumps providing the required vacuum for the whole CPTMS system. The vacuum system has three major roles:

1) To provide a vacuum environment for the whole system to transfer the ions
2) To offer a high vacuum for the Penning trap to make precise mass measurements
3) To create the gas flow inside the gas cell

Four types of pumps are used in our experiments: ***the turbo-molecular pump***, ***the mechanical pump***, ***the cryogenic pump*** and ***the helical grooved pump***. On the "cooler and gas cell" side, six turbo-molecular pumps (TP1 to TP6) backed up by three mechanical pumps (P1 to P3), and a helical grooved pump (P4), are used to pump the Helium gas introduced into the cooler and gas cell (Refer to fig 3.4). The gas cooler consists of three sections (the section 1 to section 3). A small nozzle separates each of the sections. As shown in the figure 3.4 on the next page, section 1 is connected to TP5 and TP6 backed up by P4; section 2 is connected to TP4 backed up by P3, and section 3 and the transfer line are connected to TP1 and TP2 backed up by P1. A differential pumping system is formed and the pressures are controlled by the speed of the turbo-molecular pumps and the nozzles between them. The values of the pressures used by CPTMS system are shown on the table 3.1.

GAS COOLER (T)		**CPTMS SIDE (T)**	
Cooler Section 1	5.4×10^{-1}	RFQ Trap	2.5×10^{-6}
Cooler Section 2	2.2×10^{-1}	Lens Chamber	2.0×10^{-8}
Cooler Section 3	1.1×10^{-4}	Cryo Chamber	8.4×10^{-9}
Transfer Line	1.0×10^{-7}		

Table 3.1. Typical Pressure readings in the CPTMS system

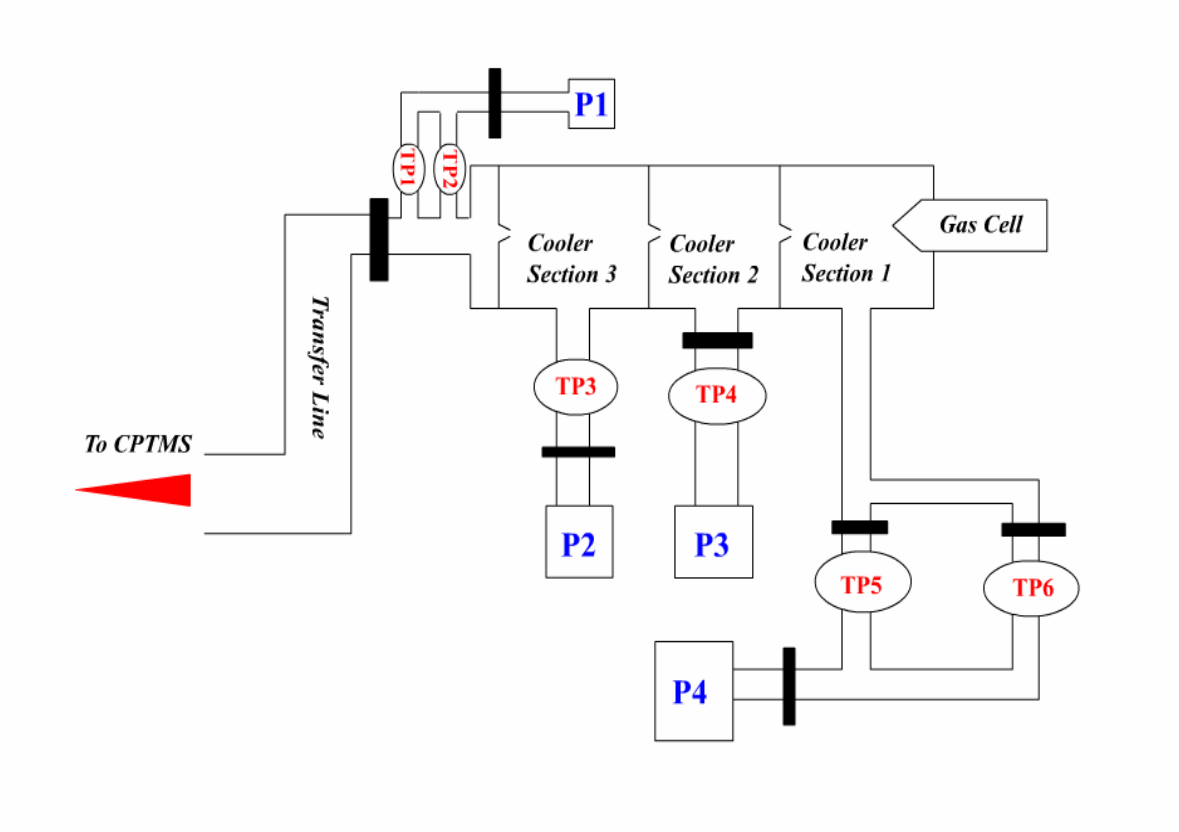

FIG. 3.4. The schematic shows the locations of the pumps used to control the pressure of the gas cooler and gas cell. There are six turbo-molecular pumps (TP1 to TP6) labeled in red and four mechanical roughing pumps (P1 to P4) labeled in blue. The black solid squares indicate the valves.

On the CPTMS side, there are five turbo-molecular pumps (TP0 to TP4), and a cryogenic pump (CP1) (see figure 3.5). Those pumps are backed by four mechanical roughing pumps (P1 to P4). TP0 and TP1 pump on the Ionization Chamber, TP2 pumps on the RFQ trap and TP3 pumps on the Lens Chamber. High vacuum (10^{-9} Torr) is needed in the Penning trap region as indicated in table 3.1. Therefore a cryogenic pump (CP1) and a turbo-molecular pump (TP4) are employed to pump down the bore of the magnet.

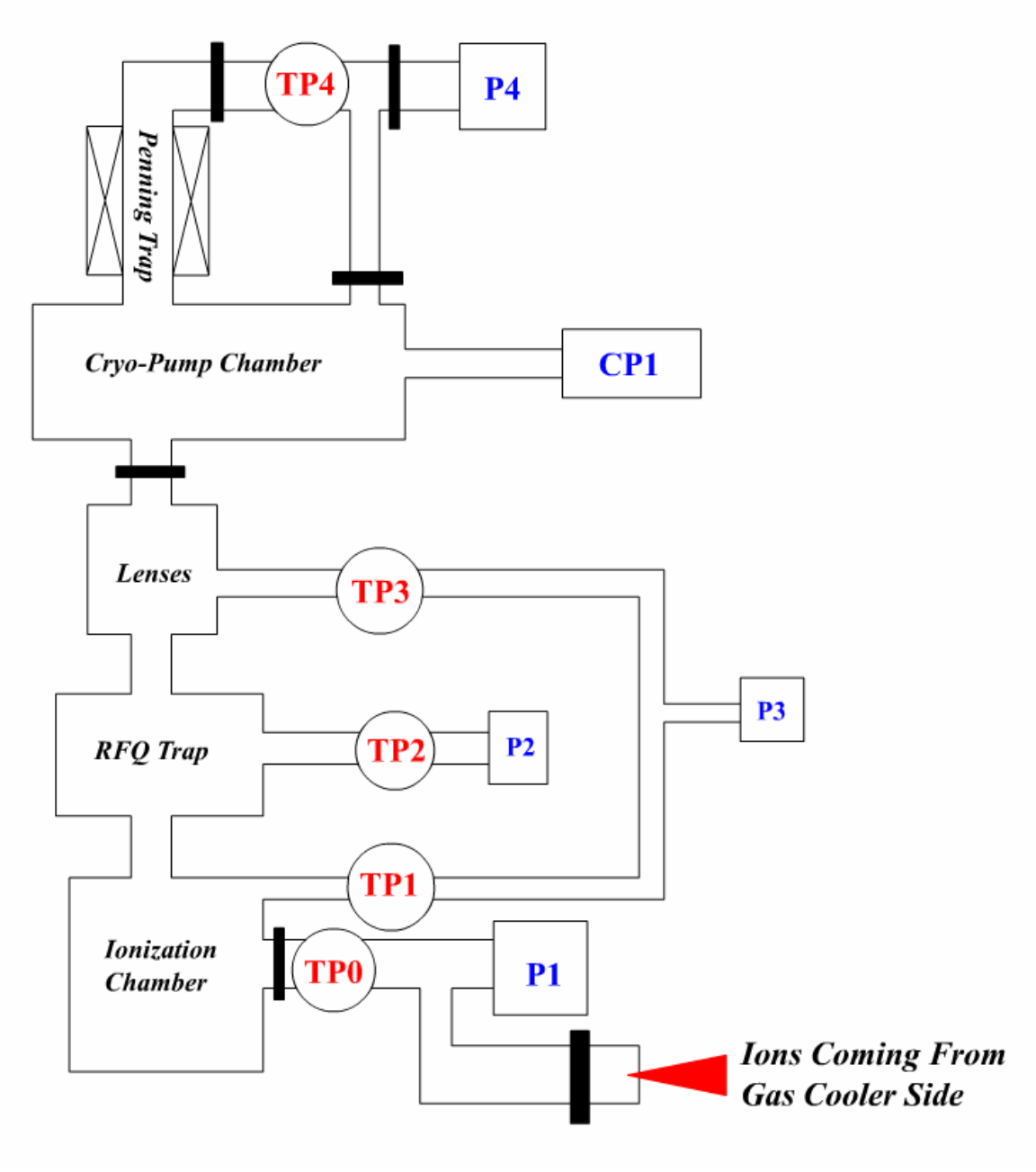

FIG. 3.5. The schematic shows the locations of the pumps used to control the pressure of the CPTMS. There are five turbo-molecular pumps (TP0 to TP4) and one cryogenic pump labeled in red, and four mechanical roughing pumps (P1 to P4) labeled in blue. The black solid squares indicate the valves.

3.3.4 The Data Acquisition and Control System

The data acquisition and control system is formed by a CAMAC (Computer Automated Measurement And Control) crate controlled by a computer through a SCSI (Small Computer Systems Interface) bus. The main task of the data acquisition system is to

1) Control the sequence and the timing for a measurement with the CPTMS system
2) Manage the excitation frequencies in the Penning trap
3) Acquire, store, display and analyze the data from the measurements.

During a mass measurement, there are four places where the ions stop. In the order along the ion path, they are: the Gas Cooler, the Isobar Separator, the RFQ trap and the Penning trap. In order to transfer the ions from the cooler to the Penning trap efficiently, the timing of the capture and ejection pulses has to be matched with each other. The logic timing settings are shown in figure 3.6. The Gas Cooler ejects the ion bunches with rate of 2Hz. The cooler ejection pulse triggers the Isobar Separator (IS) capture pulse; therefore each ion bunch is captured by the IS. The ions stay in the IS for a period of time, which is necessary to achieve separation, then ejected to the RFQ trap. On the way to the RFQ trap, ions are further selected by a $0.6\mu s$ wide deflection pulse. The RFQ trap cools the captured ions with He buffer gas and transfers them as a bunch to the Penning trap. The RFQ trap ejection rate is about 1Hz. The RFQ trap ejection pulse triggers the capture pulse on the Penning trap. When the ions are captured in the Penning trap, a dipole excitation ω_+ is applied first by the arbitrary function generator for about 100ms to remove the contaminant ions. Then, another dipole excitation ω_- is applied by

the generator for about 40ms to drive the desired ions to a certain orbit. Finally, a quadrupole excitation ω_C is employed for about 500ms to convert the ω_- motion into the ω_+ motion (refer to Chapter2 for detail). Totally, in about 640ms, the Penning trap will eject the ions to the last Micro-Channel Plate (MCP5) detector (refer to section 3.5). The multi-channel scaler (MCS) reads the number of counts on the MCP5 and combines them to obtain a time of flight (TOF) spectrum. Then the computer reads the spectra, records the raw data to the disk, and displays the spectra to the operator. At the same time, the computer sends a signal saying that the Penning trap is ready for the next capture. All the timing information is set up by the acquisition computer except the gas cooler and RFQ ejection rate, which is determined based on the number of ions we need for the mass measurements.

When a bunch of ions exit from the gas cooler system, isobar separator, or the RFQ trap, they eject with the same charge state q and roughly the same energy because of the cooling effect of the Helium buffer gas. The ions gain the same kinetic energy (E) from one position to the other in the transport system. For instance, if the distance between two position is d, the time of flight of two masses are t_1 and t_2 respectively, then the energy gain can be expressed as:

$$E = \frac{1}{2} m_1 \left(\frac{d}{t_1} \right)^2 = \frac{1}{2} m_2 \left(\frac{d}{t_2} \right)^2 \tag{3.1}$$

Based on equation 3.1, the time of flight of the ions depend on the masses:

$$\frac{m_1}{m_2} = \frac{t_1^2}{t_2^2} \tag{3.2}$$

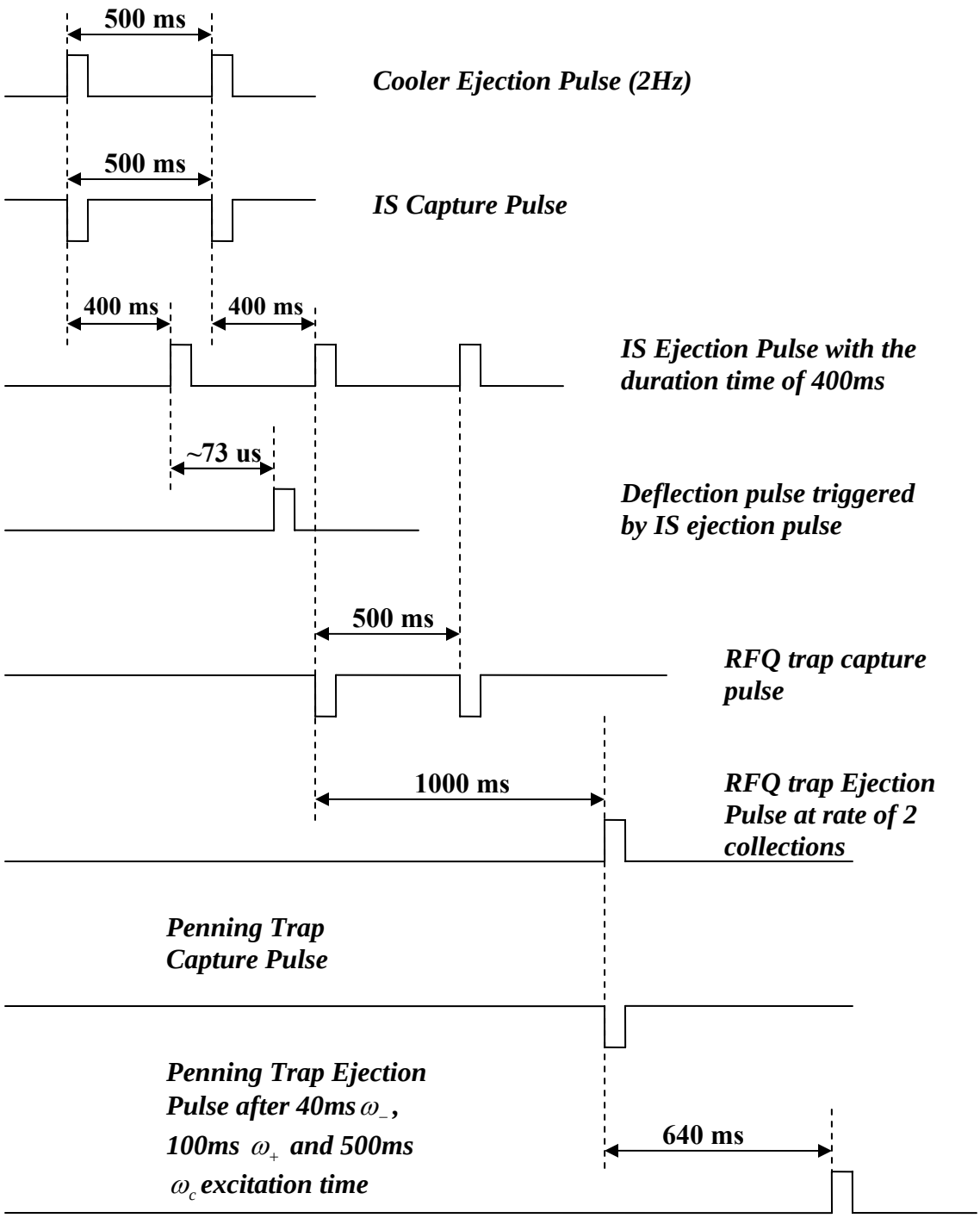

FIG. 3.6. The Typical Time sequence of the fission fragment mass measurement.

3.4 Details of the CPTMS System

3.4.1 The Ion Source

The ion source used for the mass measurements on neutron rich nuclei is a 45 μCi ^{252}Cf fission source, which produces about 1.7×10^{6} nuclear decays per second. 97% of the nuclear decays from ^{252}Cf are α decay and 3% of them are spontaneous fission. Therefore this fission source is expected to provide about 50,000 fission decays per second. Since the source is installed in front of the gas cell, less than 50% of the decays can actually enter the gas cell. The gas cell therefore is expected to capture a maximum of 25,000 fission decays per second. The following graph shows the production yield from a ^{252}Cf fission source [England1993].

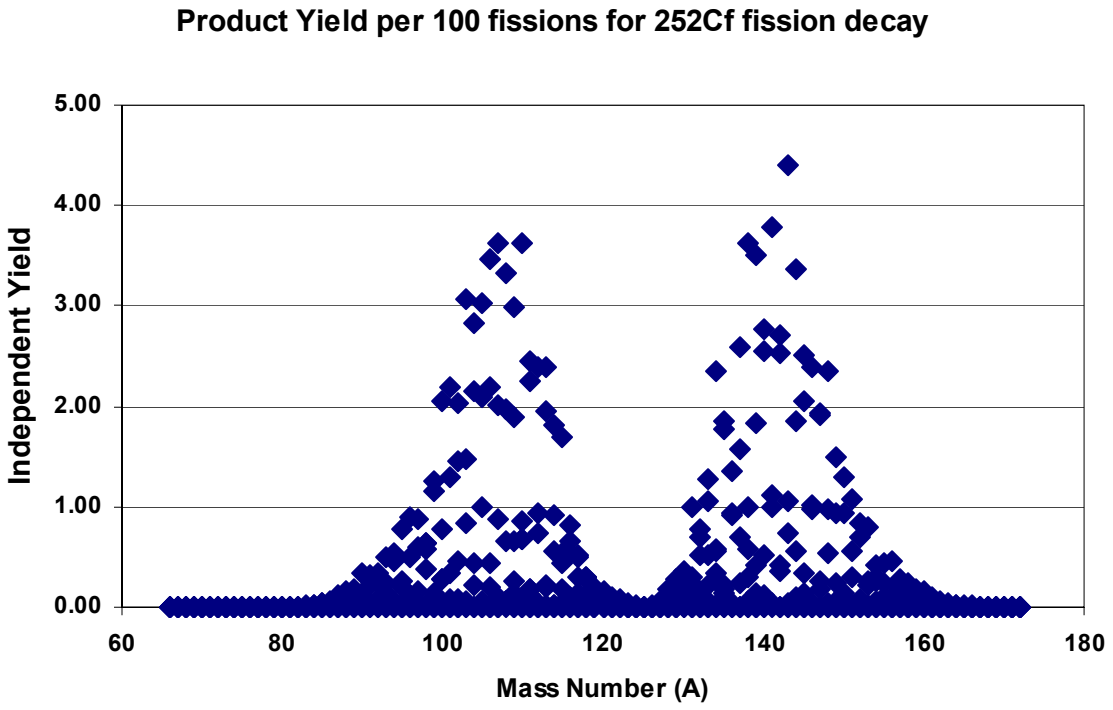

FIG. 3.7. The independent yield per 100 fissions produced from ^{252}Cf spontaneous fission decay as a function of mass number [England1993].

The reference [England1993] gives two different types of product yields: independent yields and cumulative yields. The independent yield is the production rate of the decays directly from the fissions. The cumulative yields include both the independent yields and the chain yields. The independent yield is considered in these measurements because the ions can only stay in the gas cell for less than 10ms before they are removed by the gas flow. Only independent yields can actually be detected. As shown in figure 3.7, the fission of ^{252}Cf is asymmetric. There are two fragment peaks on the figure. The lighter one around mass 110, is called the light fission fragment and the heavier one around mass 140, is called the heavy fission fragment. This thesis concentrates on the mass measurements of the lighter fission fragment, especially the nuclei with the atomic number close to 110.

3.4.2 The Gas Cell

The gas cell developed at Argonne National Lab [Savard2003] has proved to be ideal for stopping the high-energy ions. Ions with low energy spread are required for the Penning trap to make precise mass measurement. Before entering the gas cell, the fission fragment pass through a degrader to lower their energy from an initial value of ~100MeV. Each ion entering the gas cell has about 3MeV on average. The gas cell further reduces the energy spread to less than 1eV by thermalizing the incoming ions with the high purity helium buffer gas provided by the gas cylinders. The purity of the helium gas from the cylinder is 99.995%. In order to further reduce that 0.005% contaminant, a commercial purifier (made by SAES, model PS4MT3R1) and liquid nitrogen cooled “cold trap” are installed along the stainless steel gas line to purify the gas flow. The turbo-molecular

pumps continuously pump out the Helium gas in section 1 (refer to figure 3.4) creating the gas flow moving forward to the exit nozzle of the cell (refer to figure 3.9 B). The gas pressure inside the gas cell ranges from 100 to 150 Torr. By colliding with the helium gas, most of the multi-charged ions are transformed to singly or doubly charged ions. The detail structure of the gas cell is shown in figure 3.8.

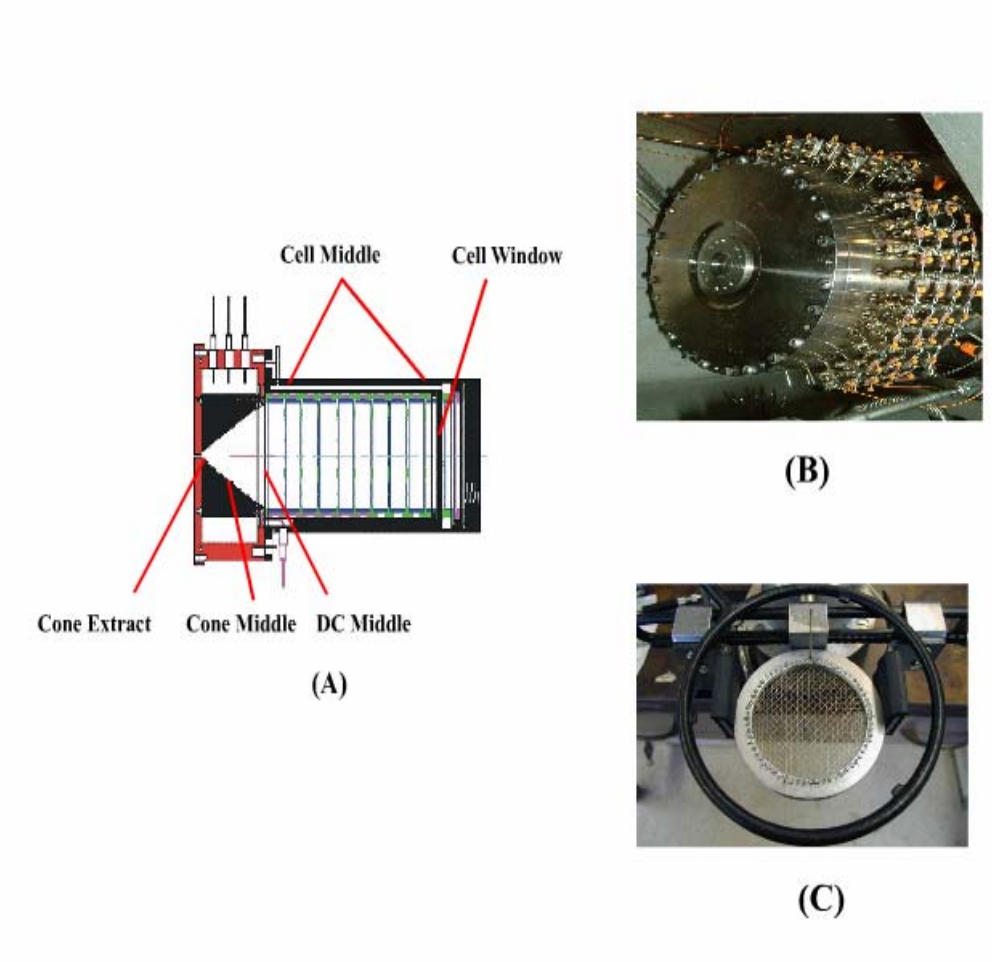

FIG. 3.8. (A) The structure of the gas cell; the labels indicate the places where the DC voltages are applied; the voltage values are given in the table 3.2. (B) The photo of the gas cell (C) The photo of the HAVAR window installed at the entrance of the gas cell.

As shown in figure 3.8 A, the gas cell consists of five parts: cell window, cell middle, DC middle, cone middle and cone extract. It has an inner diameter of 80mm and a length of 250 mm. The entrance of the gas cell (cell window) is a 1.9-mg/cm^2 thick HAVAR window as shown on the figure 3.8 C. It is made of the metal alloy wires frame covering 10% of the surface. Therefore the ion transmission efficiency of the cell window is 90%. In order to prevent the desired ions from neutralizing and forming molecules, DC voltages are applied on the five parts of the gas cell to guide the ions to the 1.3 mm diameter exit nozzle quickly, refer to the figure 3.9 A. The DC voltages applied on the gas cell forms a gradient to allow the ions move toward to the exit. The typical DC voltage settings are given on table 3.2. The gas flow and the gradient DC potential combine together to move the ions quickly to the exit.

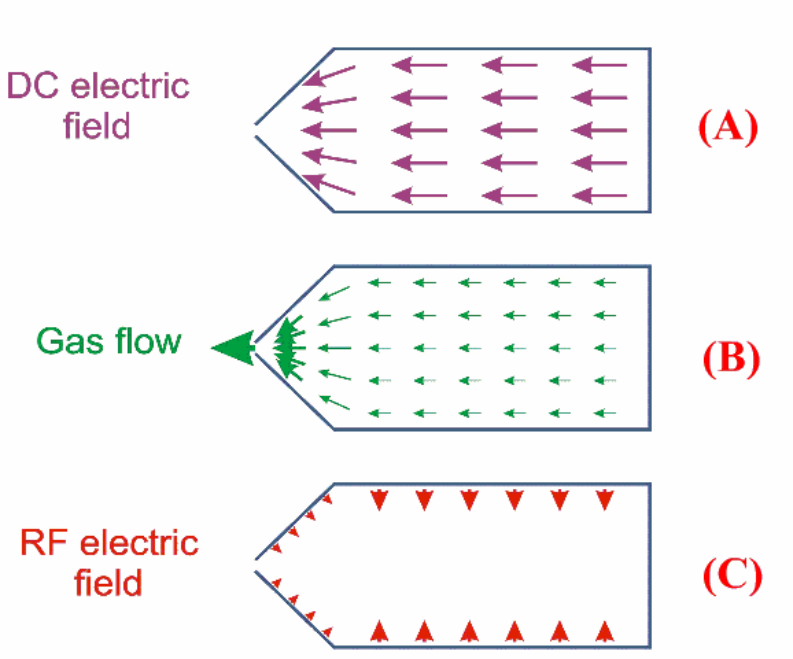

FIG. 3.9. The schematic shows how the gas cell guides and bunches the ions. (A) The DC voltage form a gradient to allow the ions moving forward; (B) The gas flow is created toward the exit of the gas cell; (C) The RF potential keeps the ions from hitting the electrode wall and increases the transferring efficiency.

Cell window	Cell middle	DC Middle	Cone middle	Cone extract	RF cone
170V	71V	56.06V	50.95V	9.05V	826KHz, 0.2Vpp

Table 3.2. This table shows the typical DC voltage settings applied on the gas cell. Also the RF frequency and amplitude applied on the gas cell cone are given.

The RF potential (the value is shown in table 3.2) applied on the gas cell keeps the ions away from the walls of the cell and therefore increases the transmission efficiency (refer to Appendix I for the mass measurement terms). As shown in figure 3.9, the combination of the gas flow, the gradient DC potential, and the RF potential allow the ions move and extract quickly and efficiently in the gas cell. The typical efficiency of the gas cell is about 30%-40%.

3.4.3 The Gas Cooler System

The gas cooler system is installed right after the gas cell along the beam transport line as shown on the figure 3.10. The main function of the gas cooler system is to remove the residual gas from the ion bunch and guide the ions to the isobar separator. The gas cooler system consists of three sections: section 1, section 2 and section 3. Each section is made of four segmented rods in order to produce the quadrupole field. There are 8 segments on each rod of section 1, 10 segments on each rod of section 2 and 25 segments on each rod of section 3. The three sections are connected by nozzles. “N1-2” indicates the nozzle between section 1 and section 2. “N2-3” indicates the nozzle between section 2 and section 3. The “last nozzle” is the exit nozzle at the end of the gas cooler system. A

differential pumping system is used to pump down each section of the gas cooler. See the previous section for details on vacuum system.

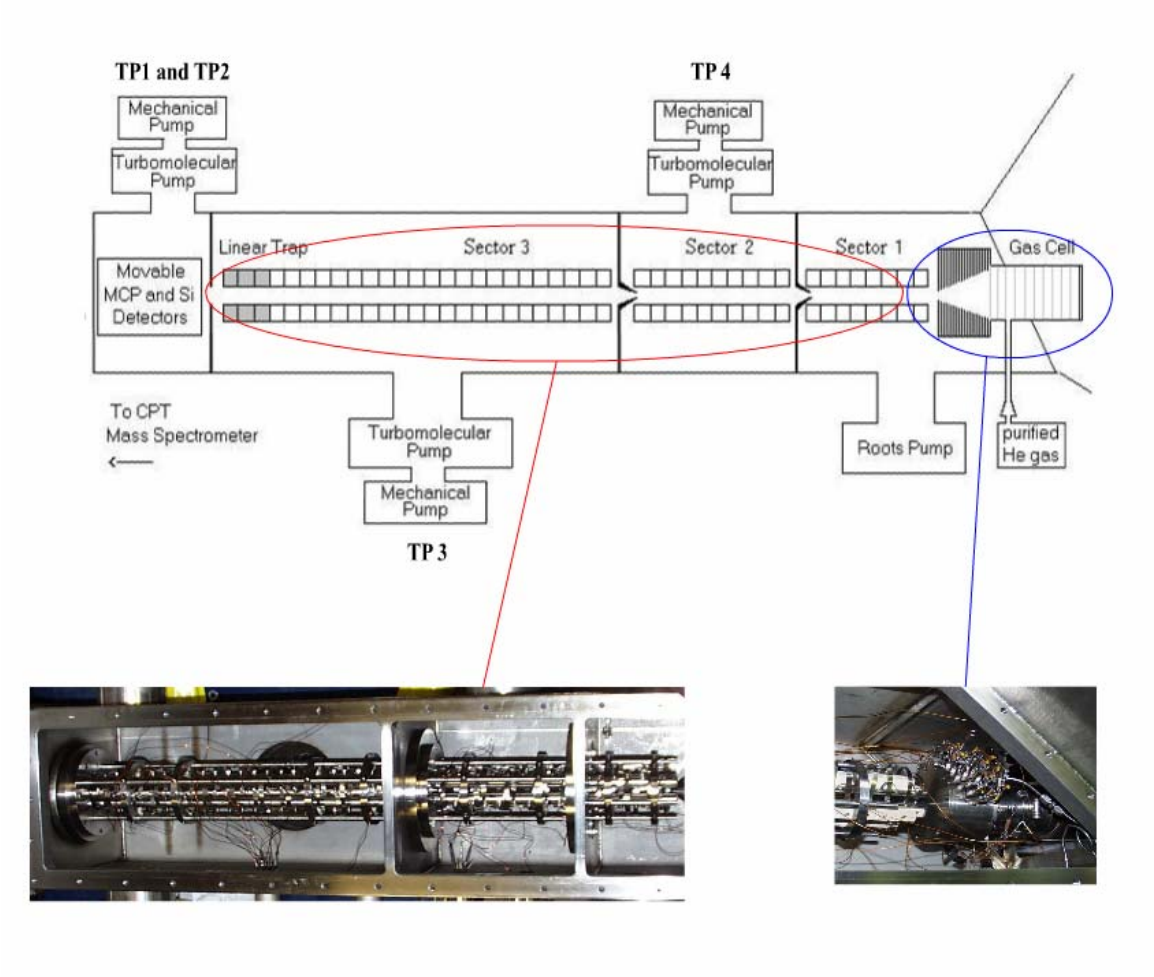

FIG. 3.10. The schematic shows the gas cell and the gas cooler system. The system consists of three sections. At the end of the section 3, there is a linear trap used to accumulate the ions. Also TP1, TP2, TP3 and TP4 are the turbo pumps formed a differential pumping system for the gas cooler system, the pressure is shown on the table 3.1.

The DC and RF voltages are applied on each section and the nozzles. The value is indicated on the table 3.3. The DC voltages form a gradient to drive the motion of the ions toward the exit of the gas cooler. The RF voltages are employed to prevent the ions

from hitting the electrodes of the cooler system. The transmission efficiency of each section is about 80%.

DC, Pulse and RF Voltages applied on the Gas Cooler												
	Sec1			Sec2			Sec3					
	DC1	DC2	N1-2	DC4	DC5	N2-3	DC7	DC8	S1	S2	S3	N3-4
DC (V)	6.60	27.07	6.62	3.37	2.55	1.45	-0.84	-1.52	-2.56	-5.09	-2.56	7.03
Pulses (V)	-	-	-	-	-	-	-	-	30	-	-4	-15
RF (Hz)	0.07Vpp@ 1066kHz			0.38Vpp@ 750kHz			0.46Vpp@ 890kHz					

Table. 3.3. DC1 to DC8 and S1 to S3 are the DC voltages applied on all the segments of each section. N1-2, N2-3, and N3-4 represent the nozzles between each section. Pulses will be applied on S1, S3 and the last nozzle on the Section 3. RF is the radio frequency applied on each section.

The last three segments of Section 3 (S1, S2 and S3) and the last nozzle (N3-4) form a linear trap. The same voltage is applied to the first part (S1) and the third part (S3) of the linear trap (see table 3.3). A lower voltage is applied the middle one (S2). S1, S2 and S3 form a harmonic potential along the ion beam axis. Combined with the residual helium gas, the linear trap accumulates and cools the ions. The DC voltage applied on the last nozzle prevents the ions from leaking out of the cooler. The cooler ejection pulse allows the ions to exit; the value is given on table 3.3. When the pulse is applied, the S1, S2 S3 and the last nozzle will form a potential gradient from +30V to –15V to push the ions out of the cooler as ion bunches. The ejected ions are then captured by the next equipment—the Isobar Separator that is installed immediately after the gas cooler system.

3.4.4 Isobar Separator

The isobar separator is a cylindrical Penning trap composed of 9 electrodes located in a compact homogeneous, conventional, water-cooled electromagnet. A magnetic field of 1 Tesla is along the axial direction (Z-axis). Figure 3.11 shows the structure of the cylindrical trap. The 9 electrodes are labelled as IS1, IS2…to IS9.

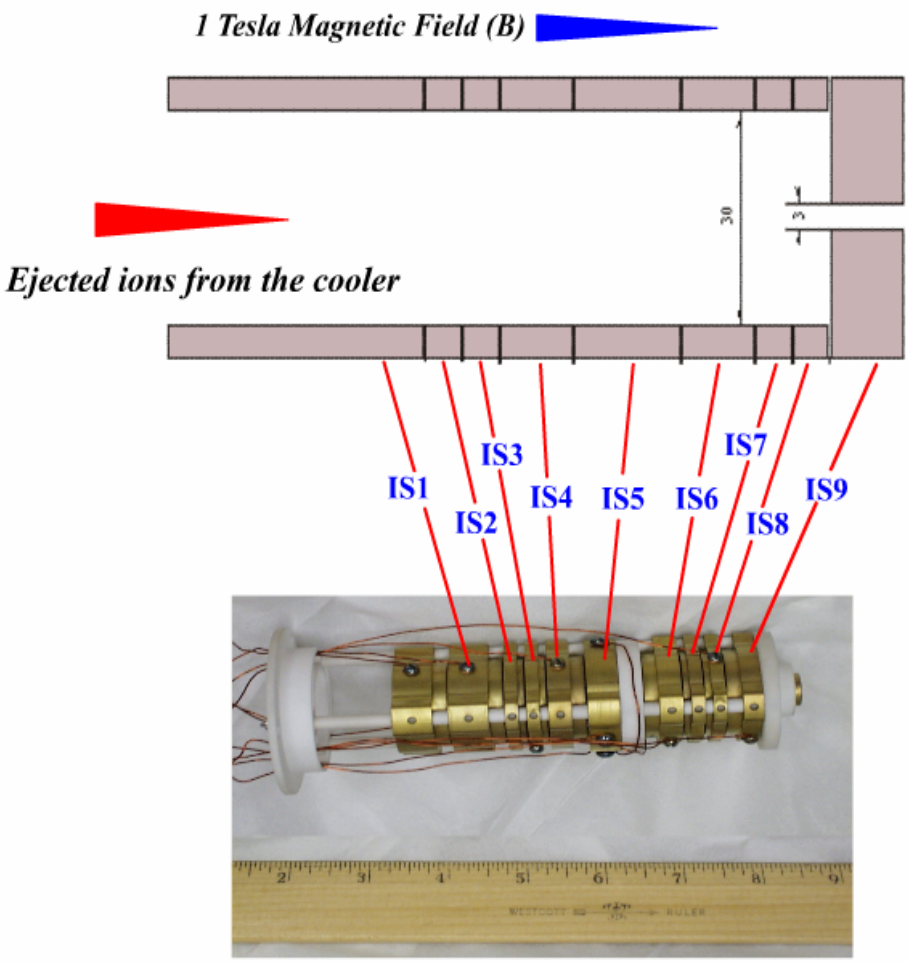

FIG. 3.11. The schematic sketch shows the structure of the isobar separator consisting of 9 electrodes. The 1 Tesla magnetic fields is applied along the axial direction.

The DC voltages are applied to the 9 electrodes along the axial direction (Z-axis) forming a harmonic potential trap with 8V depth. The typical settings of the DC voltage and the pulses are given on the following table 3.4.

	Isobar Separator DC and Pulses Voltages							
Electrodes	**IS1/IS2**	**IS3**	**IS4**	**IS5**	**IS6**	**IS7**	**IS8**	**IS9**
DC Voltages (V)	1	-1	-6	-8	-6	-1	1	20
Capture Pulse (V)	-10	-8	-6	-8	-6	-1	1	20
Ejection Pulse (V)	1	-1	80	-8	-80	-100	-100	-250

Table. 3.4. DC and Pulses Voltages applied to the Isobar Separator. The capture pulses is applied on IS1, IS2 and IS3 highlighted by the yellow shade and the ejection pulses is applied on IS4, IS6, IS7, IS8 and IS9 highlighted by the blue shade in the table.

When the capture pulse is applied, the voltages on the IS1/IS2 and IS3 are reduced to –10V and –8V respectively to allow the ions fly into the trap. The duration of the capture pulse depends on the time of flight information of the desired ions. The capture pulse has to last long enough to allow all the desired ions entering the trap. But if the duration is too long, the ions may eject back and fly out of the trap. The ejection pulse is applied by increasing the voltage on IS4 and decreasing the voltage on IS6, IS7, IS8 and IS9. The ions then are kicked out of the trap. Figure 3.12 shows the potential changes when the pulse applied on the isobar separator.

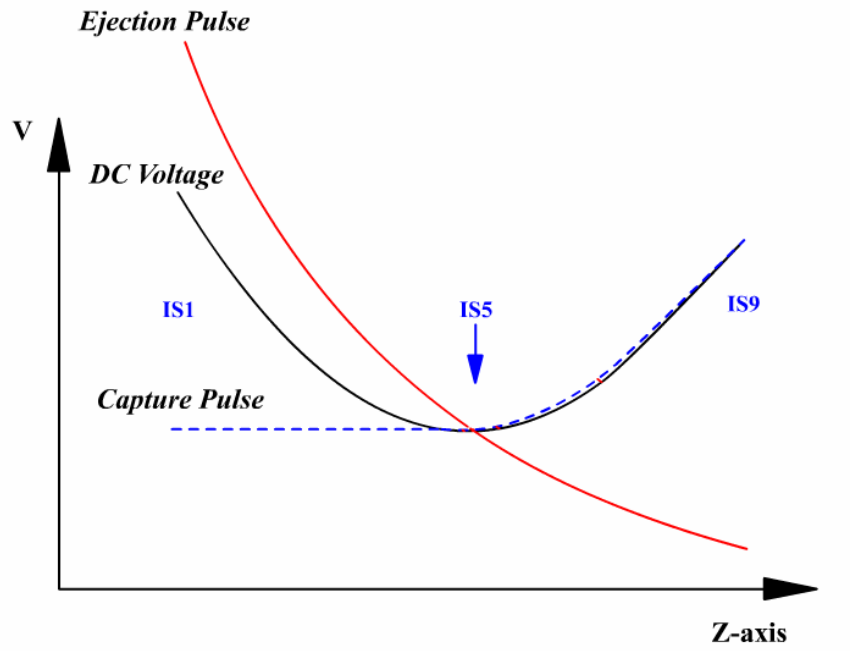

FIG. 3.12. A graph shows the DC voltages applied on the isobar separator and the potential changes when the pulses applied on it. The Y-axis represents the voltage and Z-axis represents the position of the nine electrodes along the magnetic field. The black curve shows the DC potential without any pulses; the blue dash curve shows the potential when capture pulse applied and the red solid curve show the potential when ejection pulse applied.

The duration time between capture pulse and ejection pulse indicates how long the ions stay in the isobar separator. If the duration time is short, most of the ions coming into the isobar separator will be ejected. The TOF spectrum of different masses therefore can be detected on the MCP2' detector located in the transfer line between the isobar separator and the rest the system. Figure 3.13 shows the TOF spectrum detected on the MCP2' detector in the light fission fragment mass measurement with 25ms duration time applied on the isobar separator. The transmission efficiency of the isobar separator is about 50%.

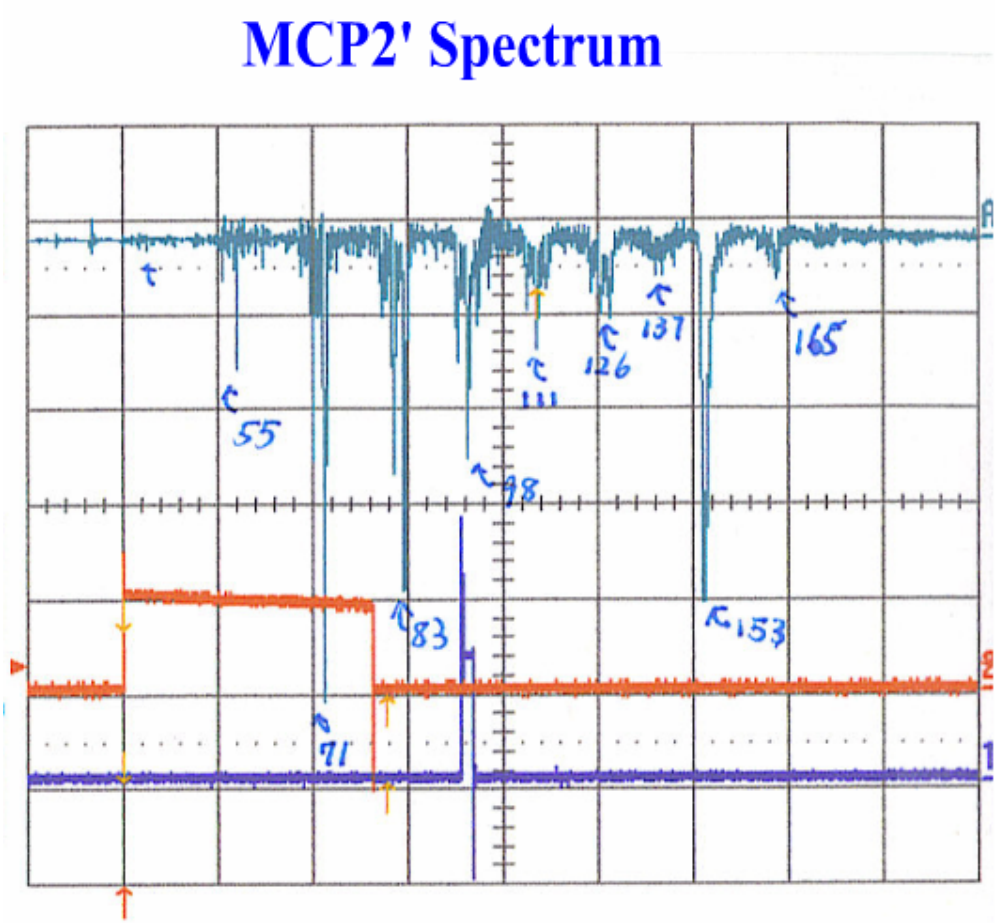

FIG. 3.13. The picture shows the spectrum detected on the MCP2' detector when the duration time on the isobar separator is set for 25ms.

The masses of those peaks on the figure 3.13 can be identified according to the time of flight of the ions traveling from the isobar separator to the MCP2' detector. The red trace indicates the isobar separator ejection pulse and blue trace indicates the deflection pulse.

As described in the chapter 2.4, the ion motion in the isobar separator (a gas-filled Penning trap) consists of three harmonic eigen-motions: an axial oscillation at a frequency ω_z and two circular motions in the radial plane with the frequencies of ω_+ (cyclotron motion) and ω_- (magnetron motion). The sum of the two radial motion

frequencies keeps constant as the true cyclotron frequency ω_C ($\omega_C = \omega_+ + \omega_-$). Therefore a quadrupole excitation at the frequency of ω_C is applied with a waveform from the SRS DS345 function generator to convert the magnetron motion of the ions to the cyclotron motion, which decays quickly through collisions of the ions with the buffer gas [Savard1991]. Similarly, the axial motion ω_z is also damped by the buffer gas. In this way, the desired ions are cooled and centered in the trap. Since this whole process is mass selective, the isobar separator has been used for removing the unwanted ion species and sending the desired ions with the low energy to the next equipment. More than 95% of the contaminant ions can be removed by the isobar separator.

3.4.5 The Deflection Pulse

A fast voltage pulse, named "deflection pulse", is applied on one of the beam transport elements to further select the desired ions (figure 3.14-A). The DC voltage on the transport element where the deflection pulse is applied is set about 750V higher than the transferring drift tube potential. Without the pulse, all the ions will be deflected here and lost at the electrode wall. The deflection pulse decreases the high DC voltage (750V) to the drift tube potential (~-1500V) to allow the ions flying through. Since the pulse only lasts for a very short period of time, only one species is allowed to pass through. The ion bunches eject from the isobar separator with roughly the same energy. Therefore, the ions with the heavier masses fly slower and the ions with the lighter masses fly faster than the desired ions in the beam transport line. By properly adjusting the width and the timing of the deflection pulse, the desired ions can be selected and the unwanted ions can be removed.

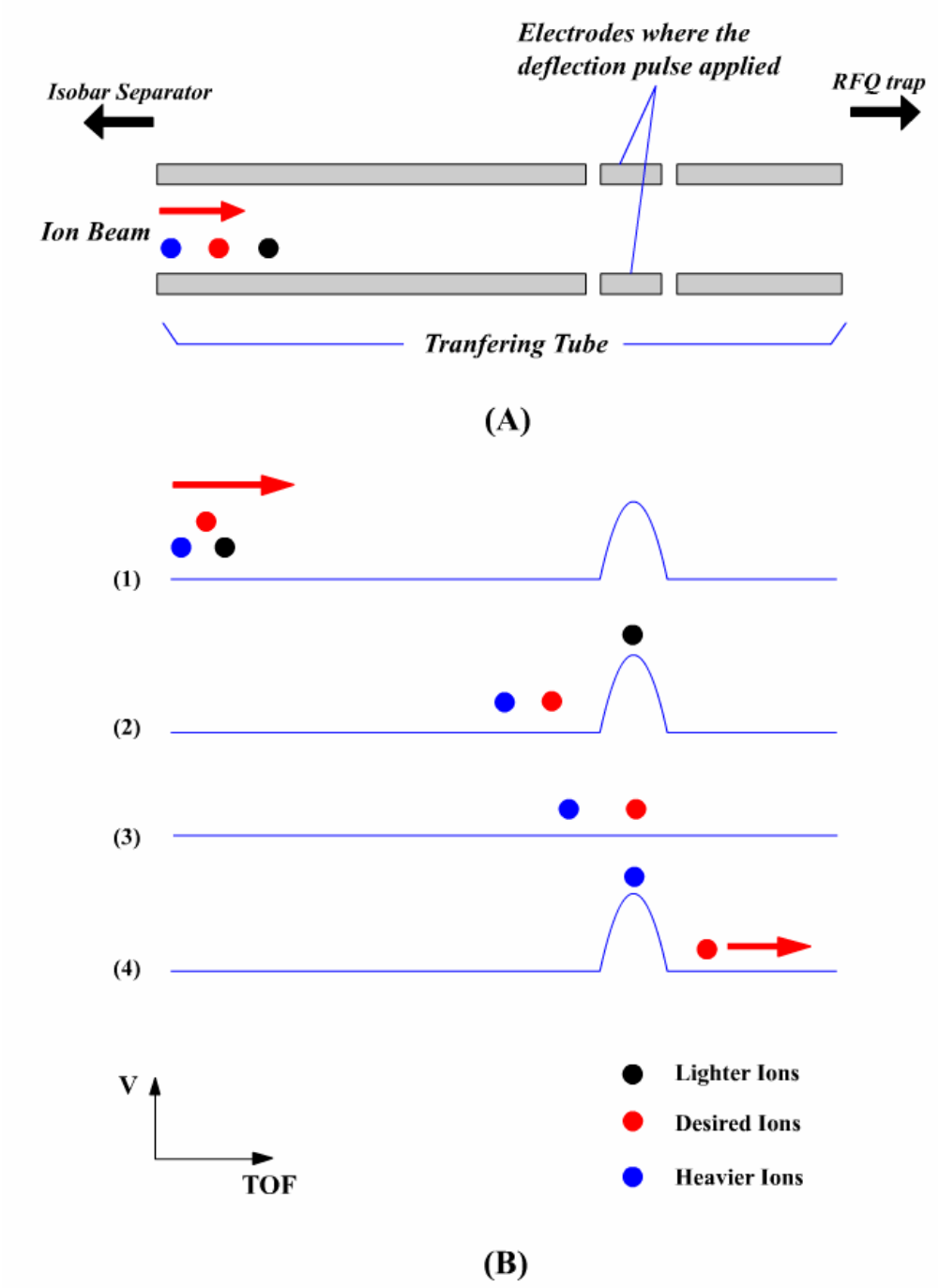

FIG. 3.14. Schematic of the deflection pulse (A) shows the electrode, located in the transfer line between isobar separator and the RFQ trap, where the deflection pulses applied. Schematic (B) shows how the deflection pulse can select the ion species. Black ball represents the ions with lighter masses, the red one represents the desired ions and the blue one represents the ions with heavier masses.

On the figure 3.14-B:

(1) The ions with different masses are ejected as a bunch from the isobar separator at the same energy.

(2) Ions arrive at the "deflection pulse" position at the different time; the lighter ones arrive earlier and are deflected to the wall.

(3) The deflection pulse is applied to decrease the DC voltage when the desired ions arrive.

(4) After the desired ions pass through the DC voltage raise again, therefore removing the heavier ions.

As shown on the figure 3.14-B, the ions with different masses arrive at the "deflection pulse" position at different time. Finally, only the desired ion species will be allowed to pass through the transport element and all the other species will be cut off. The timing of the deflection pulse can be adjusted based on equation 3.1:

$$\frac{m}{m'} = \frac{v'^2}{v^2} = \frac{t^2}{t'^2} \tag{3.1}$$

The lighter masses can be removed by tuning the deflection pulse delay and the heavier masses can be removed by adjusting the deflection pulse width. The amplitude of the pulse is adjusted high enough to allow the desired ions pass through. For the ^{109}Ru mass measurement, the width of the deflection pulse is set to ~0.8 μs to allow only mass 109 to pass through. Figure 3.15 shows the TOF spectrum detected on the MCP1 detector with the deflection pluses set up for mass 109.

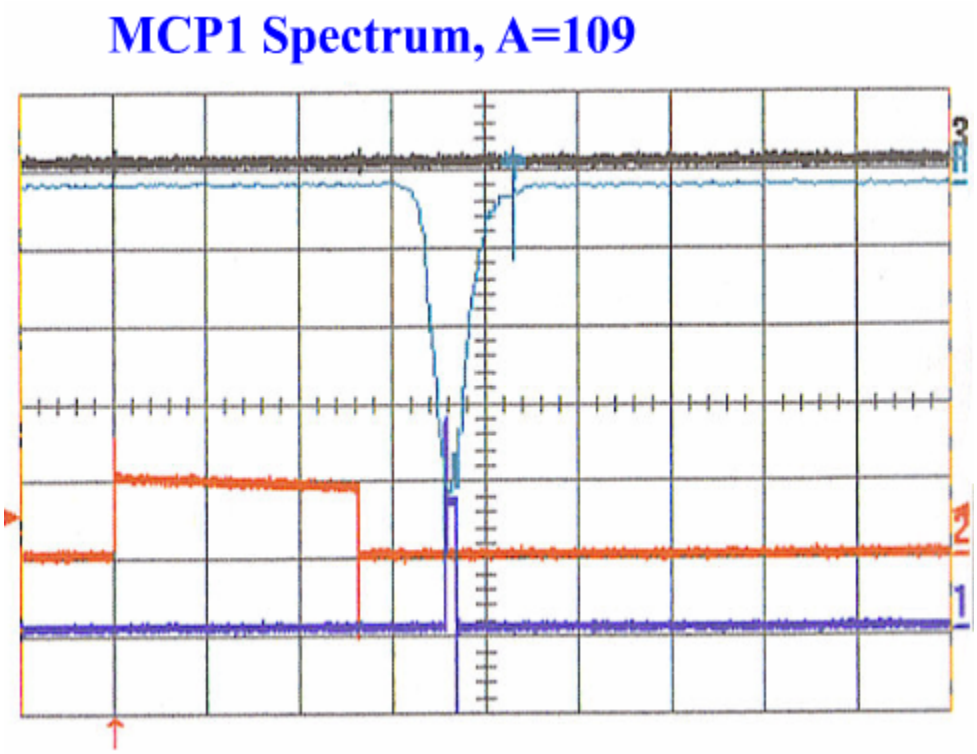

FIG. 3.15. Spectrum detected on the MCP1 detector when the deflection pulse is set up for the mass 109 and the isobar separator is used. The red trace indicates the isobar separator ejection pulse and blue trace indicates the deflection pulse.

3.4.6 The Linear RFQ Trap

The ions transferred from the isobar separator are captured in a gas filled linear RFQ trap. The gas pressure is about 3.0×10^{-3} Torr. The ions are bunched and cooled here in the RFQ trap. There are two main purposes of using the linear RFQ trap to treat the ions before sending them into the precision Penning trap:

1) To narrow the energy spread of the ion bunches. The ion bunch in the Penning trap undergoes the axial oscillation whose amplitude depends on the energy spread. If the ions have a very big energy spread, they will experience non-uniform magnetic field in the Penning trap, which will reduce the precision of

the mass measurement. The helium buffer gas is used in the RFQ trap to cool the ions and therefore reduce the energy spread.

2) To accumulate enough ions for the measurement and to match the timing sequence in each cycle of the measurement. Refer to the figure 3.6, in the typical fission fragments mass measurement, the Penning trap uses at least 640ms to finish one cycle of measurement (apply 40ms ω_-, 100ms ω_+ and 500ms ω_c excitations). The RFQ trap can use this time to accumulate and cool down the ions. Since the isobar separator ejects an ion bunch about every 500ms, the RFQ trap can collect two bunches of ions and cool them in total 1000ms. The users can decide how many bunches of ion need to be collected in making the mass measurement. When enough cooled ions are accumulated and the Penning trap is empty, the RFQ trap is ready to eject the ions to the Penning trap.

Similar to the RFQ trap in the last section of the cooler system, this linear RFQ trap consists of four segmented parallel rods forming a two-dimensional quadrupole field on the radial plane. On the figure 3.16, (A) shows the structure of the linear RFQ trap, (B) the quadrupole potential made by the linear RFQ trap; (C) and (D) are photos of the RFQ trap. The RF signal is applied on the rods through an amplifier. Based on the theory introduced on the chapter 2, the ions with certain range of masses will be accumulated and confined according to the RF frequency and amplitude applied on the rods.

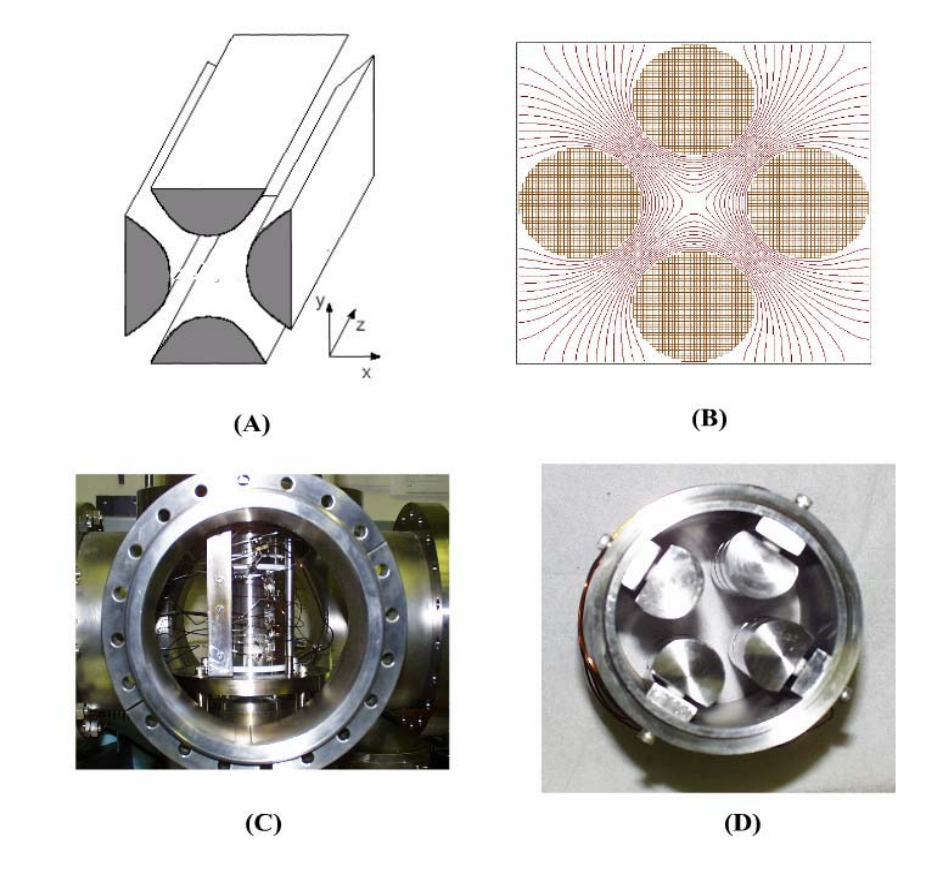

FIG. 3.16. The schematic sketch of RFQ trap (A) Shows the structure of the linear RFQ trap; (B) made by the SIMION program simulating the quadrupole potential on the radial plane inside the RFQ trap; (C) the photo of the linear RFQ trap replaced the old Paul trap and installed in the steel cross; (D) the photo of the RFQ trap.

Each rod in the RFQ trap consists of three segments as seen on the figure 3.17-A. A potential well is created along the axial direction, when a lower voltage (V2) is applied on the middle segment of each rod as shown on the figure 3.17-B. In the capture mode, the ions fall into the potential well and get cooled by colliding with the buffer gas. Both the energy and the energy spread of the ions are reduced. Finally, the ions will settle to the bottom of the potential well. When several bunches of ions are collected, an ejection pulse will be applied to kick them out by increasing V1 and decreasing V2.

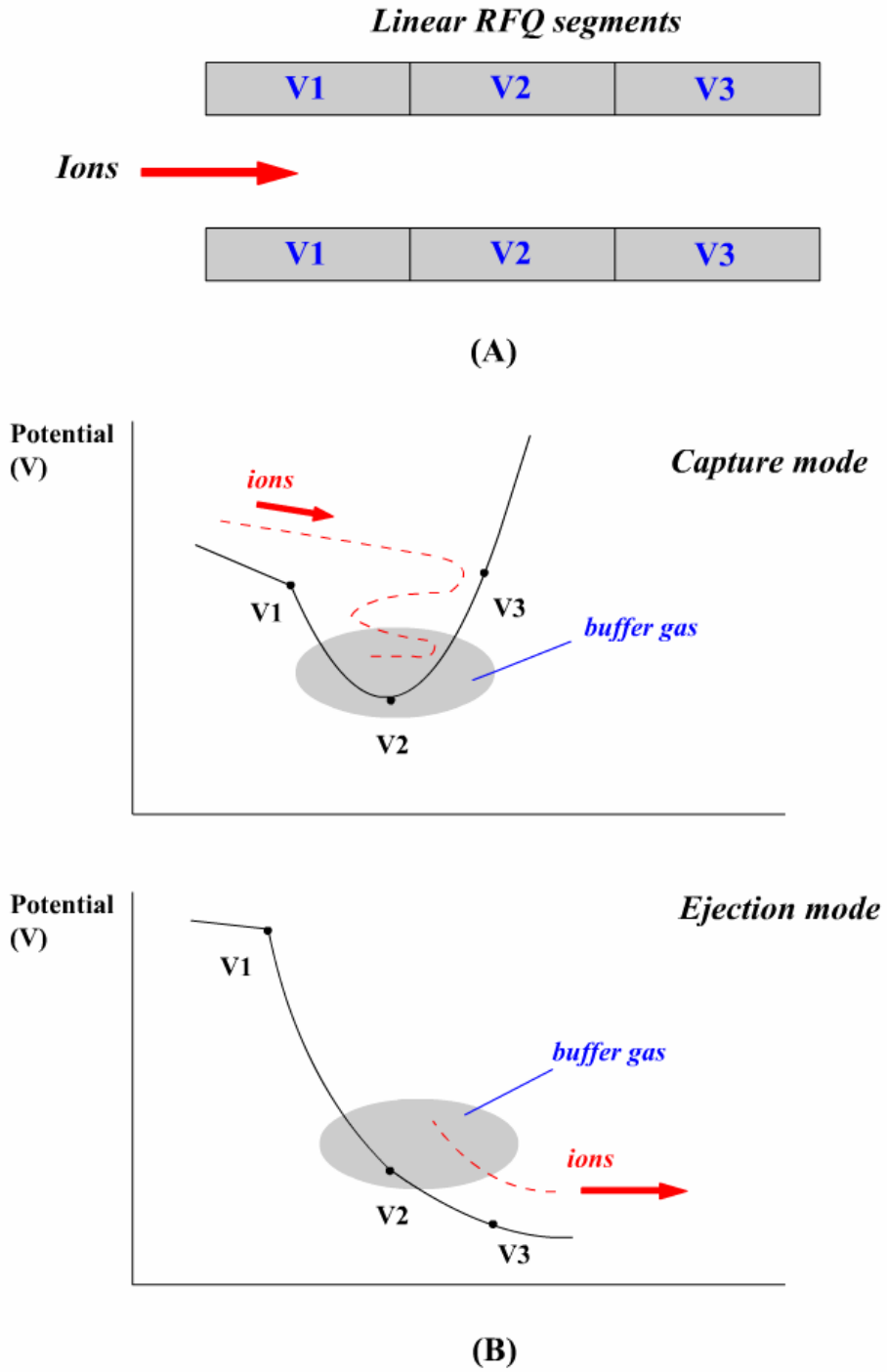

FIG. 3.17. Schematic sketch of RFQ trap (A) shows the three segments on each rod of the RFQ trap, V1, V2 and V3 are the potential applied on each segment. (B) Shows the capture and ejection potential for the linear RFQ trap, ions are captured and cooled during the capture mode and ejected with low energy on the ejection mode.

The MCP3 detector is used to detect the ions ejected from the RFQ trap. Using A=109 mass measurement as an example, the figure 3.16 shows the TOF spectrum of ions (molecule C_8H_{13}) on MCP3 detector.

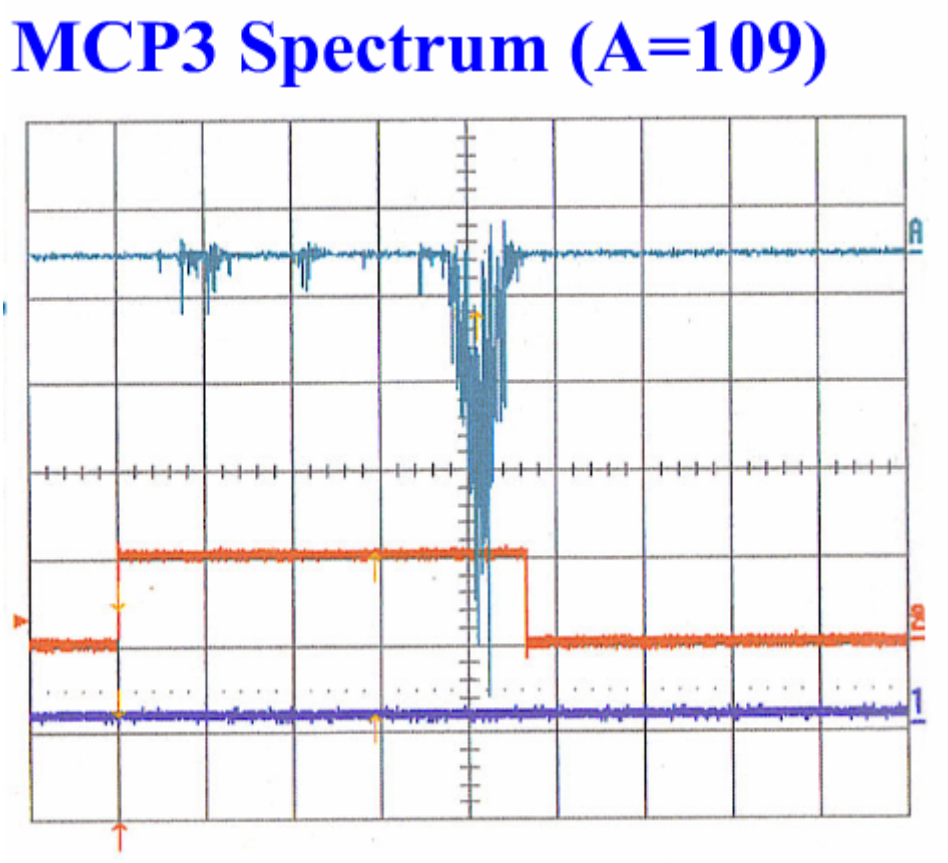

FIG. 3.18. The picture shows the TOF spectrum detected on the MCP3 detector. The peak shows the mass 109.

3.4.7 The Penning Trap

The Penning trap located in a super-conducting magnet (B=5.9T) consists of two end caps, a ring electrode and correction electrodes. The detailed structure of the Penning trap is given on the figure 3.19. In the ideal Penning trap as described in the chapter 2.3 the potential surfaces should be continuous and infinite. However, in reality, we can only

use limited surface. Also entrance holes have to be made on the end caps to allow the ions flying through. Therefore, correction rings and correction tubes are necessary to make a fine adjustment to the established potential. A 0.5cm aperture is made on both top end-cap and bottom end-cap. The ring electrode of the Penning trap has been divided into four parts, which allows both of the dipole and quadrupole excitations being applied [Bollen1990]. All of the Penning trap electrodes are composed of gold-plated oxygen-free high purity copper to avoid the magnetic effects.

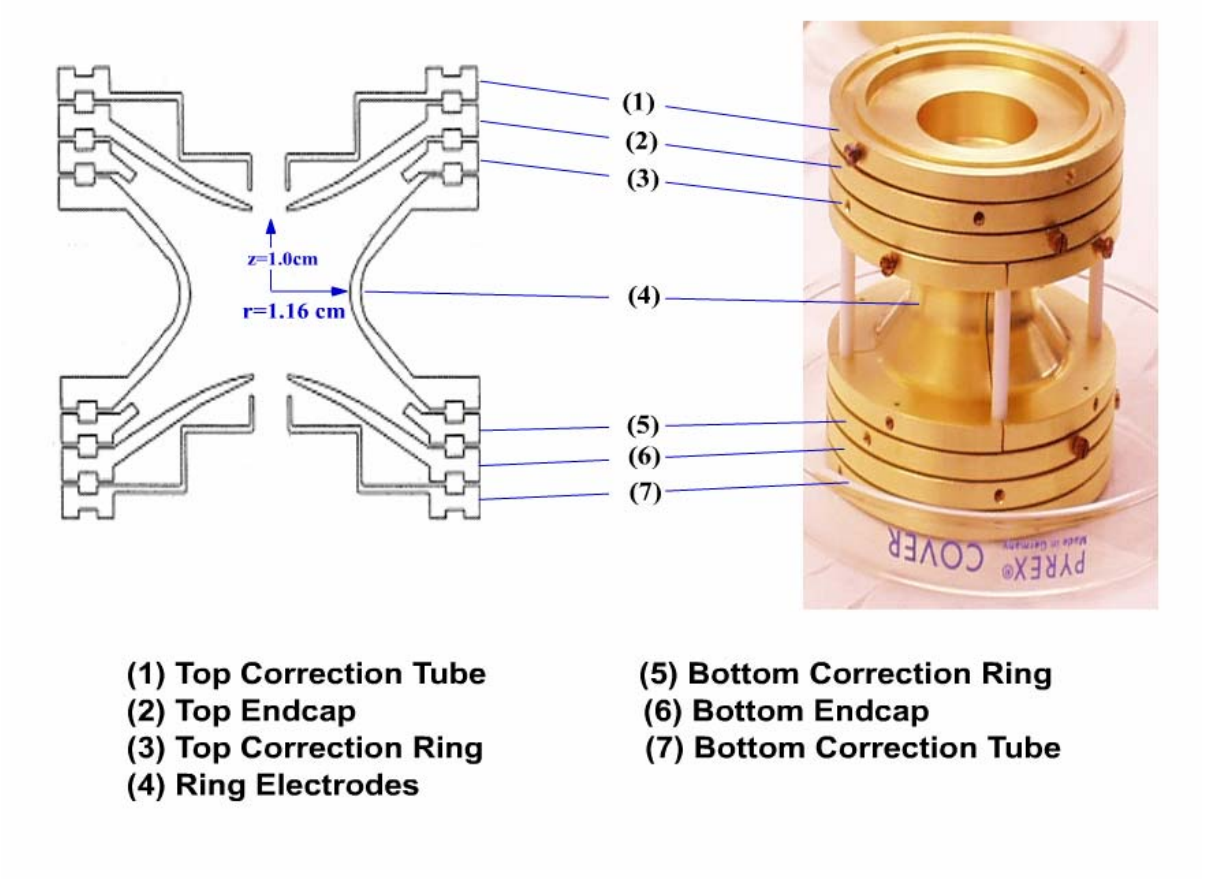

FIG. 3.19. The detailed structure of the precision Penning trap used in the CPTMS system is shown on the left and the photo is given on the right.

During a mass measurement, proper DC voltages are applied to the Penning trap to form a harmonic potential on the axial direction. In the radial direction, a ω_+ dipole excitation at the selected frequency is applied first to increase the orbit of cyclotron motion of contaminant ions and finally remove them from the trap (refer to chapter 2.3). The amplitude and the duration time of this ω_+ excitation are carefully chosen to remove the contaminant ions without disturbing the desired ions. After the previous cleaning process, a dipole ω_- excitation is employed to drive the desired ions to an initial orbit. As described in chapter 2.3, ω_- excitation is mass unselective. Therefore all the ions in the Penning trap will be driven to the same orbit. Typically, the ω_- excitation frequency is about 1590kHz, the excitation amplitude is about 0.016V and the excitation duration time is 40ms. Finally a quadrupole excitation with frequency of ω_c ($\omega_c = qB/m$) is applied to convert the initial magnetron motion to the cyclotron motion of the desired ions. The accurate mass value of the desired ion can be obtained by comparing the cyclotron frequency between the desired ion and the corresponding reference ion. The excitation duration time and the excitation amplitude are properly chosen to make sure the full conversion from the magnetron motion to the cyclotron motion (refer to chapter 2.3.2).

Once the quadrupole excitation is completed, the ions are ejected from the Penning trap to the last Micro-Channel Plate (MCP) detector through the magnetic field. Due to the interaction between the orbital magnetic moment of the ions and the magnetic field gradient, the radial energy of the ions will be converted to axial energy (refer to chapter 2.5 about TOF technique). The drift tube installed above the Penning trap is long enough to allow a full conversion. The excited ions fly faster than the others. That's why we can obtain a peak on the TOF (Time of Flight) spectrum. Finally, the masses of the

isotopes can be determined by the resonance frequency on the spectrum (refer to the Appendix II for the TOF spectra).

3.4 Detectors for ions and radioactivity

There are two types of ion detectors used in our experiments: ***Silicon Detectors*** and ***Micro-Channel Plate (MCP) detectors***. There are three silicon detectors applied on the CPTMS system. Si1' detector is installed behind the isobar separator and before the 90-degree beam transport line. Si2' detector is installed after the beam transport line. The ratio of the activity counts between Si1' and Si2' detectors indicates the efficiency of the 90-degree beam transport line. Typically, the transmission efficiency of the 90-degree transport line is about 90%. Si3 detector is installed behind the linear RFQ trap. The counts ratio between Si3 detector and Si2' detector shows the efficiency of the deflection pulse plus the RFQ trap plus the transfer line. There are totally five MCP detectors used in the system. MCP1' detector is installed at the same position as Si1' detector. MCP2' detector is installed at the same position as Si2' detector. MCP1, MCP3 and MCP5 detectors are installed behind the deflection pulse, the RFQ trap and the Penning trap respectively to detect the ions coming out of those equipments.

In some of the cases, both detectors are located at the same position, such as Si1' and MCP1' detectors, Si2' and MCP2' detectors, and Si3 and MCP3 detectors. Therefore they have been mounted on the same holder as shown on the following figure 3.20. The holder is attached to a feed-through that can be moved up and down to select different detectors.

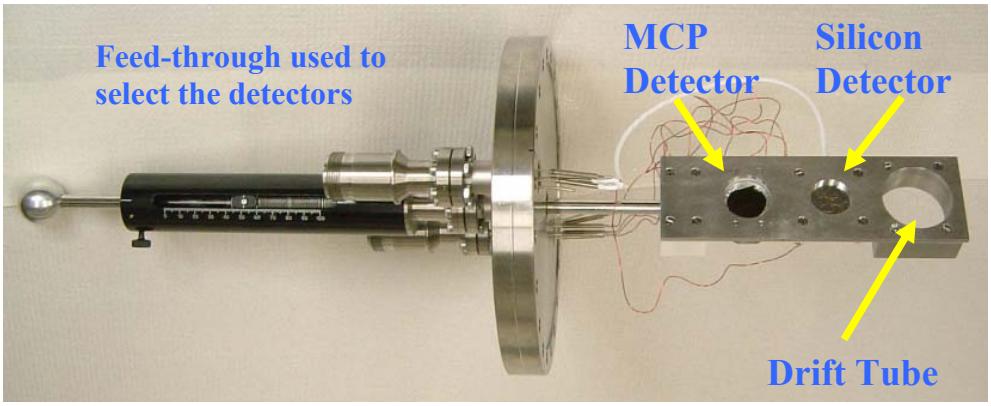

FIG. 3.20. The picture of the detectors. The holder and the linear-motion feed through are shown on the following picture. Either drift tube, MCP detector or Silicon detector can be placed facing the ion beam.

3.4.1 The Silicon Detectors

The silicon detectors are used to determine the number of the radioactivities by counting the radioactive decays. When the β decay particles pass through the detector, the electron-hole pairs are created and the resulting charges can be collected by applying a biased potential. During our experiment, the bias voltage is about +90V. The signal goes through the amplifier and is sent to the oscilloscope. The threshold of the signal pulse amplitude is set to a certain value in order to get rid of the noise at low amplitude. An aluminium foil, applied with –1900V, is installed in front of each of the silicon detectors to gather the ions.

3.4.2 The MCP Detectors

The MCP detectors are used to test the performance of the beam transport elements by measuring the number of the ions hitting the detector. Also the MCP detectors provide the time of flight information of the measured ions. The MCP detector

is a fabricated plate having thousands of independent channels. The figure 3.21 shows the real MCP detector compared with a two-dollar Canadian coin. The single ion enters the channel and produces an initial electron from the channel wall. This secondary electron is accelerated by an electric field and produces more electrons when it hits the channel surface. Produced electrons repeat the same process to create more and more electrons. Finally a single ion hitting the plate produces a cloud of several thousand electrons. In our experiment, the typically bias of MCP detectors ranges from –1900 V to –2300 V. The efficiency of the MCP detector is about 40%.

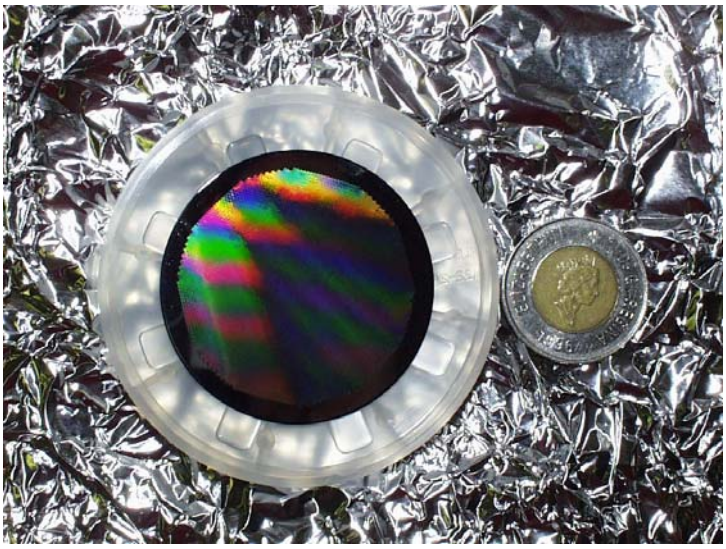

FIG. 3.21. Photo of the MCP detector. The detector are shown on the left and compared with a Canadian two-dollar coin on the right.

Chapter 4

Results and Data Analysis

4.1 Results

The precise mass measurements of four neutron-rich isotopes (^{108}Tc, ^{108}Ru, ^{109}Ru and ^{110}Ru) from the lighter ^{252}Cf fission fragment peak (refer to figure 3.7) have been successfully done using the CPT mass spectrometer. This is the first time that masses of fission fragments have been directly measured with a mass spectrometer. The TOF spectra related to the mass measurements are shown on Appendix II. The computer program automatically fits the TOF spectrum by minimizing the reduced χ^2 value and finally gives us the centroid frequency ω_c and associated uncertainties. The reduced χ^2 measures how well the function fits the data. It can be expressed as:

$$\chi^2 = \frac{1}{N-P} \cdot \sum_{1}^{N} \left(\frac{1}{\sigma_i^2} \cdot (Y - Y_i)^2 \right) \tag{4.1}$$

Where σ_i is the uncertainty of each data point, Y is the value from the fitting function ($Y = f(Y_i)$), Y_i is the value of each data point, N is the total number of the data points and P is the degree of freedom of the fitting function Y. In the mass measurements, the reduced χ^2 also equals to the ratio of the external error and the internal error:

$$\chi^2 = \frac{\sigma_{ext}^2}{\sigma_{\text{int}}^2} \tag{4.2}$$

where σ_{int} is the internal error, which can be expressed as:

$$\sigma_{\text{int}} = \sqrt{\frac{1}{\sum_{1}^{i} \frac{1}{\sigma_i^2}}} \tag{4.3}$$

where σ_{ext} is the external error and has the format of:

$$\sigma_{ext} = \sqrt{\frac{1}{N-P} \cdot \frac{\sum_{1}^{i} \left(\frac{1}{\sigma_i^2} \cdot (Y - Y_i)^2 \right)}{\sum_{1}^{i} \frac{1}{\sigma_i^2}}} \tag{4.4}$$

Table 4.1 shows measured frequencies of the activities and corresponding reference molecules.

Reference Molecule	Centroid Frequency (Hz)	Uncertainty (Hz)	Reduced CHI-Square	Isotope	Centroid Frequency (Hz)	Uncertainty (Hz)	Reduced CHI-Square
C_8H_{12}	836628.92	0.03	1.15	^{108}Tc	837988.76	0.18	1.82
C_8H_{12}	836628.91	0.03	1.55	^{108}Ru	838053.15	0.15	0.59
C_8H_{13}	828900.68	0.03	1.27	^{109}Ru	830334.39	0.17	1.09
C_8H_{13}	828900.60	0.07	0.56	^{109}Ru	830334.26	0.10	0.85
C_8H_{13}	828900.57	0.07	3.23	^{109}Ru	830334.09	0.22	0.95
C_8H_{13}	828900.27	0.02	1.87	^{109}Ru	830334.34	0.12	0.64
C_8H_{14}	821313.53	0.08	2.21	^{110}Ru	822775.76	0.25	0.94
C_8H_{14}	821313.58	0.05	1.91	^{110}Ru	822774.52	0.16	1.69
C_8H_{14}	821313.58	0.05	1.91	^{110}Ru	822774.30	0.22	2.17
C_8H_{14}	821313.58	0.06	1.44	^{110}Ru	822776.08	0.59	0.89
C_8H_{14}	821313.75	0.04	1.80	^{110}Ru	822774.87	0.12	0.98

Table. 4.1. Frequencies of the calibration molecules and the corresponding activities. There are four different measurements for ^{109}Ru and five different measurements for ^{110}Ru. The reduced χ^2 of each measurement is also listed.

Internal error characterizes the precision of the data. External error describes the data scatter of the points from the produced value. In the table 4.1, the final error (uncertainty) is chosen from either internal error or external error, depended on whichever is bigger.

In the Penning trap mass measurements, the ratio of the masses and the ratio of the cyclotron frequencies are equal based on the following equation 4.5:

$$R = \frac{(m - e \cdot m_e)/e}{(m_{ref} - e_{ref} \cdot m_e)/e_{ref}} = \frac{\omega_{ref}}{\omega} \tag{4.5}$$

Where R is the ratio, m is the mass of the ion, m_e is the mass of the electron, and e is the charge state. ω_{ref} and ω are the centroid frequencies of the reference molecule and the activity respectively. The following table 4.2 lists the frequency ratio and its statistics error calculated from the data in the table 4.1.

Isotope	Reference Molecular	Frequency Ratio (Reference/Isotope)	Statistics Error
^{108}Tc	C_8H_{12}	0.998377254	0.000000222
^{108}Ru	C_8H_{12}	0.998300530	0.000000186
^{109}Ru	C_8H_{13}	0.998273334	0.000000213
^{109}Ru	C_8H_{13}	0.998273388	0.000000143
^{109}Ru	C_8H_{13}	0.998273559	0.000000282
^{109}Ru	C_8H_{13}	0.998272898	0.000000151
^{110}Ru	C_8H_{14}	0.998222812	0.000000319
^{110}Ru	C_8H_{14}	0.998224378	0.000000206
^{110}Ru	C_8H_{14}	0.998224645	0.000000271
^{110}Ru	C_8H_{14}	0.998222480	0.000000720
^{110}Ru	C_8H_{14}	0.998224154	0.000000152

Table. 4.2. The table of the frequency ratio. It lists the frequency ratio between reference molecules and corresponding isotope. The statistical uncertainty is given.

Since both isotopes and reference molecules are singly charged during the light fission fragments measurements, the equation 4.5 can be changed to:

$$m = R \cdot \left(m_{ref} - m_e\right) + m_e \qquad (4.6)$$

Where m_{ref} is the mass of reference molecule, which comes from the AME 2003 [Audi2003]. The masses of these reference molecules are well known to high accuracy (about 10^{-10}). The masses of light fission fragments can be calculated from the reference masses. The masses of the calibration molecules and the calculated masses of the isotopes are listed below in table 4.3:

Isotope	Calibration Molecules	Mass of Molecules (μ u)	Mass of the Isotope (μ u)	Uncert. (μ u)
^{108}Tc	C_8H_{12}	108093900.38	107918492.37	24.02
^{108}Ru	C_8H_{12}	108093900.38	107910198.94	20.13
^{109}Ru	C_8H_{13}	109101725.42	108913344.11	23.26
^{109}Ru	C_8H_{13}	109101725.42	108913350.04	15.59
^{109}Ru	C_8H_{13}	109101725.42	108913368.62	30.82
^{109}Ru	C_8H_{13}	109101725.42	108913296.56	16.49
^{110}Ru	C_8H_{14}	110109550.45	109913866.08	35.18
^{110}Ru	C_8H_{14}	110109550.45	109914038.47	22.74
^{110}Ru	C_8H_{14}	110109550.45	109914067.91	29.79
^{110}Ru	C_8H_{14}	110109550.45	109913829.54	79.23
^{110}Ru	C_8H_{14}	110109550.45	109914013.81	16.71

Table. 4.3. The table of the atomic masses. The table shows the atomic masses calculated from the reference molecules and measured frequencies based on the equation 4.6. The masses of molecules come from the AME2003 mass table.

As shown on the table 4.3, there are four different masses for ^{109}Ru and five different masses for ^{110}Ru. Taking the weighted average of each mass, we can obtain the final masses listed on table 4.4. The weighted average masses are calculated based on the following equation:

$$m_{weighted} = \frac{\sum_{1}^{i} \frac{m_i}{\sigma_i^2}}{\sum_{1}^{i} \frac{1}{\sigma_i^2}} \tag{4.7}$$

Where m_i is each one of the measured masses and σ_i is its uncertainty. The error of the weighted average mass is:

$$\sigma_{weighted} = \sqrt{\frac{1}{\sum_{1}^{i} \frac{1}{\sigma_i^2}}} \tag{4.8}$$

Isotope	Masses in this work (μ u)	Uncert. (μ u)	AME 2003 (μ u)	Uncert. (μ u)	Δ (μ u)	Precision
^{108}Tc	107918492.37	24.02	107918461.23	135.77	31.14	2.23E-07
^{108}Ru	107910198.94	20.13	107910173.47	124.71	25.48	1.87E-07
^{109}Ru	108913332.44	15.43	108913203.23	70.95	129.21	1.42E-07
^{110}Ru	109914008.54	29.96	109914136.04	57.16	-127.50	2.73E-07

Table. 4.4. The comparison of the measured masses from this work and the masses from the AME 2003 mass table

Table 4.4 lists the masses from CPTMS measurements and the masses from AME2003 mass table. The "**Δ**" in the table is the difference between the measured masses and the

AME 2003 masses. The precision of the measurement is also given on table 4.4 (refer to Appendix I for the spectrometry terms). All of the four neutron-rich isotopes ^{108}Tc, ^{108}Ru, ^{109}Ru, and ^{110}Ru have been measured up to a precision of 10^{-7}. Figure 4.1 shows the mass difference versus isotopes.

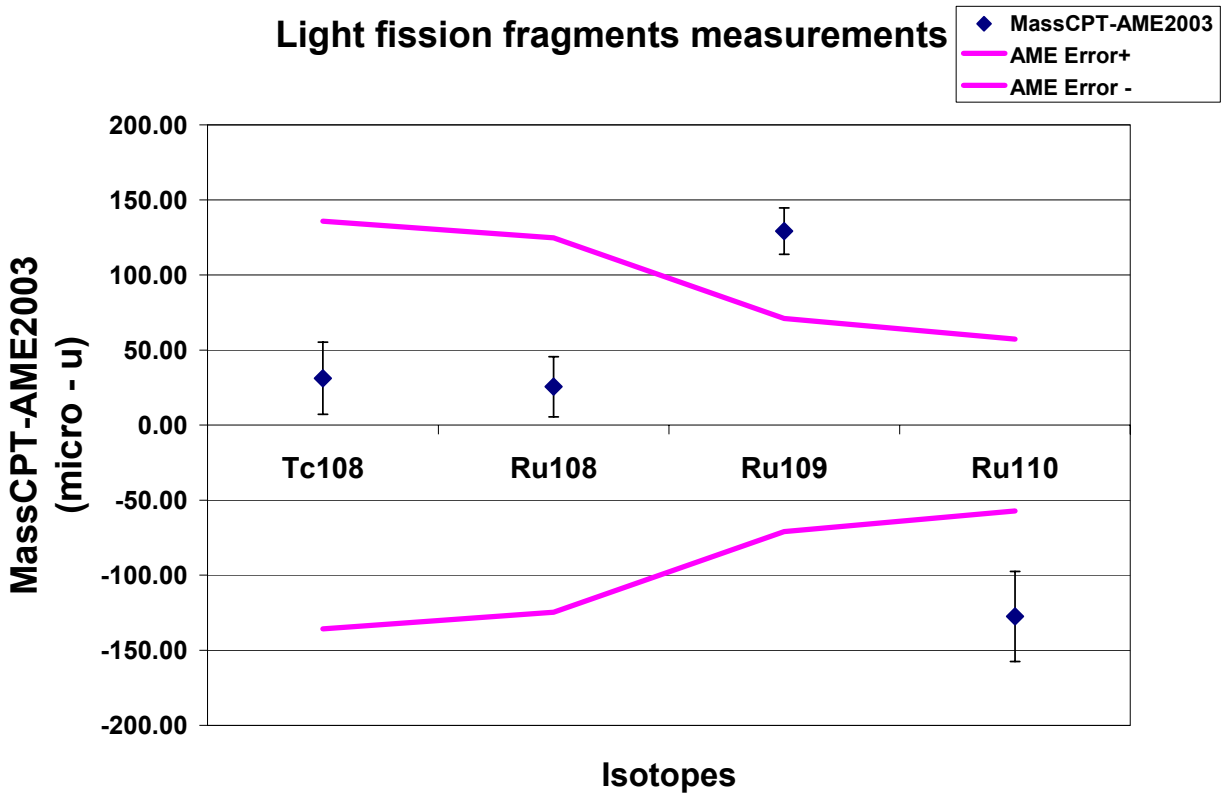

FIG. 4.1. Mass comparisons between CPT measured value and AME2003 [Audi2003] mass value. Two purple lines indicate the plus and minus errors from the AME 2003. The uncertainty of each data point on this figure comes from the mass measurements of present work.

Compared with the AME (Atomic Mass Evaluation) 2003 [Audi2003], our mass measurements yield a better precision than the mass table. The masses of ^{108}Tc and ^{108}Ru agree with the atomic mass values from AME 2003, while the masses of ^{109}Ru and ^{110}Ru do not agree.

4.2 Discussion

4.2.1 Systematic Effects

Systematic effects can shift the cyclotron frequency ω_c of desired ions in a Penning trap during measurement. As shown in the previous section, the statistical uncertainty of the light fission fragment mass measurement is approximately 10^{-7}. If the systematic error is bigger than 10^{-7}, then the systematic effects have to be considered in the mass measurement results.

There are two different types of systematic effects from the CPTMS system: avoidable systematic effects and unavoidable systematic effects. The major avoidable systematic effects are caused by:

1) The presence of contaminant ions in each ion bunch
2) The number of the desired ions in the Penning trap
3) The energy spread of the desired ions in the Penning trap

Although the avoidable systematic effects cannot be completely prevented, it can be minimized by properly operating the CPTMS system. The systematic effect caused by the contaminant ions can be minimized by correctly adjusting the frequency, duration timing and amplitude of the ω_+ dipole excitation applied on the Penning trap (refer to chapter 3.3.7). The Coulomb interaction between the trapped ions may influence the resonant cyclotron frequency. The frequency shift caused by the ion number effect is about 10^{-9} per detected ion [Sharma2004]. During the light fission fragment measurement, less than 10 ions are kept in the Penning trap for each measurement cycle. Therefore the systematic effect caused by the ion number can be ignored on the light fission fragment mass measurement with the precision of 10^{-7}. In order to minimize the systematic effect

caused by the energy spread, a slow "evaporation pulse" is applied on the Penning trap electrodes shortly to reduce the trapping potential from its nominal value. This allows ions with relative high kinetic energy to escape in the axial direction. When the trapping potential returns to its normal value, the ions are cooled to the centre of the trap and occupy only a small volume.

The stability of the magnetic field could cause an unavoidable systematic effect. As described in chapter 2 ($\omega_c = qB/m$), the resonant cyclotron frequency is dependent on the magnetic field. Monitoring the magnetic field therefore is necessary. Fortunately, the magnetic field of the CPT magnet is extremely stable. The stability of the magnet is observed to be on parts in 10^{10} per hour [Clark2005]. Typically, each mass measurement including the reference molecule and the desired isotopes was made within a day. More details of systematic effects can be found in the reference [Clark2005].

4.2.2 Comparing the Measured masses with existing data and the AME2003

Figure 4.1 shows that two of the mass measurement results in this work (^{108}Tc and ^{108}Ru) agree with the AME2003 [Audi2003] value while the other two masses (^{109}Ru and ^{110}Ru) do not agree. The atomic mass values in the AME2003 are derived from the adjusted value in the table of the reference [Wapstra2003], which is the first part of the AME2003 atomic mass evaluation. The adjusted values are calculated from the input data based on a least-squares evaluation method [Wapstra2003]. The input data come from the nuclear reaction, decay and mass spectrometric results. The following schematic diagram

and table illustrate the input data and connections related to the isotopes measured by the CPTMS system.

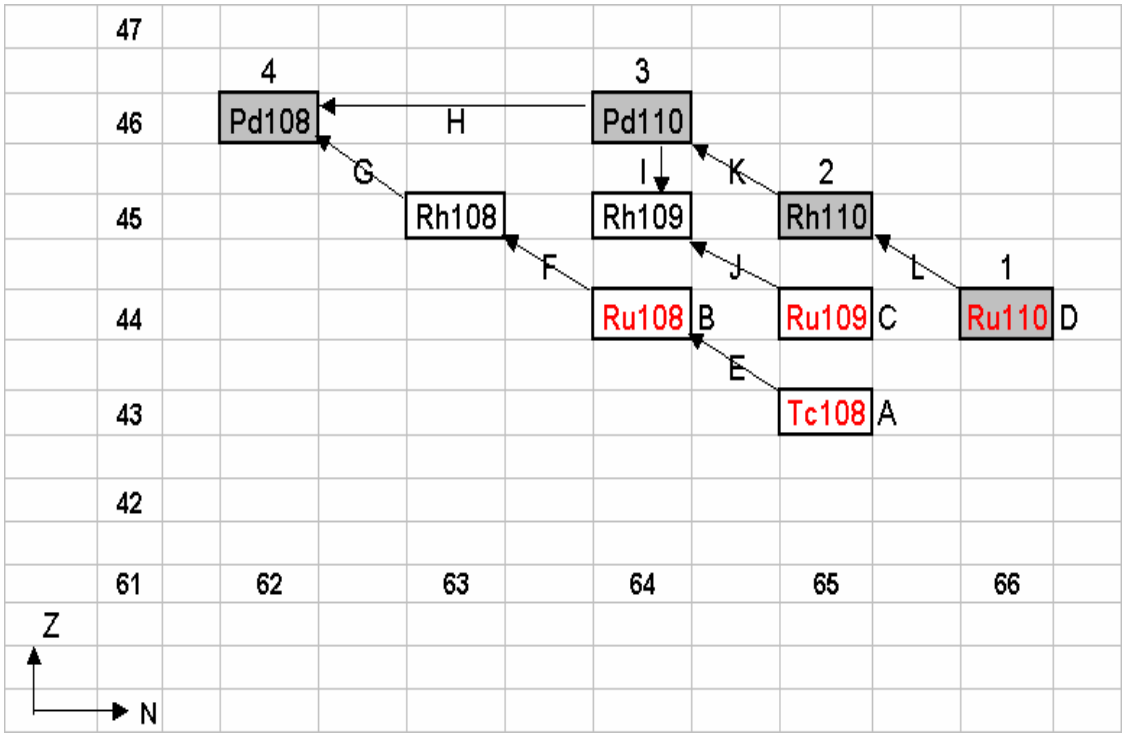

FIG. 4.2. The diagram shows the connection of nine isotopes. The horizontal direction represents the neutron number and the vertical direction represents the proton number. The isotopes and the connections are label with letters and numbers. The detailed descriptions of the labels are given in table 4.5.

Label	Isotopes	Measured Masses (μ u)	Uncertainty (μ u)	Notes / References
A	^{108}Tc	107918492	24	Mass from this work
B	^{108}Ru	107910199	20	Mass from this work
C	^{109}Ru	108913332	15	Mass from this work
D	^{110}Ru	109914009	30	Mass from this work
1	^{110}Ru	107903886	6	Mass Measurement [Kolhinen2003]
2	^{110}Rh	109905161	9	Mass Measurement [Kolhinen2003]
3	^{110}Pd	109911292	84	Mass Measurement [Damerow1963]
4	^{108}Pd	109914101	77	Mass Measurement [Damerow1963]

(A)

Label	Reactions	Input Data (μu)	Uncertainty (μu)	References
E	^{108}Tc ($\beta-$) ^{108}Ru	8288	54	[Graefenstedt1989]
F1	^{108}Ru($\beta-$) ^{108}Rh	1412	107	[Pierson1962]
F2	^{108}Ru($\beta-$) ^{108}Rh	1524	199	[Graefenstedt1989]
F3	^{108}Ru($\beta-$) ^{108}Rh	1481	86	[Jokinen1992]
F4	^{108}Ru($\beta-$) ^{108}Rh	1449	64	[Jokinen1994]
F5	Weighted average	1455	45	
G	^{108}Rh($\beta-$) ^{108}Pd	4836	113	[Graefenstedt1989]
H	^{110}Pd (p, t) ^{108}Pd	2001252	16	[Kuheld1975]
I1	^{110}Pd (d, ^{3}He) ^{109}Rh	996416	5	[Kaffrell1987]
I2	^{110}Pd (t, ^{4}He) ^{109}Rh	996437	27	[Flynn1982]
J	^{109}Ru($\beta-$) ^{109}Rh	4466	70	[Graefenstedt1989]
K	^{110}Rh($\beta-$) ^{110}Pd	5797	107	[Pinston1970]
L	^{110}Ru($\beta-$) ^{110}Rh	3017	54	[Jokinen1991]

(B)

Table. 4.5. Table (A) and (B) explain the labels in the figure 4.2. (A) A to D labels the masses measured by the CPTMS system. 1 to 4 labels the masses from the other mass spectrometry measurements. The measured masses and their uncertainties are given respectively. The references are shown in the last column. (B) E to L labels the reactions between each two isotopes. The input data (the reaction Q value) are given respectively. Also the references are indicated.

In the AME2003 mass table, the atomic masses of ^{108}Ru, ^{109}Ru and ^{108}Tc were derived from the nuclear reactions only. Now the atomic masses of those isotopes have been directly measured by the CPTMS system with high precision. Therefore the mass measurement results presented here can be used to double check the atomic masses of those isotopes in the mass table as well as the nuclear reaction Q value between any two isotopes. The red symbols in figure 4.2 (^{108}Tc, ^{108}Ru, ^{109}Ru, and ^{110}Ru) represent the measured masses in this work; the solid gray squares (^{108}Pd, ^{110}Pd, ^{110}Rh, and ^{110}Ru) stand for the spectrometric masses measured by the other research groups. The mass measurements results are shown on table 4.5 (A). The arrows in figure 4.2 indicate the

nuclear reactions and decays between each two isotopes, and the direction of the arrows represents the direction of the nuclear reactions. The nuclear reaction Q values are shown on table 4.5 (B). F1 to F4 in this table are the four results from different β decay measurements and F5 is the weighted average of these values. I1 and I2 are the two different nuclear reactions between ^{110}Pd and ^{109}Rh, used to determine their masses.

Among the nine masses in figure 4.2, seven of them have been directly measured by mass spectrometers. The atomic masses can also be calculated through the nuclear reaction Q values. Therefore we can compare the derived masses and the directly measured masses and tell which input data are reliable and which ones are suspicious. The following table 4.6 shows the comparison of the measured masses from this work and the input data from AME2003.

Check spectrometric mass	**Mass Difference (μu)**	**Uncertainty (μu)**	**Note**
D-1	-92	83	Compare measurement of ^{110}Ru
Check one reaction connection			
A-B-E	6	62	Check connection E
3-4-H	23	19	Check connection H
2-3-K	333	137	Check connection K
1-2-L	-208	126	Check connection L
D-2-L	-300	104	Check connection L
Check two reaction connections			
(B-4)-(F+G)	21	123	Check connection F and G
(D-3)-(L+K)	33	124	Check connection L and K
(C-3)-(J-I1)	121	72	Check connection I and J
(C-3)-(J-I2)	142	72	Check connection I and J
Weighted Average	132	51	Check connection I and J

Table. 4.6. The table shows the results of checking the input data. The letters and the numbers are the labels from table 4.5. For example "D-1" represents the mass differences between ^{110}Ru from mass measurement in this paper and ^{110}Ru from the JYFLTRAP mass measurement [Kolhinen2003].

In figure 4.2, there are three nuclear reaction chains connecting all of the nine isotopes:

1) From ^{108}Tc to ^{109}Ru
2) From ^{109}Ru to ^{110}Ru, and
3) From ^{108}Tc to ^{110}Ru.

If all of the nine atomic masses are consistent with each other, the difference between any two of them should match the nuclear reaction Q value along the reaction chain. If they didn't match, either the nuclear reaction value or the directly measured masses is suspected.

Check CPT masses against others

^{110}Ru has been measured by both the CPTMS system and the JYFLTRAP. The results agree with each other according to table 4.6 (D-1).

Connections between adjacent nuclides

The connections E, H, K and L in figure 4.2 can be directly checked. According to the table 4.6, the connection E and the connection H are consistent with their mass difference, while K and L do not agree. The mass difference between ^{110}Rh and ^{110}Pd is higher than the reaction value (connection K) by about 300 μu. The mass difference between ^{110}Ru and ^{110}Rh is lower than the reaction value (connection L) by about 300 μu. It seems the mass of ^{110}Rh shifts about 300 μu. The isomer state might be existed in this case. One more precise mass measurement of the isotope ^{110}Rh will resolve the problem.

More complex connections

In table 4.6, connections of (G, F), (K, L) and (I, J) have been checked. (G+F) and (K+L) agree with the corresponding mass differences, while (J-I) do not agree. The connection (K+L) matches with the mass difference between two reliable masses ^{110}Pd and ^{110}Ru. The difference between the connection I and the connection J do not agree with the mass difference between ^{110}Pd and ^{109}Ru. Since the atomic mass of ^{110}Pd is reliable, the suspicions value lies on the mass value of ^{109}Ru, the link I and the link J. For the link I, there are two different reaction Q value measurements and they agree with each other (refer to table 4.5 B). So the value of link I is probably more reliable than the link J. The direct mass measurement of ^{109}Rh will clarify this problem.

4.2.3 Comparing measured masses with the mass models

Precise mass measurements have been widely used to test the nuclear mass models. In 1935, the "semi-empirical mass formula" was first presented by Von Weizacker using the liquid-drop model [Weizsacker1935]. This mass model treats the nuclei as a droplet of liquid. Since then, improvements have been made to this original mass formula. Until now the Finite-Range Droplet Model (FRDM), which combines both the macroscopic effects and the microscopic corrections, has become one of the most popular mass models. The atomic mass excesses of 8979 nuclei ranging from ^{16}O to A=339 were calculated based on the FRDM and presented in reference [Moller1995]. The measured masses from this work can be used to test the mass values from the FRDM mass table. Table 4.7 shows comparison of the mass excesses between our values and the FRDM values.

Proton (Z)	Neutron (N)	Isotope	Measured Masses Excess (MeV)	FRDM Mass Excess (MeV)	Δ (MeV)
44	64	Ru108	-83.65	-83.26	-0.39
44	65	Ru109	-80.73	-80.43	-0.30
44	66	Ru110	-80.10	-79.41	-0.69

Table. 4.7. Table shows the mass excess from the measurements and the mass excess from FRDM calculation. The differences of the mass excesses are given on the last column.

Plots the "Δ" value against the species in the table 4.7. It suggests that the FRDM overestimates the atomic mass of ^{108}Ru, ^{109}Ru and ^{110}Ru. It seems a trend that the mass difference increases when the atomic number gets bigger.

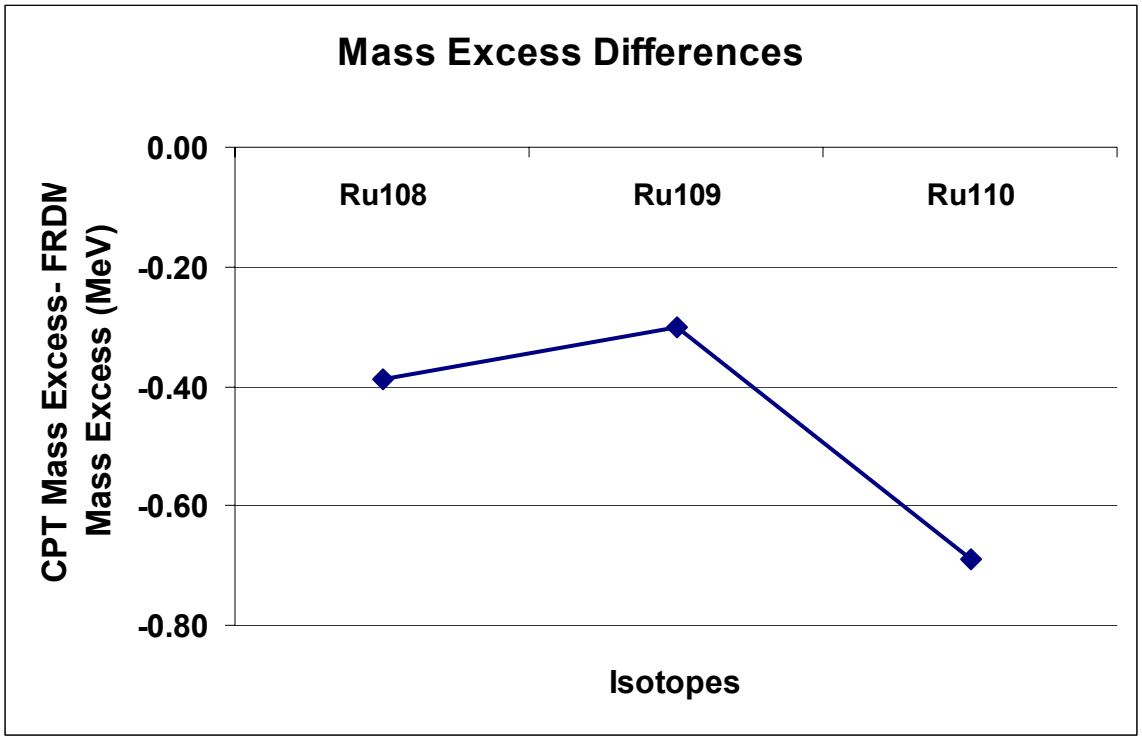

FIG. 4.3 The plot of the mass excess differences between CPT measured value and the FRDM calculated value.

From the microscopic point of view, the Hartree-Fock mass formula provides a sound theoretical basis and a very good fit to the mass data. The HFBCS-1 mass table was built in 2001 based on the Hartree-Fock (HF) method and the BCS pairing approach [Goriely2001]. Using the same method, we can test the masses from HFBCS mass model. Table 4.8 shows the comparison of the measured mass excess value and calculated mass excess value. By plotting the "Δ" value in the table 4.8, we get the figure 4.4. Based on figure 4.4, it suggests that the HFBCS mass model underestimates the atomic mass of ^{108}Ru and ^{109}Ru, and predicted the mass of ^{110}Ru correctly. The data suggest a possible trend that the mass difference increases when the atomic number decreases.

Proton (Z)	Neutron (N)	Mass Number (A)	Isotope	Measured Mass Excess (MeV)	HFBCS Mass Excess (MeV)	Δ (MeV)
44	**64**	**108**	**Ru108**	-83.65	-83.70	0.05
44	**65**	**109**	**Ru109**	-80.73	-80.80	0.07
44	**66**	**110**	**Ru110**	-80.10	-80.10	0.00

Table. 4.8. Comparison of the mass excess between CPT value and HF-BCS value. This table lists the measured mass excess and the mass excess from the HF-BCS nuclear mass table [Goriely2001]. The Δ is the difference between our mass excess and HF-BCS mass excess.

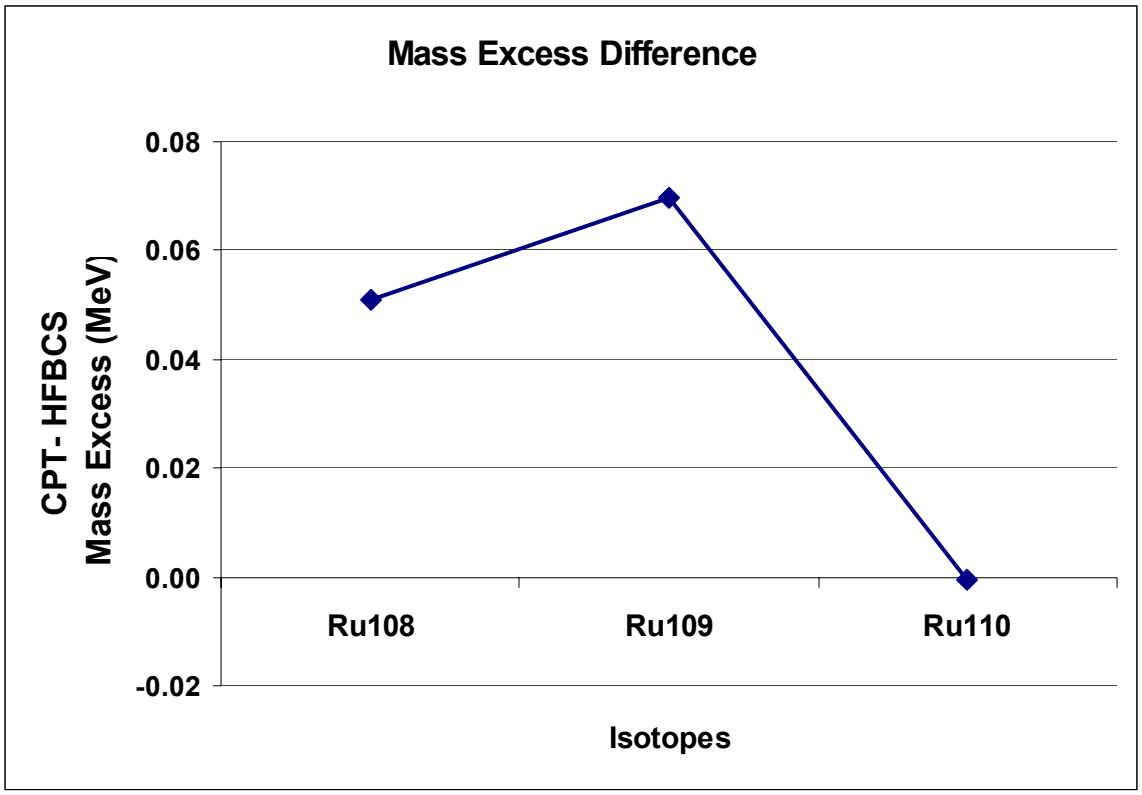

FIG. 4.4. The plot shows the difference between measured mass excess and the mass excess from the HF-BCS mass table.

As far as the three measured masses are concerned, the HFBCS mass model predicts the masses much better than the FRDM.

Chapter 5

Summary and Outlook

5.1 Summary

Ion traps have been widely used to conduct precise mass measurements [Savard1997]. The Canadian Penning Trap Mass Spectrometer (CPTMS) located at Argonne National Laboratory consists: the mechanical system, the electronic system, the vacuum system and the data acquisition/control system. It has proved an ideal apparatus to provide the precise and reliable mass values [Clark2004].

Precise mass measurements of light ^{252}Cf fission fragments have been made using the CPTMS system. It is the first time the light fission fragments were measured by a mass spectrometer. The precise mass measurements of four neutron-rich isotopes (^{108}Tc, ^{108}Ru, ^{109}Ru and ^{110}Ru) were presented in this thesis. Compared with the mass values in the AME2003 mass table, all of our measurements yield a better precision. The measured masses of ^{108}Tc and ^{108}Ru agree with the AME2003 value; while ^{109}Ru and ^{110}Ru do not agree. For the atomic mass of ^{110}Ru, our mass measurements are consistent with the mass measurement from the JYFLTRAP group [Kolhinen2003]. Based on the link checking results in chapter 5.2, there are reasons to suspect the nuclear reaction Q value between ^{109}Rh and ^{109}Ru, the atomic mass of ^{110}Rh and the reaction values between ^{110}Pd and

^{110}Rh. In order to clarify this situation, precise mass measurements of ^{110}Rh and ^{109}Rh are needed.

5.2 Outlook

For the outlook of the CPTMS system, more mass measurements of the light ^{252}Cf fission fragments will be made. The future mass measurements will benefit from a stronger ^{252}Cf fission source in addition to the ongoing improvements to the CPTMS system. A 7 Tesla super conducting magnet and a new Penning trap have already been installed to replace the old isobar separator. A mass resolving power greater than 100,000 is expected, which is enough to completely remove the contaminant molecules. The new isobar separator will make the mass measurements faster and more precise. A new data acquisition and control system is in preparation, which will significantly reduce the human efforts and mistakes. The whole system will become more automatic and easy-to-control.

The mass measurements of fission fragments will continue playing an important role in testing the nuclear reaction Q value and in understanding the astrophysical processes as well. More than half of elements in the universe heavier than iron are synthesized by the rapid neutron-capture process (r-process). Mass measurements of neutron-rich isotopes close to the r-process path are critical to network calculations that are used to explain the natural abundance of the nuclides produced by this astrophysical process.

Appendix I

The Mass Spectrometry Terms

"High precision and high accuracy" are the ultimate goal of a precise mass measurement. Efficiency, precision, accuracy and resolution are the most commonly used and important terms in mass measurements. They describe how well the mass measurement has been done.

Efficiency

Efficiency is the ratio of the effective output to the total input in any system. For the CPTMS system, the efficiency describes how well the equipment can transfer the ions. For instance, if 1000 desired ions come into one of the transport elements and 800 of them come out, we can say the efficiency of this transport element in this event is about 80%. During the experiments, it is important to make sure all of the equipment is working efficiently.

Precision

Precision of the masses can be expressed as the following equation:

$$P(precision) = \frac{\Delta m}{m} \tag{1.1}$$

Where, P is the precision of the measurement, m is the measured mass value and Δm is the uncertainty of that value. In the Penning trap mass measurements, since

$m = qB/\omega_c$ (refer to the chapter 2.2) the precision can also be expressed in terms of the measured cyclotron frequency:

$$P(precision) = \frac{\Delta m}{m} = \frac{q \cdot B \cdot \Delta\omega}{\omega_c^2} \cdot \frac{\omega_c}{q \cdot B} = \frac{\Delta\omega_c}{\omega_c} \tag{1.2}$$

The CPT mass spectrometer has been proved to be an ideal machine to perform high precision mass measurements. The precision of the mass measurement described in this paper reaches 10^{-7}.

In our mass measurements, the precision of the measurement can be expressed as [Clark2005]:

$$P(precision) = \frac{\Delta m}{m} = \frac{m}{qB} \frac{C}{T_{RF} \cdot \sqrt{N}} \tag{1.3}$$

Where, q is the charge, B is the magnetic field, C is a constant, T_{RF} is the excitation time and N is the total number of the desired ions. Based on equation 1.3, there are four ways to increase the precision:

1) Use stronger magnetic field. In the CPTMS system, a super-conducting magnet is used to provide a 5.9T homogeneous magnetic field.
2) Use higher charge state. Due to the buffer gas cooling, most nuclides from the ion source become singly or doubly charged ions in the fission fragments measurement.
3) Use longer excitation time. However a very long excitation time may cause the loss of the ions due to the half-life of the nuclides. Losing desired ions may decrease the precision of measurements. Therefore the excitation time needs to be considered together with the number of desired ions transferred to the Penning trap.

4) Increase the number of desired ions. However, it doesn't mean to transfer as much ions as possible to the precision Penning trap. Because the cleaning process of the Penning trap never reach 100% efficiency, the more ions are transferred to the Penning trap, the more contaminant ions will be mixed among desired ions. The presence of contaminant ions reduces the TOF depths of the cyclotron resonance spectra. Therefore cleaning process is also very important in performing a high precision mass measurement. Also too many desired ions used for each measurement cycle results in the systematic effect as described in chapter 4.2. In a word, the excitation time and the number of desired ions used for the precise mass measurement need to be considered carefully.

Accuracy

Accuracy of the measurement is how close the measured value is to the "real" value. In our measurement, the "theoretical" value can be wrong. We only know the calibration masses accurately.

The result of each measurement will be in one of the four following situations: 1) low accuracy and low precision, 2) high accuracy but low precision, 3) low accuracy but high precision and 4) high accuracy and high precision. More explanation are given below to clarify the difference of each situation:

1) The measurements are in low accuracy and low precision. In this situation, all the data points are far away from the "real" value and they all have big uncertainties.
2) The measurements are in low accuracy but high precision. In this situation, most of the data points are far away from the "real" value, but they have small

uncertainties. If the data form a gaussian distribution, the centre of the distribution will be off from the real value, but the FWHM (Full Width Half Maximum) of the distribution is narrow.

3) The measurements are in high accuracy but low precision. In this situation, most of the data points are close to the "real" value, but they have big uncertainties.
4) The measurements are in high accuracy and high precision. In this situation, most of the data points are close to the "real" value and they all have very small uncertainties. It is the goal of our measurements.

Mass Resolution

Mass Resolution shows the ability of the apparatus to separate ions of similar masses. In our experiment, it can be calculated with the following equation:

$$R(resolution) = \omega_c \Big/ FWHM \tag{1.4}$$

Where, ω_c is the cyclotron frequency of a certain mass in the Penning trap and FWHM refers to Full Width Half Maximum of the data distribution. The resolution of the Isobar Separator is calculated in such way shown on the chapter 3.3. For the last Penning trap of the system, the FWHM is given as:

$$FWHM \sim \frac{0.89}{T_{RF}} \tag{1.5}$$

Therefore longer excitation period gives smaller FWHM, hence higher resolution.

Appendix II

Acronyms

AME: Atomic Mass Evaluation

CAMAC: Computer Automated Measurement and Control

CPT: Canadian Penning Trap

CPTMS: Canadian Penning Trap Mass Spectrometer

FRDM: Finite-Range Droplet Model

HFBCS: Hartree-Fock Bardeen Cooper Schrieffer

IS: Isobar Separator

MCP: Micro-Channel Plate

RFQ: Radio Frequency Quadrupole

SCSI: Small Computer Systems Interface

TOF: Time of Flight

Appendix III

The TOF spectra of the light fission fragment mass measurements are presented here. A quadrupole excitation of 500ms was applied on each measurement. The horizontal axis represents the sweeping frequencies. The vertical axis represents the time of flight of the ions and the unit is ¼ of the real timing in μs .

1) ^{108}Tc

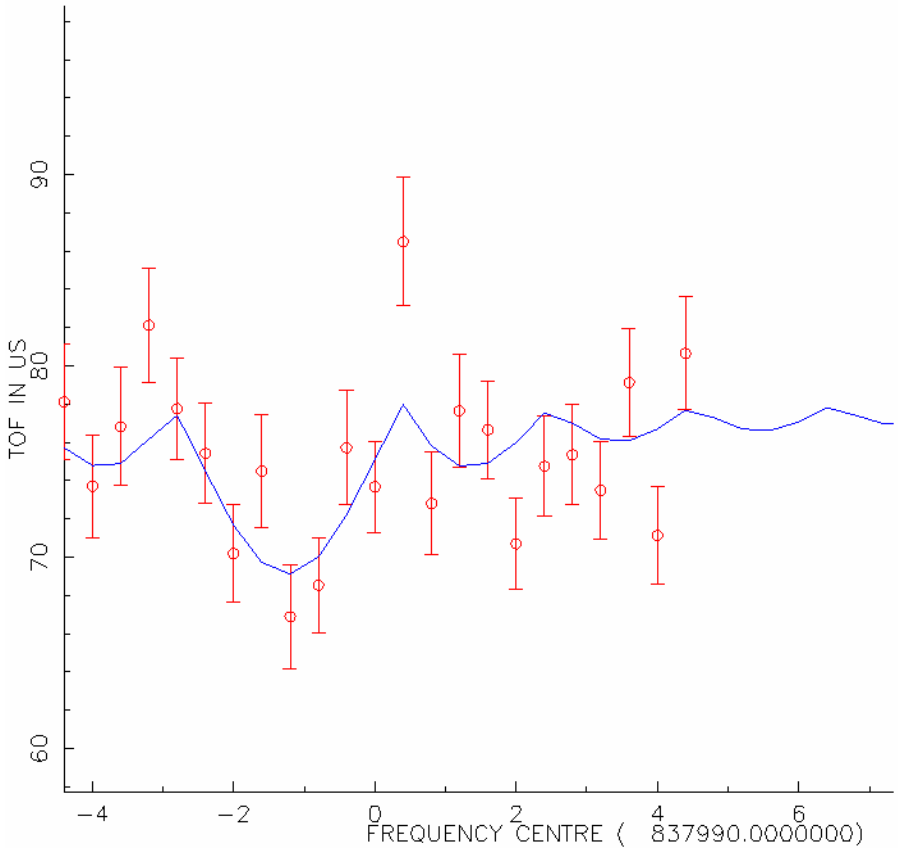

2) ^{108}Ru

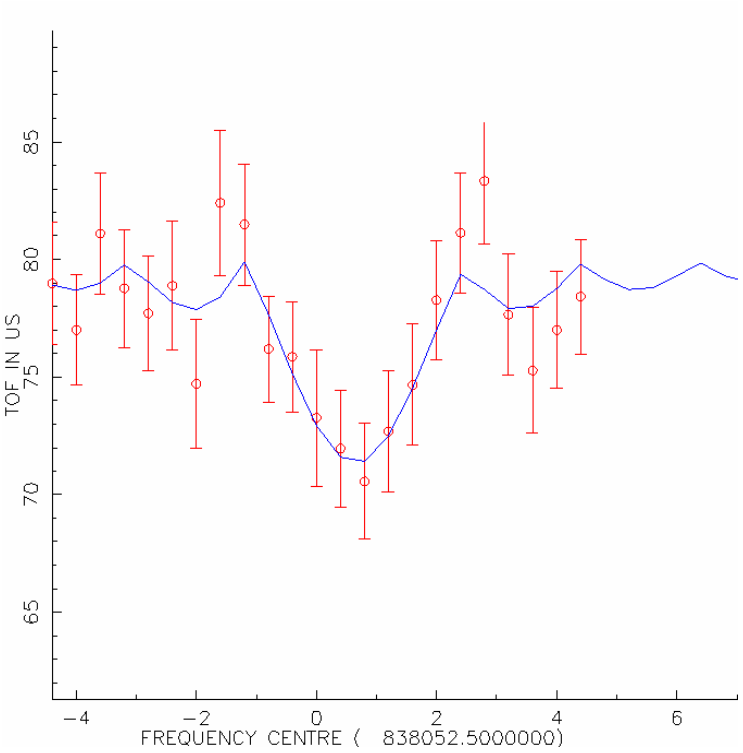

3) ^{109}Ru

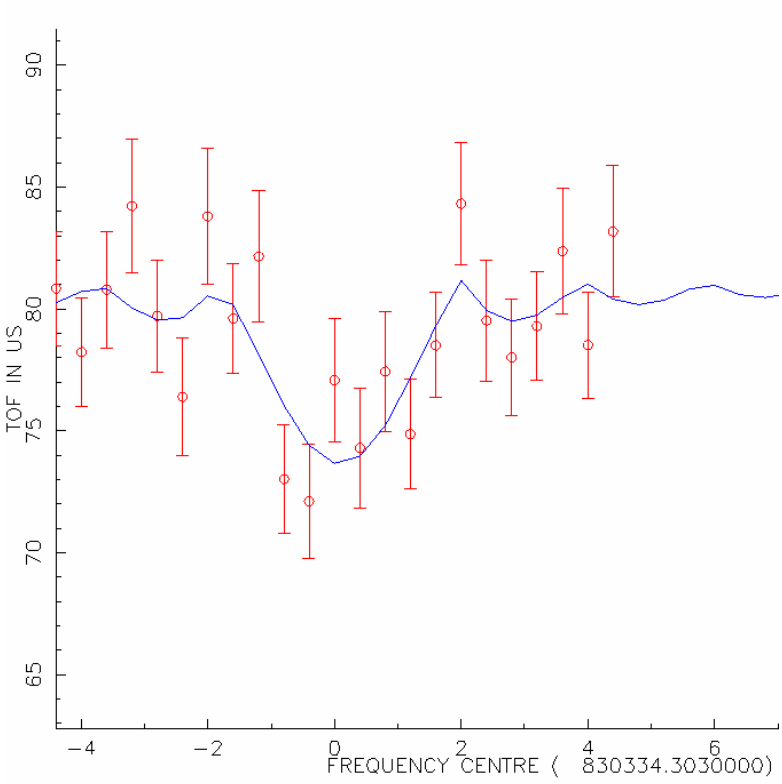

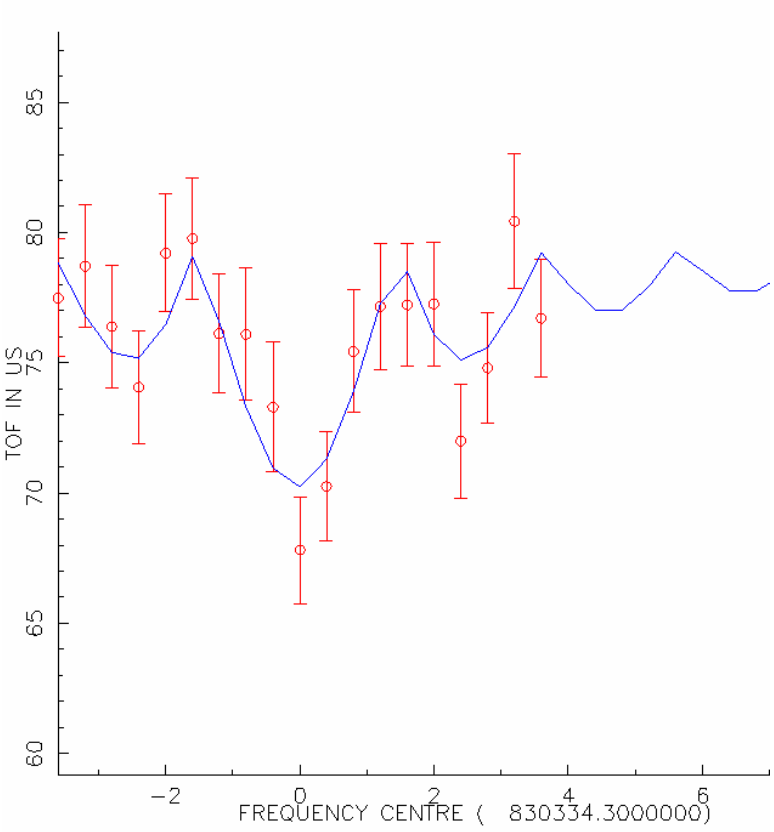
TOF IN US
60
65
70
75
80
85
−2
0
2
4
6
FREQUENCY CENTRE (830334.3000000)

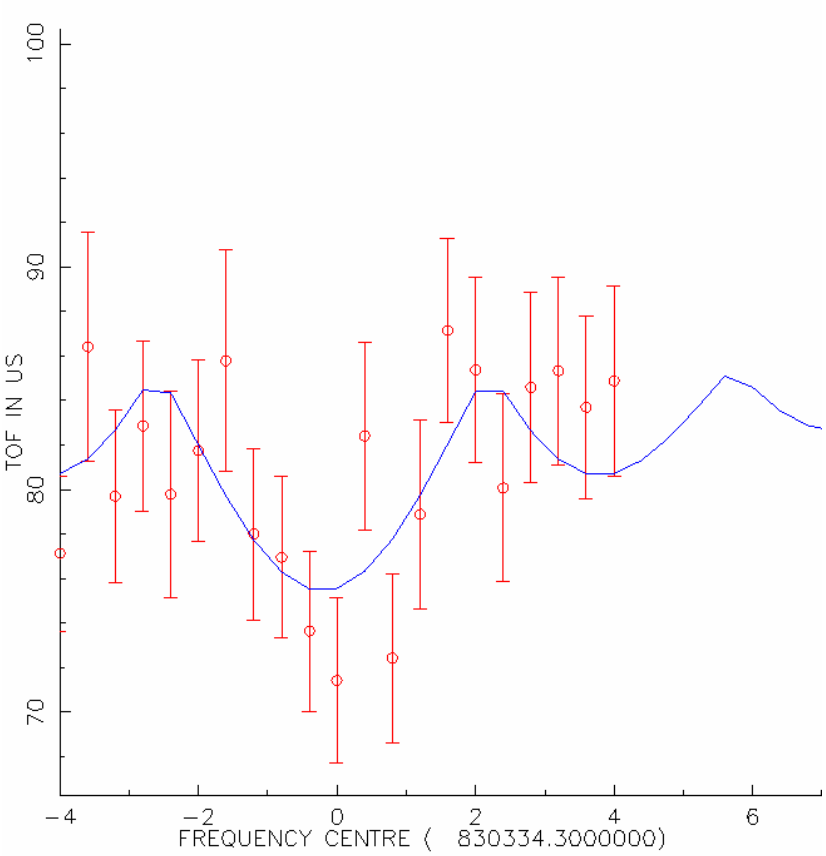
TOF IN US
70
80
90
100
−4
−2
0
2
4
6
FREQUENCY CENTRE (830334.3000000)

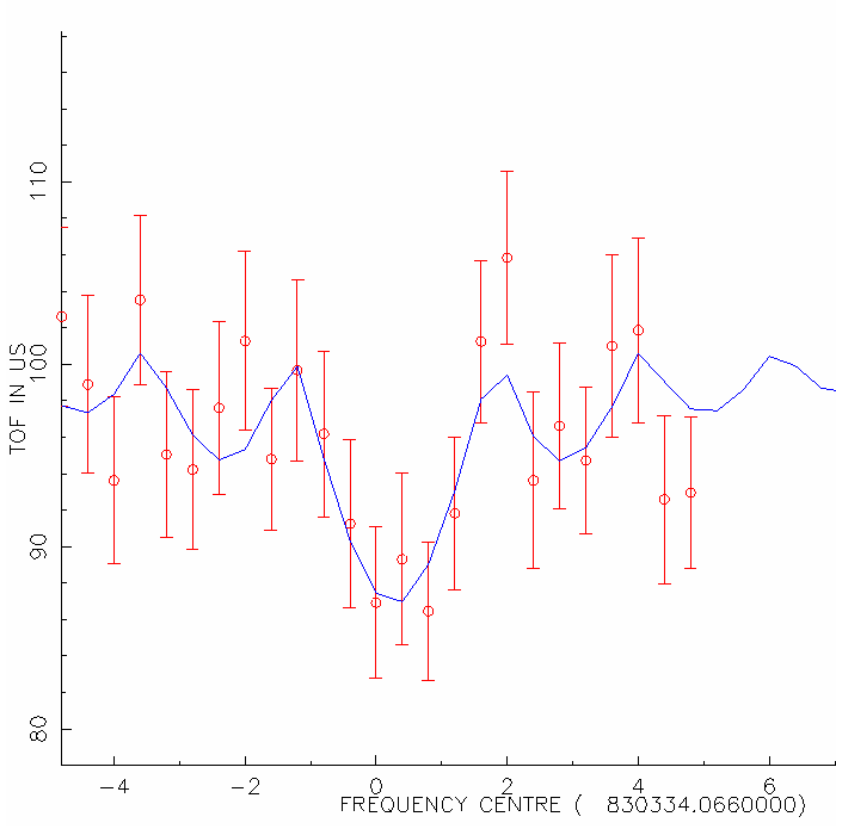
TOF IN US
80
90
100
110
−4
−2
0
2
4
6
FREQUENCY CENTRE (830334.0660000)

4) ^{110}Ru

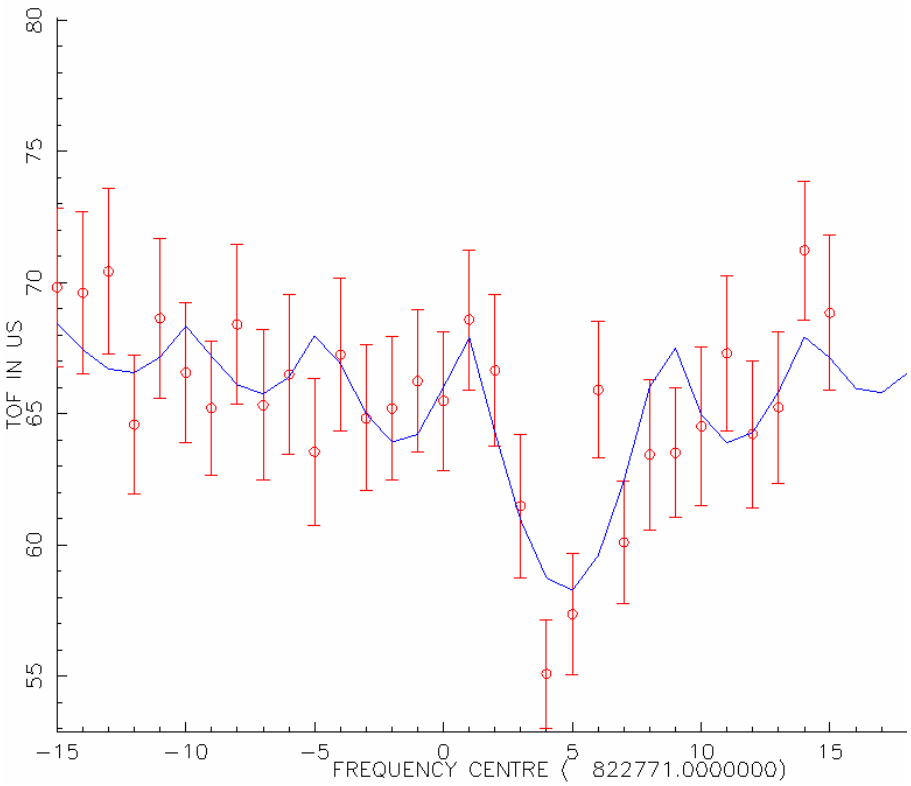
TOF IN US
55
60
65
70
75
80
−15
−10
−5
0
5
10
15
FREQUENCY CENTRE (822771.0000000)

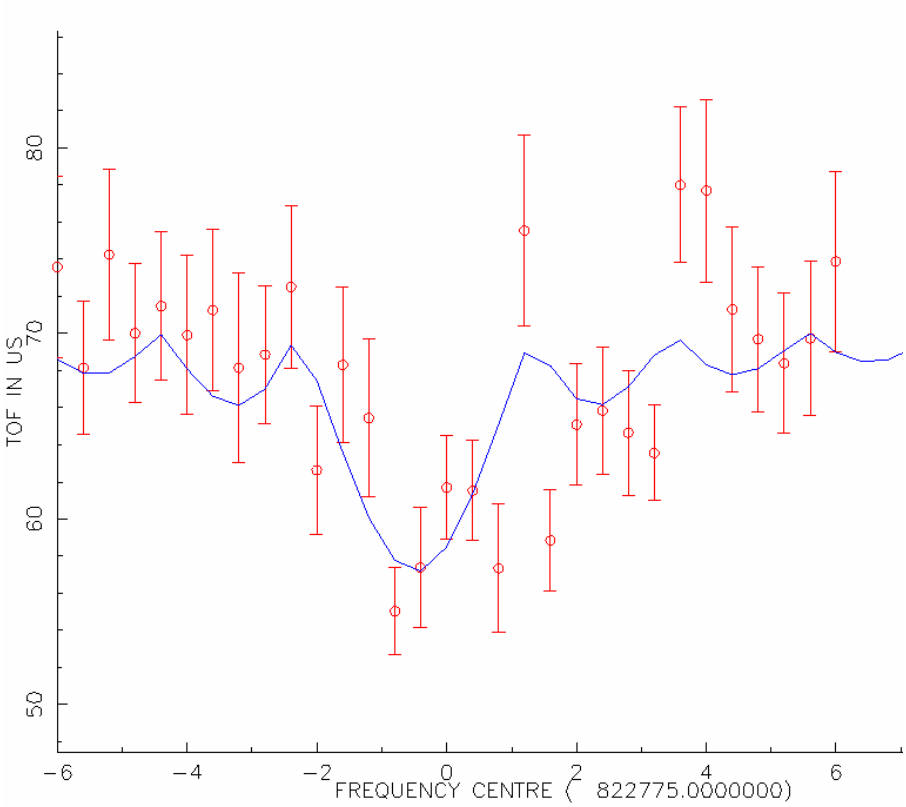
TOF IN US
50
60
70
80
−6
−4
−2
0
2
4
6
FREQUENCY CENTRE (822775.0000000)

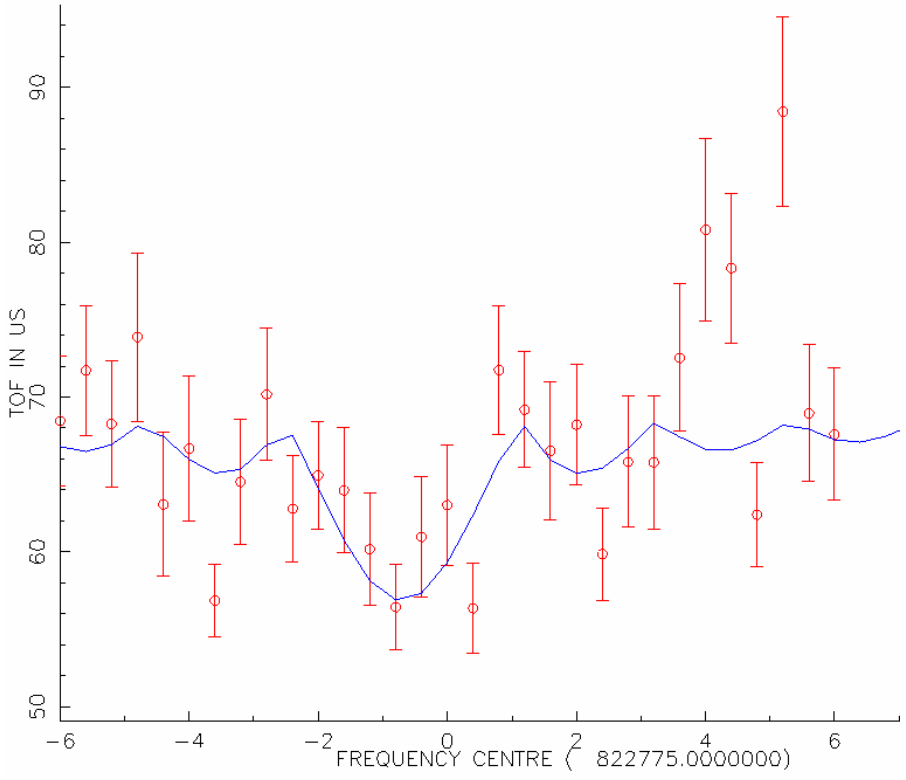
TOF IN US
50
60
70
80
90
−6
−4
−2
0
2
4
6
FREQUENCY CENTRE (822775.0000000)

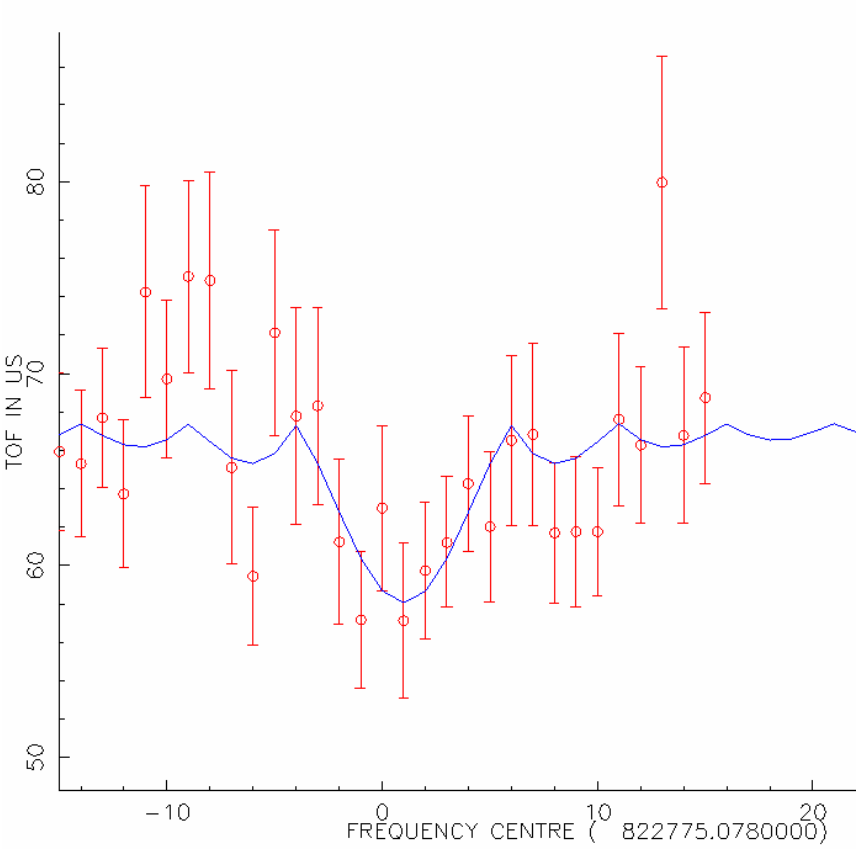
TOF IN US
80
70
60
50
−10
0
10
20
FREQUENCY CENTRE (822775.0780000)

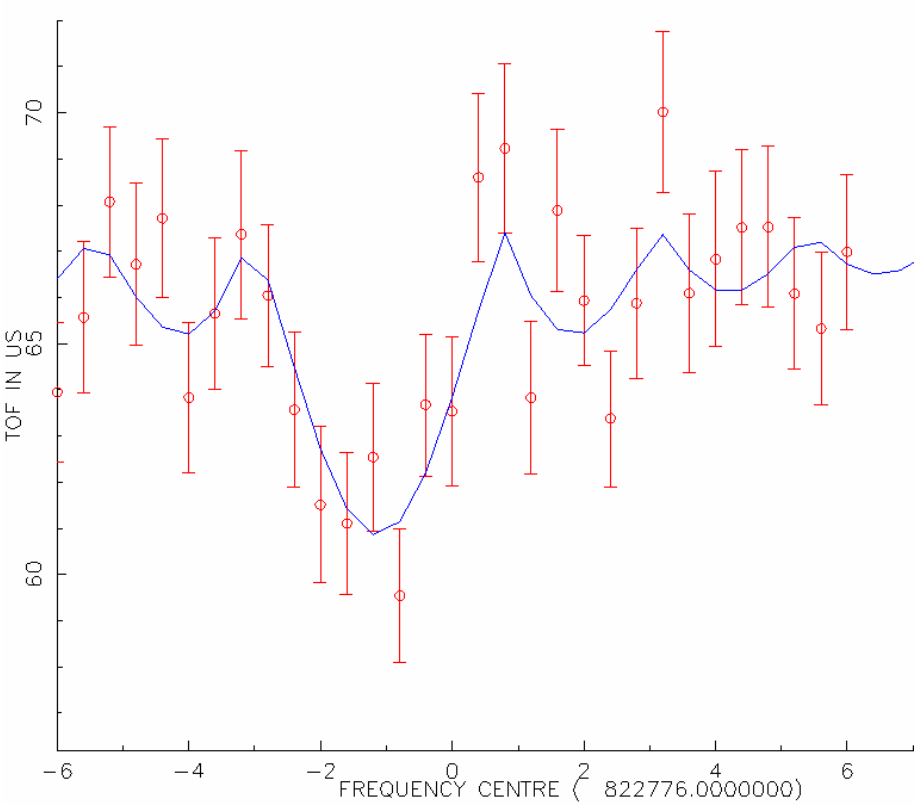
TOF IN US
70
65
60
−6
−4
−2
0
2
4
6
FREQUENCY CENTRE (822776.0000000)

Reference:

[Aston1920] Aston, 1920, Nature (London) 105,617.

[Audi2003] G. Audi, A. H. Wapstra, and C. Thibault *The AME2003 atomic mass evaluation (II) Tables, graphs and references,* Nuclear Physics A 729 (2003) 337-676.

[Barber1964] R. C. Barber, R. L. Bishop, L. A. Cambey, H. E. Duckworth, J. D. Macdougall, W. McLatchie, J. H. Ormrod & P. van Rookhuyzen (1964). *Proceedings of the Second International Conference on Nuclidic Masses,* ed. Johnson, W. H., pg. 393. Vienna: Springer-Verlag.

[Barber1971] R.C. Barber, R. L. Bishop, Duckworth, H. E., Meredith, J. O., Southon, F. C. G., van Rookhuyzen, P and Williams, P. (1971). *Review of Scientific Instruments*, **42**, 1.

[Bollen1990] G. Bollen, R. B. Moore, G. Savard and H. Stolzenberg, *The Accuracy of Heavy Ion Mass Measurements Using TOF-ICR in a Penning Trap* 1990.

[Bollen1996] G. Bollen, S. Becker, *ISOLTRAP: a tandem Penning trap system for accurate on-line mass determination of short-lived isotopes* Nucl. Instrum. Methods A 368 (1996) 675-697.

[Bollen2002] G. Bollen, Eur. Phys. J. A 15 (2002) 237.

[Bollen2003] G. Bollen and S. Schwarz, Nucl. Instrum. Methods Phys. Res., Sect. B 204, 466-473 (2003)

[Boudreau2001] Chantal Boudreau, *The Transport of Radioactive Ions in a Gas Filled Radio Frequency Quadrupole Mass Filter System* Master Thesis (2001)

[Brown1970] Lowell S. Brown and Gerald Gabrielse, *Geonium theory: Physics of a single electron or ion in a Penning trap* (1970)

[Clark2003] J. A. Clark *et al*., Nucl. Instrum. Methods Phys. Res., Sect. B 204, 487 (2003)

[Clark2004] J. A. Clark, G. Savard, K. S. Sharma, and *et al*., *Precise Mass Measurement of ^{68}Se, a Waiting-Point Nuclide along the rp Process*, Phys. Rev. Lett. 92. 192501 (2004)

[Clark2005] J. A. Clark, PhD thesis, University of Manitoba (2005)

[Damerow1963] Richard A. Damerow, Richard R. Ries, and Walter H. Johnson, *Atomic Masses from Ruthenium to Xenon* 132, pp. 1673-1681

[Dawson1976] P.H. Dawson (editor), *Quadrupole Mass Spectrometry and Its Applications*, Elsevier, Amsterdam (1976)

[Denison1971] D. R. Denison, J. Vac. Sci. & Tech. 8, 266 (1971)

[Dilling2003] J. Dilling, P. Bricault, M. Smith, and H. -J. Kluge. Nucl. Instrum. Methods Phys. Res., Sect. B 204, 492-496 (2003)

[Duckworth1990] Duckworth, H. E., Barber, R. C. and Venkatasubramaniam, V. S. (1990). *Mass Spectroscopy* (2^{nd} edition), pg 148, Cambridge University Press

[England1993] T. R. England and B. F. Rider, Evaluation and Compilation of Fission Product Yields LA-UR-94-3106 ENDF-349

[Flynn1982] E. R. Flynn, F. Ajzenberg-Selove, Ronald E. Brown, J. A. Cizewski, and J. W. Sunier *Erratum: Proton hole states in neutron rich nuclei near A=100,* Phys. Rev. C 25, 2851–2852 (1982)

[Goriely2001] S. Goriely, F. Tondeur, J. M. Pearson, At. Data Nucl. Data Tables 77, 311 (2001)

[Graf1980] G. Graff, H. Kalinowsky, and J. Traut. *A Direct Determination of the Proton Electron Mass Ratio Z*. Phys. A 297, 35-9 (1980)

[Graefenstedt1989] M. Graefenstedt, P. Jurgens, etc. *Experimental Beta-Decay Energies of Very Neutron-Rich fission Products with* $107 \leq A \leq 109$ Zeitschrift Physik A 334, 239-245 (1989)

[Jokinen1991] A. Jokinen, J. Aysto and etc. Zeitschrift Physik A 340, 21 (1991)

[Jokinen1992] A. Jokinen, Nuclear Physics A 549, 420

[Jokinen1994] A. Jokinen, PhD thesis,

[Kaffrell1987] N. Kaffrell, P. Hill, J. Rogowski, and H. Tetzlaff, Nuclear Physics A 470, 141

[Kellerbauer2002] Alban Kellerbauer, PhD thesis, the Ruperto-Carola Unviersity of Heidelberg, Germany

[Kolhinen2003] V. Kolhinen, PhD thesis, the University of Jyvaskyla

[Koni1995] M. Konig, G. Bollen, H. –J. Kluge, T. Otto, and J. Szerypo. *Quadrupole Excitation of Stored Ion Motion at the True Cyclotron Frequency*. Int. J. Mass Spectrum. Ion Proc. 142, 95-116 (1995)

[Krane1987] Krane, Kenneth S. (1987), Introductory Nuclear Physics

[Kuheld1975] A. W. Kuhfeld, Nuclear Physics A 247,152

[Lunney2003] D. Lunney, J. M. Pearson, and C. Thibault. *Recent trends in the determination of nuclear masses* Reviews of Modern Physics Volume 75, No.3 (2003)

[McDa1973] E. W. McDaniel and E. A. Mason. *The Mobility and Diffusion of Ions in Gases. Wiley*, New York (1973)

[Moller1995] P. Moller, J. R. Nix, W. D. Myers, W. J. Swiatecki, At. Data Nucl. Data Tables 59, 185 (1995)

[NASA] *http://imagine.gsfc.nasa.gov/docs/teachers/elements/imagine/05.html* Created by NASA

[Paul1989] W. Paul. Rev. Mod. Phys. 62 (1989) 531

[Penning1936] F. M. Penning, Physica 3 (1936) 873

[Pierson1962] William R. Pierson, Henry C. Griffin, and Charles D. Coryell *Characterization of Ru^{107}, Ru^{108}, Rh^{107}, and Rh^{108}*, 127 pp. 1708-1722

[Pinston1970] J.A. Pinston, F. Schussler, Nuclear Physics A 144, 42

[Radon2000] T. Radon *et al*., Nucl. Phys. A 677 (2000) 75

[Savard1991] G. Savard, S. Becker, G. Bollen, H. -J. Kluge, R. B. Moore, T. Otto, L. Schweikhard, H. Stolzenberg, and U. Wiess. *A New Cooling Technique for Heavy Ions in a Penning Trap.* Phys. Lett. A. 158, 247-52 (1991)

[Savard1997] G. Savard. "*Ion Trap Technology at Accelerator Facilities"* Nucl. Instr. And Meth. , B126 (1997) 361

[Savard2003] G. Savard *et al*., Nucl. Instrum. Methods Phys. Res., Sect. B 204, 582 (2003)

[Savard2004] G. Savard, J. A. Clark, *et al., Q value of the super-allowed decay of ^{22}Mg and the calibration of the $^{21}Na\ (p,\gamma)$ experiment* Phy. Rev. C. 70, 042501® (2004)

[Savard2005] G. Savard, F. Buchinger, J.A. Clark, *et al*. *Q value of the super-allowed decay of ^{46}V and its influence on V_{ud} and the CKM matrix unitarity,* in preparation.

[Sharma1998] K. S. Sharma *et al*., in: Proc. Int. Conf. Exotic Nuclei and Atomic Masses ENAM'98, Shanty Creek, USA, 1998, AIP, 1998, p. 103

[Sharma2004] K. S. Sharma *et al*., in: Proc. Int. Conf. Exotic Nuclei and Atomic Masses ENAM'04, Pine Mountain, Georgia, USA, 2004, Eur. Phys. J. A. 25, s01, 45-46(2005)

[Szerypo2002] Szerypo J. L, Jokinen A., Kolhinen V.S., Nieminen A.; Rinta-Antila S., Aysto J. Nuclear Physics A, Volume 701, Number 1, 22 April 2002, pp. 588-591(4)

[Vaz2002] Joseph V. F. Vaz *Precision Mass Measurements of Selected Isotopes of Platinum* PhD thesis (2002)

[Wang2005] J. C. Wang, F. Buchinger, J. A. Clark, *et al*. *Precise mass measurement of neutron-rich nuclei from fission fragments of* ^{252}Cf, in preparation.

[Wapstra2003] A. H. Wapstra, G. Audi, and C. Thibault *The AME2003 atomic mass evaluation (I) Evaluation of input data, adjustment procedures,* Nuclear Physics A 729 (2003) 129-336

[Weizsacker1935] C. F. von Weizacker, Z. Phys. 99, 431 (1935)